An Investigation of Crop Senescence Patterns Observed in Palouse Region Fields Using Satellite Remote Sensing and Hydrologic Modeling

A Thesis

Presented in Partial Fulfillment of the Requirements for the

Degree of Master of Science

with a

Major in Environmental Engineering

in the

College of Graduate Studies

University of Idaho

by

Matthew A. Yourek

Major Professor: Erin Brooks, Ph.D.

Committee Members: David Brown, Ph.D.; Jan Eitel, Ph.D.

Department Administrator: Ching-An Peng, Ph.D.

January 2016

AUTHORIZATION TO SUBMIT THESIS

This thesis of Matthew Yourek, submitted for the degree of Master of Science with a Major in Environmental Engineering and titled “An Investigation of Crop Senescence Patterns Observed in Palouse Region Fields Using Satellite Remote Sensing and Hydrologic Modeling,” has been reviewed in final form. Permission, as indicated by signatures and dates below, is now granted to submit final copies to the College of Graduate Studies for approval.

Major Professor: _____Date: _____
Erin Brooks, Ph.D.

Committee Members: _____Date: _____
David Brown, Ph.D.

_____Date: _____
Jan Eitel, Ph.D.

Department Administrator: _____Date: _____
Ching-An Peng, Ph.D.

ABSTRACT

Precision agriculture (PA) recognizes that every area of a field does not respond equally to equal inputs. Growers in the Palouse region know this from the yields they obtain. Scientists know this from carefully designed experiments, and casual observers know this from the patchwork of green, yellow, and brown they see within the rolling wheat fields come July. Crop yields are driven by water in this dryland farming region, and the colors are senescence (or ageing) patterns caused mainly by water stress. Soils, topography, and climate all combine to form the unique micro-environments in which crops grow in Palouse fields, producing a high level of spatial complexity. In this thesis, intensive field monitoring and soil mapping are used to parameterize and evaluate a modified version of the SMR hydrologic model. A linkage is investigated between soil measurements, landscape hydrology, and crop patterns observed by the high-resolution RapidEye™ multispectral imager.

ACKNOWLEDGEMENTS

I foremost would like to thank my advisor, Dr. Erin Brooks, for committing himself to my success, even while his responsibilities to others were many. In particular, I am appreciative of him helping me set manageable research objectives, for providing thoughtful suggestions whenever it came time to communicate results through presentations and writing, and for his enthusiasm toward my work expressed through a willingness to lend his fullest attention whenever I wanted advice. I have applied many of his keen insights about modeling and data interpretation/analysis in this thesis.

I received two full years of funding through a research assistantship with the Biological and Agricultural Engineering Department at the University of Idaho in which I aided Dr. Brooks in his research as a member of the "Brooks Lab Group". This team of undergraduate and graduate students has been dedicated to field and lab research activities, and nearly all of the field data of Chapter two, and all the hydrological and meteorological data of Chapter 3 were collected, processed, and organized by members of the Brooks Lab Group, members of which I wish to acknowledge collectively. Obviously, without data there would be no thesis.

Funding for my research position originated from the Site-Specific Climate-Friendly Farming project grant, sponsored by the U.S. Department of Agriculture's National Institute of Food and Agriculture and awarded to the Washington State University (WSU) Crop & Soil Sciences Department. I would like to thank Dr. Dave Huggins, USDA-ARS adjunct faculty at WSU, for providing unrestricted access to his lab for soil sample storage and processing. I would also like to acknowledge Margaret Davies, Associate in Research at WSU, for running all of our soil nitrate analyses.

The detailed soil mapping presented in Chapter 3 is the work of Matteo Poggio, WSU Soil Science doctoral graduate and Caley Gasch, post-doctoral research associate for Dr. David Brown of the WSU Crop & Soil Sciences Department. Field data collection was headed by Matteo Poggio and geostatistical analysis and mapping by Caley Gasch.

DEDICATION

I would like to honor my parents—they have contributed immeasurably to this work through their love and fervent support at each stage in my education.

TABLE OF CONTENTS

LIST OF TABLES

LIST OF FIGURES

CHAPTER 1: INTRODUCTION

1. BACKGROUND

1.1. The New Green Revolution

Across the world the "Green Revolution" brought a drastic boost in the production of staples, especially of wheat and rice (Pingali and Raney, 2005), and chronic food deficits of developing countries subsided (Pingali, 2012). The Green Revolution also introduced a new paradigm in agricultural research and practice founded on the belief that growing conditions could, and should, be manipulated so as to improve upon what nature alone could provide, i.e. if rainfall is limiting--then irrigate--if nutrients are lacking--then fertilize, etc. (Food and Agriculture Organization, 1996). While cropping systems have certainly become more productive, a concomitant outcome of this methodology has been the degradation of soil and water resources through erosion processes, transport of soluble agrichemicals in runoff to surface waters, and leaching of nitrate to groundwater (Ongley, 1996). In addition to contributing water pollution, agriculture is also the number one source of anthropogenic (human-caused) emissions of the potent greenhouse gas, nitrous oxide (Forster *et al*., 2007). Now with the global population projected to increase by over a third and global demand for food to increase by 70% by the year 2050 (Food and Agriculture Organization, 2009), and given the scarcity of arable land, the need is clear both for resource conservation and another dramatic boost in crop production—a new Green Revolution.

1.2. Proximal and Remote Sensing in Precision Agriculture

Ideally the goals of producing more food and minimizing environmental impact would intersect with the farmer's desire to ensure the profitability of his/her operation. Because it addresses the needs of society and the farmer alike, precision agriculture (PA) has been an important vehicle of change in the agricultural sector. A general definition that captures the key aspects of PA is provided by Dobermann *et al.* (2004) who defined it as: "a systems approach to managing soils and crops to reduce decision uncertainty through better understanding and management of spatial and temporal variability." Thus PA is not simply a suite of technologies or a set of management strategies, but a system primarily aimed at helping the farmer make better decisions.

A plethora of proximal soil and plant sensors are either commercially available or are being researched in order to provide quality spatial data to farm managers (see Viscarra Rossel *et al*., 2011 for a comprehensive review). The most widely-implemented proximal sensing technology for inferring physical soil properties has been electromagnetic induction (EMI) (Adamchuk *et al.*, 2004;

Doolittle and Brevik, 2014). Electromagnetic surveys directly measure apparent electrical conductivity of the soil, which has been related to soil depth (Kitchen *et al.* 1999), clay content (Triantafilis and Lesch, 2005), soil salinity (Corwin and Lesch, 2003), soil moisture (Kachanoski *et al*., 1988; Allred *et al*., 2005), exchangeable Ca^{2+} and Mg^{2+} (McBride *et al.*, 1990), and soil organic carbon (Korsaeth *et al.*, 2008). There are now commercially available sensors, based on EMI technology, that measure bulk soil electrical conductivity while conducting standard tillage operations (Veris Technologies, Salina, KS). Many large farming operations across the U.S. now have access to detailed soil electrical conductivity maps for their fields. Another technology uses visible and near-infrared (VNIR) sensors to detect optical properties of the soil related to soil physical properties (Mouazen *et al*., 2007; Knadel *et al*., 2015). Proximal soil sensing devices that measure variability in soil resistance/strength using tractor or truck-mounted hydraulically-driven soil probes (Domsch *et al.*, 2006; Tekin *et al*., 2008) are being developed for commercial use and are likely to become more widely used by growers and agricultural consultants. A considerable amount of research has also been applied to the development of mobile VNIR sensors for precision management (Maleki *et al.*, 2007; Mouazen *et al.*, 2007; Christy, 2008). In addition to surface soil measurements, VNIR sensors have been used for measuring soil profiles (Ben-Dor *et al.*, 2008). Recently Poggio *et al*. (2015) have developed and assessed a VNIR-cone penetrometer assembly for concurrent determination of bulk density and soil texture with depth.

In addition to proximal sensing methods wherein measurements are made close to or in direct content with the soil/crop, methods for determining soil properties and monitoring crop vitality have been developed using remote sensing (RS) instruments mounted on aircraft and satellites. These instruments have sensor arrays that detect light reflected from the ground in discrete wavebands. In crops, the fraction of incident sunlight reflected (reflectance) in visible and near-infrared wavebands is directly linked to leaf chemical and structural properties. Indices consisting of ratios and differences of waveband reflectance have been shown to correlate highly with LAI, biomass, chlorophyll, and leaf N content (e.g. Jordan, 1969; Rouse *et al*., 1973; Tucker, 1978; Huete, 1988; Barnes *et al.*, 2000; Daughtry *et al.*, 2000; Haboudane *et al*., 2002; Rodriguez *et al*., 2006; Eitel *et al*., 2011). Writing optimistically of the future role of RS in PA, Moran *et al*. (1997) identified eight opportunities for RS to bridge information gaps, among which are: converting point samples to field maps, mapping crop yield, mapping soil variability, monitoring seasonally variable soil and crop characteristics, and determining the cause of variability in crop production. Despite rapid advances in satellite technology that have made it possible to access data at high spatial (<5 m)

and temporal (<6 days) resolutions, the potential of RS has been largely unrealized owing to a large disconnect between the product developer, who generally lacks farming experience, and the farmer who by-and-large lacks familiarity with RS imagery and its interpretation (Seelan *et al*., 2003).

1.3. Prediction of Water Stress in Crops Using Remote Sensing and Hydrologic Modeling

The difference between plant temperature and air temperature has been used as an indicator of water stress since the 1970's (Idso and Ehrler, 1976). Subsequent development of the crop water stress index (CWSI) was based on the relationship between canopy temperature, air temperature, and vapor pressure deficit (Idso *et al*., 1981; Jackson *et al*; 1981). Early on, it was recognized that variations in canopy density posed a key limitation to use of the CWSI for the inference of soil water patterns. Multiple studies (Moran *et al*., 1994; Carlson *et al*., 1995; Clarke, 1997; Gillies *et al*., 1997) suggested that the confounding influence of canopy density on the water stress signal could be dampened by normalizing the CWSI with an estimation of fractional vegetation cover made from a spectral vegetation index (VI). Sandholt *et al*. (2002) later developed an empirical simplification of the CWSI, called the temperature dryness vegetation index (TVDI) that uses thermal detection of land surface temperature combined with the normalized difference vegetation index (NDVI) calculated from satellite RS data. All these indices and similar variants (Zhang *et al*., 2014; Shafian and Maas, 2015) rely on the physical process of evaporative cooling for their determination. For example, a water-stressed plant will transpire less (and be warmer) than a well-watered plant. Likewise a dry soil will evaporate less than a wet soil. Application of water stress indices to soil moisture estimation assumes soil moisture in the rooting zone and at the surface, rather than evaporative demand of the atmosphere (vapor pressure deficit), to be primary drivers of ET rate.

In agricultural watersheds, and especially in dryland cropping systems, availability of water within the root zone is a dominant control on crop growth and yield. Both vertical fluxes of water (precipitation, deep percolation, evapotranspiration) and lateral fluxes of water (subsurface flow, runoff), together with soil properties (wilting point and field capacity), determine the stored plant available water (PAW). There is a great need for hydrologic models that can simulate both surface runoff generation as well as the spatio-temporal variation of soil moisture at the precision management scale (a few meters) (Lake *et al*., 1997; Taylor *et al*., 2009).

1.4. Regional Site Description

The Columbia Plateau in Washington, Idaho, and Oregon is covered in loess ranging from a few meters to 75 m in thickness. The deepest deposits form a region of land in eastern Washington known as "The Palouse" (Busacca, 1989). These deep eolian loess hills have provided a fertile bed for

cultivating the soft white winter wheat for which the region is famous (Washington Wheat Commission, 2009). Palouse loess was blown in by south-westerly winds, with coarser grains settling in the west, closer to the sediment source (Busacca and McDonald, 1994). Moving east into northern Idaho, the loess cover gradually thins until little-to-no unweathered loess remains above the uppermost paleosol (buried soil), which is expressed as either an argillic (Bt) or fragipan (Btx) horizon (Busacca, 1989).

The Palouse region has a Mediterranean-like moisture regime characterized by cool, moist winters and warm, dry summers (Soil Survey Staff, 2006). Approximately 60% of precipitation occurs from November to March (Kaiser, 1967). Within the Palouse region there is a discernable east-west climate gradient reflected in mean annual precipitation, mean annual temperature, and elevation. Regional soil diversity in the Palouse reflects these climatic differences. Soils in the intermediate precipitation (450-700 mm) and high (>700 mm) annual precipitation zones show visible signs of clay eluviation with subsequent illuviation in argillic and fragipan layers. These hydraulically restrictive horizons support perched water tables (PWTs) during the wet season. When water perches on sloping land, the resulting lateral water movement is often significant (Reuter *et al*., 1998; Brooks *et al*., 2004; McDaniel *et al*., 2001, 2008). Soils to the west, in the low precipitation zone (< 450 mm), are less developed in terms of clay illuviation and generally have deeper topsoil horizons. As a result, PWTs develop much less frequently in the western parts of the Palouse region (Brooks *et al*., 2012).

Wind and topography drive effective precipitation patterns at the hillslope scale. Effective precipitation is defined as the difference between precipitation and ET and is greatest on northeast-facing slopes where snowdrifts tend to accumulate (Brooks *et al*., 2012). Southwest-facing slopes are drier by comparison, accumulating less snow and receiving more direct sunlight to drive soil evaporation (Rockie, 1951). Differences in moisture have resulted in more advanced erosion on the wetter northeast-facing slopes and the typical Palouse hillslope profile in which the land slopes more steeply (30-55%) on the northeast-facing side (Rockie, 1951).

While erosion is a natural process that has shaped the Palouse landscape over eons, cultural practices have greatly accelerated the rate of topsoil erosion (Frazier *et al*., 1983; McCool *et al*., 2001). It has been estimated that erosion, which has primarily been associated with winter wheat production, has resulted in the loss of approximately that 40% of the fertile Palouse topsoil (Pimentel *et al*., 1995). Recognition of this problem has resulted in widespread adoption of agricultural Best Management Practices (BMPs) to control erosion and prevent further degradation of soil fertility (Brooks *et al.*, 2010). According to a 1998 USGS report, the BMPs leading to the greatest reduction in

erosion within the Palouse River Basin have been planting shrubs and trees, no-till seeding, and conservation tillage (Ebbert and Roe, 1998). Kok *et al.* (2009) estimated that wide implementation of conservation technologies and farming systems in the Pacific Northwest dryland cropping region slowed topsoil loss from a rate of 45 Mg ha^{-1} yr^{-1} in 1975 to 11 Mg ha^{-1} yr^{-1} in 2005.

1.5. Summary

The productivity of existing farmland will need to increase greatly in order to meet the nutritional needs of a rapidly growing global population. Increased food production must not come at the expense of sustainable use of soil and water resources. The duality of this goal has been the impetus behind the conservation farming movement, and of equal importance, the growth of PA. Precision technologies, including proximal and remote sensing, provide growers with data they need to make better field-scale management decisions. Hydrologic models capable of simulating dominant hydrologic processes operating in a landscape have potential for predicting patterns of PAW and crop water stress and might therefore be useful for evaluating management strategies. New sensor technologies and improved hydrologic models can be of great benefit to site-specific management activities from zone mapping, to yield forecasting, to water quality risk assessment. Cropping systems of the Palouse region have an opportunity to embrace PA in a way that is well suited to the unique landscape, climate, and soil morphology of the region. By doing so, the Palouse can maintain its standing among world leaders in wheat production.

2. MOTIVATION STATEMENTS AND THESIS OUTLINE

1. Site-specific farm management strategies need to be developed for the Palouse dryland cropping region based upon a sound understanding of the linkage between landscape hydrologic processes, soils, topography, and climate.

2. There is a need for tools and technologies that enable reliable prediction of water availability at any point within a field.

Chapter two of this thesis uses extensive field measurements to explore variability in cropping patterns (crop type, crop growth, and crop development) observed with 5 m resolution RapidEye™ satellite imagery. This study is exploratory in nature and is aimed at identifying soil attributes, either directly measured or derived from the observed data, having a statistically significant correlation with spectral vegetation indices (VIs). Key drivers of crop response (growth, development, and yield) related to topography, soil, and water are investigated at four agricultural fields that are managed with no-till or minimal-tillage and are located across the Palouse soil-climate gradient. Key attributes are compared and contrasted by climate sub-region.

In chapter three, a modified version of the SMR landscape hydrology model is assessed at the same field sites as are explored in chapter two. The modified version of the model simulates changes in PAW within a dynamic root zone throughout the growing season. The model simulates formation of a perched water table above a restricting layer, subsurface lateral flow, and saturation excess runoff. Chapter four opens with an integrated discussion on implications of this work for site-specific field management in the Palouse region and ends with a summary of key findings.

3. REFERENCES

Adamchuk VI, Hummel JW, Morgan MT, Upadhyaya SK. 2004. On-the-go soil sensors for precision agriculture. *Computers and Electronics in Agriculture* **44**: 71-91. DOI: 10.1016/j.compag.2004.03.002

Allred BJ, Ehsani MR, Saraswat D. 2005. The impact of temperature and shallow hydrologic conditions on the magnitude and spatial pattern consistency of electromagnetic induction measured soil electrical conductivity. *Transactions of the American Society of Agricultural Engineers* **48**(6): 2123-2135.

Barnes EM, Clarke TR, Richards SE, Colaizzi PD, Haberland J, Kostrzewski M, Waller P, Choi C, Riley E, Thompson T, Lascano RJ, Li H, Moran MS. 2000. Coincident detection of crop water stress, nitrogen status and canopy density using ground-based multispectral data. In *Proceedings of the Fifth International Conference on Precision Agriculture, Bloomington, Minnesota, USA, 16-10 July, 2000*, Robert PC, Rust RH, Larson WE (eds). American Society of Agronomy: Madison, WI; 1-15.

Ben-Dor E, Heller D, Chudnovsky A. 2008. A novel method of classifying soil profiles in the field using optical means. *Soil Science Society of America Journal* **72**(4): 1113-1123. DOI: 10.2136/sssaj2006.0059

Brooks ES, Boll J, McDaniel PA. 2012. (Chapter 10) Hydropedology in seasonally dry landscapes: the Palouse region of the Pacific Northwest, USA. In *Hydropedology: Synergistic Integration of Soil Science and Hydrology*, Lin H (ed). Academic Press: Elesevier B.V.; 329-350.

Busacca AJ. 1989. Long quaternary record in eastern Washington, U.S.A., interpreted from multiple buried paleosols in loess. *Geoderma* **45**(2): 105–122. DOI: 10.1016/0016-7061(89)90045-1

Busacca AJ, McDonald EV. 1994. Regional sedimentation of late Quaternary loess on the Columbia Plateau: sediment source areas and loess distribution patterns. In *Regional Geology of Washington State*, Lasmanis R, Cheney ES (eds). *Washington Division of Geology and Earth Resources Bulletin* **80**: 181-190.

Carlson TN, Gillies RR, Schmugge TJ. 1995. An interpretation of methodologies for indirect measurement of soil water content. *Agricultural and Forest Meteorology* **77**: 191-205. DOI: 10.1016/0168-1923(95)02261-U

Christy CD. 2008. Real-time measurement of soil attributes using on-the-go near infrared reflectance spectroscopy. *Computers and Electronics in Agriculture* **61**: 10-19. DOI: 10.1016/j.compag.2007.02.010

Clarke TR. 1997. An empirical approach for detecting crop water stress using multispectral airborne sensors. *HortTechnology* **7**(1): 9-16.

Corwin DL, Lesch SM. 2003. Application of soil electrical conductivity to precision agriculture: theory, principle, and guidelines. *Agronomy Journal* **95**(3): 455-471. DOI: 10.2134/agronj2003.4550

Daughtry CST, Walthall CL, Kim MS, Brown de Colstoun E, McMurtrey III JE. 2000. Estimating corn leaf chlorophyll concentration from leaf and canopy reflectance. *Remote Sensing of Environment* **74**(2): 229-239. DOI: 10.1016/S0034-4257(00)00113-9

Dobermann A, Blackmore S, Cook SE, Adamchuk VI. 2004. Precision farming: challenges and future directions. In *Proceedings of the 4th International Crop Science Congress, 26 Sep—1 Oct 2004, Brisbane, Australia* [online]. Accessed December 12, 2015 at www.cropscience.org.au.

Domsch H, Ehlert D, Giebel A, Witzke K, Boess J. 2006. Evaluation of the soil penetration resistance along a transect to determine loosening depth. *Precision Agriculture* **7**: 309-326. DOI: 10.1007/s11119-006-9009-6

Doolittle JA, Brevik EC. 2014. The use of electromagnetic induction techniques in soil studies. *Geoderma* **223-225**: 33-45. DOI: 10.1016/j.geoderma.2014.01.027

Ebbert JC, Roe RD. 1998. Soil erosion in the Palouse River Bain: Indications of improvement, Fact Sheet FS-069-98, U.S. Geological Survey. Accessed December 12, 2015 at http://wa.water.usgs.gov/pubs/fs/fs069-98/.

Eitel JUH, Vierling LA, Litvak ME, Long DS, Schulthess U, Ager AA, Krofcheck DJ, Stoscheck L. 2011. Broadband, red-edge information from satellites improves early stress detection in a New Mexico conifer woodland. *Remote Sensing of Environment* **115**(12): 3640-3646. DIO: 10.1016/j.rse.2011.09.002

Food and Agriculture Organization. 1996. Lessons from the green revolution: toward a new green revolution. In *World Food Summit, 13-17 November, Rome, Italy* [online]. Food and Agriculture Organization of the United Nations. Accessed December 12, 2015 at http://www.fao.org/docrep/003/w2612e/w2612e06a.htm.

Food and Agriculture Organization. 2009. Global agriculture toward 2050. In *How to Feed the World in 2050: High-Level Expert Forum, 12-13 October 2009, Rome, Italy* [online]. Food and Agriculture Organization of the United Nations. Accessed December 12, 2015 at http://www.fao.org/fileadmin/templates/wsfs/docs/Issues_papers/HLEF2050_ Global_ Agriculture.pdf.

Forster P, Ramaswamy V, Artaxo P, Berntsen T, Betts R, Fahey DW, Haywood J, Lean J, Lowe DC, Myhre G, Nganga J, Prinn R, Raga G, Schultz M, Van Dorland R. 2007. (Chapter 2) Changes in atmospheric constituents and in radiative forcing. In *Climate Change 2007: The Physical Science Basis*, Solomon S, Qin D, Manning M, Chen Z, Marquis M, Averyt KB, Tignor M, Miller HL (eds). Cambridge University Press: Cambridge, United Kingdom; 129-234.

Frazier BE, McCool DK, Engle CF. 1983. Soil erosion in the Palouse: an aerial perspective. *Journal of Soil and Water Conservation* **38**(2): 70-74.

Gillies RR, Carlson TN, Cui J, Kustas WP, Humes KS. 1997. A verification of the `triangle' method for obtaining surface soil water content and energy fluxes from remote measurements of the Normalized Difference Vegetation Index (NDVI) and surface radiant temperature. *International Journal of Remote Sensing* **18**(15): 3145-3166.

Haboudane D, Miller JR, Tremblay N, Zarco-Tejada PJ, Dextraze L. 2002. Integrated narrow-band vegetation indices for prediction of crop chlorophyll content for application to precision agriculture. *Remote Sensing of Environment* **81**(2-3): 416-426. DOI: 10.1016/S0034-4257(02)00018-4

Huete AR. 1988. A soil-adjusted vegetation index (SAVI). *Remote Sensing of Environment* **25**(3): 295-309. DOI: 10.1016/0034-4257(88)90106-X

Idso SB, Ehrler WL. 1976. Estimating soil moisture in the root zone of crops: a technique adaptable to remote sensing. *Geophysical Research Letters* **3**(1): 23-25. DOI: 10.1029/GL003i001p00023

Idso SB, Jackson RD, Pinter Jr. PJ, Reginato RJ, Hatfield JL. 1981. Normalizing the stress-degree-day parameter for environmental variability. *Agricultural Meteorology* **24**(1): 45-55. DOI: 10.1016/0002-1571(81)90032-7

Jackson RD, Idso SB, Reginato RJ, Pinter Jr. PJ. 1981. Canopy temperature as a crop water stress indicator. *Water Resources Research* **17**(4): 1133-1138. DOI: 10.1029/WR017i004p01133

Jordan CF. 1969. Derivation of leaf-area index from quality of light on the forest floor. *Ecology* **50**(4): 663-666. DOI: 10.2307/1936256

Kachanoski RG, Gregorich EG, Van Wesenbeeck IJ. 1988. Estimating spatial variations of soil water content using noncontacting electromagnetic inductive methods. *Canadian Journal of Soil Science* **68**: 715-722. DOI: 10.4141/cjss88-069

Kaiser VG. 1967. Soil erosion and wheat yields in Whitman County, Washington. *Northwest Science* **41**(2): 86-91.

Kitchen NR, Sudduth KA, Drummond ST. 1999. Soil electrical conductivity as a crop productivity measure for claypan soils. *Journal of Production Agriculture* **12**(4): 607-617.

Knadel M, Thomsen A, Schelde K, Greve MH. 2015. Soil organic carbon and particle sizes mapping using vis-NIR, EC and temperature mobile sensor platform. *Computers and Electronics in Agriculture* **114**: 134-144. DOI: 10.1016/j.compag.2015.03.013

Korsaeth A, Riley H, Kvaerno SH, Vestgarden LS. 2008. Relations between a commercial soil survey map based on apparent electrical conductivity (ECa) and measured soil properties on a moronic soil in southeast Norway. In *Handbook of Agricultural Geophysics*, Allred BJ, Daniels JJ, Ehsani MR (eds). CRC Press, Taylor and Francis Group: Boca Raton, Florida; 225-231.

Lake JV, Bock GR, Goode JA (eds). 1997. *Precision Agriculture: Spatial and Temporal Variability of Environmental Quality, No. 210* [ebook]. CIBA Foundation Symposium; 18-30.

Maleki MR, Mouazen AM, Ramon H, De Baerdemaeker J. 2007. Optimisation of soil VIS-NIR sensor-based variable rate application system of soil phosphorus. *Soil & Tillage Research* **94**: 239-250. DOI: 10.1016/j.still.2006.07.016

McBride RA, Gordon AM, Shrive SC. 1990. Estimating forest soil quality from terrain measurements of apparent electrical conductivity. *Soil Science Society of America Journal* **54**(1): 290-293. DOI: 10.2136/sssaj1990.03615995005400010047x

McCool DK, Huggins DR, Saxton KE, Kennedy AC. 2001. Factors affecting agricultural sustainability in the Pacific Northwest, USA: an overview. In *Sustaining the Global Farm--Selected papers from the 10th International Soil Conservation Organization Meeting, May 24-29, 1999, West Lafayette, IN*, Stott DE, Mohtar RH, Steinhardt GC (eds). International Soil Conservation Organization in cooperation with the USDA and Purdue University, West Lafayette, IN; 255-260. Accessed December 13, 2015 at http://topsoil.nserl.purdue.edu/nserlweb-old/isco99/pdf/ISCOdisc/SustainingTheGlobalFarm/P222-McCool.pdf.

McDaniel PA, Gabehart RW, Falen AL, Hammel JE, Reuter RJ. 2001. Perched water tables on Argixeroll and Fragixeralf hillslopes. *Soil Science Society of America Journal* **65**: 805-810.

McDaniel PA, Regan MP, Brooks E, Boll J, Barndt S, Falen A, Young SK, Hammel JE. 2008. Linking fragipans, perched water tables, and catchment-scale hydrological processes. *Catena* **73**: 166-173. DOI: 10.1016/j.catena.2007.05.011

Moran MS, Clarke TR, Inoue Y, Vidal A. 1994. Estimating crop water deficit using the relation between surface-air temperature and spectral vegetation index. *Remote Sensing of Environment* **49**(3): 246-263. DOI: 10.1016/0034-4257(94)90020-5

Moran MS, Inoue Y, Barnes EM. 1997. Opportunities and limitations for image-based remote sensing in precision crop management. *Remote Sensing of Environment* **61**(3): 319-346. DOI: 10.1016/S0034-4257(97)00045-X

Mouazen AM, Maleki MR, De Baerdemaeker J, Ramon H. 2007. On-line measurement of some selected soil properties using a VIS-NIR sensor. *Soil & Tillage Research* **93**: 13-27. DOI: 10.1016/j.still.2006.03.009

Ongley ED. 1996. FAO irrigation and drainage paper 55: Control of water pollution from agriculture, 111pp. Food and Agriculture Organization of the United Nations. Accessed December 12, 2015 at ftp://ftp.fao.org/agl/aglw/docs/idp55e.pdf.

Pimentel D, Harvey C, Resosudarmo P, Sinclair K, Kurz D, McNair M, Crist S, Shpritz L, Fitton L, Saffouri R, Blair R. 1995. Environmental and economic costs of soil erosion and conservation benefits. *Science* **267**(5201): 1117-1123.

Pingali PL. 2012. Green revolution: Impacts, limits, and the path ahead. In *Proceedings of the National Academy of the Sciences of the U.S.A. Journal* **109**(31): 12302-12308.

Pingali PL, Raney T. 2005. From the green revolution to the gene revolution: How will the poor fair?, ESA Working Paper No. 05-09, 17pp. Food and Agriculture Organization of the United Nations. Accessed December 12, 2005 at http://www.fao.org/3/a-af276t.pdf.

Poggio M, Brown DJ, Bricklemeyer RS. 2015. Laboratory-based evaluation of optical performance for a new soil penetrometer visible and near-infrared (VisNIR) foreoptic. *Computers and Electronics in Agriculture* **115**: 12-20. DOI: 10.1016/j.compag.2015.05.002

Reuter RJ, McDaniel PA, Hammel JE, Falen AL. 1998. Solute transport in seasonal perched water tables in loess-derived soilscapes. *Soil Science Society of America Journal* **63**: 977–983.

Rockie WA. 1951. Snowdrift erosion in the Palouse. *Geographical Review* **41**: 34-48.

Rodriguez D, Fitzgerald GJ, Belford R, Christensen LK. 2006. Detection of nitrogen deficiency in wheat from spectral reflectance indices and basic crop eco-physiological concepts. *Australian Journal of Agricultural Research* **57**: 781-789. DOI: 10.1071/AR05361

Rouse Jr. JW, Haas RH, Schell JA, Deering DW. 1973. Monitoring vegetation systems in the Great Plains with ERTS. In *Proceedings of the Third ERTS Symposium, Washington, DC, 10-14 December 1972*, NASA SP-351. National Aeronautics and Space Administration: Washington, DC; 309-317.

Sandholt I, Rasmussen K, Andersen J. 2002. A simple interpretation of the surface temperature/vegetation index space for assessment of surface moisture status. *Remote Sensing of Environment* **79**(2-3): 213-224. DOI: 10.1016/S0034-4257(01)00274-7

Seelan SK, Laguette S, Casady GM, Seielstad GA. 2003. Remote sensing applications for precision agriculture: a learning community approach. *Remote Sensing of Environment* 88(1-2): 157-169. DOI: 10.1016/j.rse.2003.04.007

Shafian S, Maas SJ. 2015. Index of soil moisture using raw Landsat image digital count data in Texas High Plains. *Remote Sensing* **7**: 2352-2372. DOI: 10.3390/rs70302352

Soil Survey Staff. 2006. *Keys to Soil Taxonomy, Tenth Edition*. U.S. Department of Agriculture-Natural Resources Conservation Service, Washington, DC.

Taylor JA, Tisseyre B, Acevedo-Opazo C, Lagacherie P. 2009. Field-scale model of the spatio-temporal vine water status in a viticulture system. In *Precision Agriculture '09*, Van Henton EJ, Goense D, Lokhorst C (eds). Wageningen Academic Publishers: The Netherlands; 537-550.

Tekin Y, Kul B, Okursoy R. 2008. Sensing and 3D mapping of soil compaction. *Sensors* **8**(5): 3447-3459. DOI: 10.3390/s8053447

Triantafilis J, Lesch SM. 2005. Mapping clay content variation using electromagnetic induction techniques. *Computers and Electronics in Agriculture* **46**: 203-237. DOI: 0.1016/j.compag.2004.11.006.

Tucker CJ. 1978. Red and photographic infrared linear combinations for monitoring vegetation, Technical Memorandum 79620, 34pp. National Aeronautics and Space Administration--Goddard Space Flight Center: Greenbelt, MD.

Viscarra Rossel RA, Adamchuk VI, Sudduth KA, McKenzie NJ, Lobsey C. 2011. (Chapter 5) Proximal soil sensing: an effective approach for soil measurements in space and time. In *Advances in Agronomy, Vol. 113, 1-359,* Sparks DL (ed). Academic Press: San Diego, CA and Waltham, MA; 238-282.

Washington Wheat Commission. 2009. Washington wheat facts 2008-2009. Washington Wheat Commission. Accessed December 12, 2015 at http://admin.aghost.net/images/E0177801/2008WF4WebSmHomepage.pdf.

Zhang D, Tang R, Zhao W, Tang B, Wu H, Shao K, Zhao-Lang L. 2014. Surface soil water content estimation from thermal remote sensing based on the temporal variation of land surface temperature. *Remote Sensing* **6**(4): 3170-3187. DOI: 10.3390/rs6043170

CHAPTER 2: AN EVALUATION OF CROPPING PATTERNS RECORDED BY RAPIDEYE™ SATELLITE IMAGERY IN A DRYLAND GRAIN PRODUCTION REGION

1. INTRODUCTION

1.1. Background

It is a maxim of site-specific management that all areas of a field do not produce equal crop. It is also commonly understood by growers and consultants alike that much of the yield variability can be attributed to spatially-variable soil properties. However, obtaining sufficient data to appropriately represent heterogeneous soils in a farmed landscape is both labor intensive and costly (Sadler *et al.*, 1997). As a result, there has been considerable interest since the 1990's in developing methods that use easily-measured ancillary variables to spatially interpolate primary soil properties (Zhang *et al*., 1992; Wilcox *et al*., 1994; Lopez-Grenados *et al*., 2002, 2005). Common sources of ancillary data include electromagnetic induction surveys (Sudduth *et al*., 2005), digital elevation models (Moore *et al*., 1993), visible and near-infrared (VNIR) spectroscopy (Stoner and Baumgardner, 1981), and remote sensing (Ben-Dor, 2002).

Efforts to date have focused on both hyperspectral (Dematte *et al*., 2001; Gomez *et al*., 2008; Jaber *et al*., 2011; Dutta *et al*., 2015) and multispectral remote sensing (Dematte *et al*., 2004, 2005; Sullivan *et al*., 2005; Ahmed and Iqbal, 2014; Ballabio *et al*., 2014) for soil classification and mapping of soil properties based on soil reflectance. Examples of soil properties that have been mapped with remote sensing (RS) instruments include soil organic carbon (Chen *et al*., 2000; Chang and Laird, 2002; Jaber *et al*., 2011), soil salinity (Eldeiry and Garcia, 2010; Allbed *et al*., 2014), soil texture (Barnes and Baker, 2000; Liao *et al*., 2013; Ahmed and Iqbal, 2014), and cation exchange capacity (Bishop and McBratney, 2001). These studies have regarded reflectance by vegetation as a source of noise that obscures the soil signal and that should be removed if possible. However, remote sensing of the crop canopy can reveal information about the underlying soil, which supplies vital nutrients and water for plant growth.

Important opportunities have arisen for field-scale agricultural management as a result of advances made within the last decade in multispectral imaging from satellite platforms. Since 2008, the RapidEye™ constellation of five identical satellites has been capable of providing images at 6.5 m resolution (re-sampled to 5m pixels after orthorectification) with repeat coverage every 5.5 days (BlackBridge, 2012). RapidEye™ sensors detect light in five bands from the visible to near-infrared, including the red-edge. More recently in 2014, the WorldView-3 satellite was launched with on-board sensors measuring reflectance in wavebands at even higher spatial (1.24 m) resolution and

temporal (4.5 d repeat coverage) frequency (Satellite Imaging Corporation, Tomball, TX). Satellite data are frequently used to calculate indices of crop greenness, biomass, LAI, land cover, and various biochemical properties of the canopy. The physical basis for these spectral vegetation indices (VIs) are well established, with reviews by Bauer *et al*. (1986) and Pinter *et al*. (2003) relating in particular to management of agricultural crops. The most commonly used VI for a wide variety of applications has been the Normalized Difference Vegetation Index (NDVI). It is an established indicator of plant biomass, leaf area index (LAI), and fractional vegetation cover (Rouse *et al*., 1974; Tucker, 1979; Carlson and Ripley, 1997), and has been used for decades to predict crop yields (e.g. Tucker 1980; Aase and Siddoway, 1981; Rasmussen, 1992; Raun *et al.*, 2001; Sultana *et al*., 2014).

Work by Carter (1993, 1994) has demonstrated the special importance of the absorption band near 700 nm for detection of environmental stressors (dehydration, nutrient deficiency, and extreme temperatures, among others) in many plant species. A distinct feature of the light absorption spectrum of green vegetation is the region of transition from high absorption in the far-red (680-700 nm) by chlorophyll to high reflectance (low absorption) in the near-infrared (725-760 nm) (Cho and Skidmore, 2006). This region, from 700 to 725 nm is known as the red-edge (Clevers *et al*., 2000). It has been shown in numerous studies that light absorption in red-edge wavelengths is highly correlated with leaf chlorophyll and foliar leaf N (Horler *et al*., 1983; Carter and Knapp, 2001; Cho and Skidmore, 2006). The availability of a red-edge band sets RapidEye™ apart from most other broadband multispectral imagers and provides unique opportunities for regional mapping of crop nitrogen (N). For example, Perry *et al*. (2012) demonstrated how the Canopy Nitrogen Index (CNI), calculated using only the red-edge and red bands of RapidEye™ could be combined with measurements of dry biomass to predict plant N at the paddock scale. In another study, Ramoelo *et al*. (2012) used multiple regression with altitude and the NIR-to-red ratio (R_{NIR}/R_{RED}) of RapidEye™ as covariates to predict canopy N of Savannah grass.

The process by which leaves change color from green, to yellow, to brown is called senescence. Leaf senescence is regulated by environmental stressors such as extremes of temperature, water shortage, and nutrient deficiency, as well as by internal factors like age and reproductive development (Gan and Amasino, 1997). Environmental regulators can induce senescence prematurely, which often depresses crop yields. A common approach to detection of water stress with RS has been multi-sensor imaging in which fractional vegetation cover from a VI is combined with thermal detection of land surface temperature in order to draw inferences about evapotranspiration (ET) rates of different soil-crop combinations (Carlson *et al*., 1995; Gillies *et al*.,

1997). For example, the crop water stress index (CWSI) determines water stress based on the surface-air temperature difference for a given percent cover (Moran *et al*., 1994). Sandholt *et al*. (2002) developed an empirical simplification of the CWSI, called the temperature dryness vegetation index, which requires measurement of a VI and radiant surface temperature only. In a separate approach, Temimi *et al*. (2010) combined terrain attributes with remote sensing data to define a modified topography-based wetness index, which emphasizes the close interrelationship between vegetation, topography, and soil moisture patterns.

Attempts have also been made to predict soil moisture from VIs directly. Adegoke and Carleton (2002) compared surface soil moisture with NDVI calculated from bands of the Advanced Very High Resolution Radiometer (AVHRR) satellite. They found concurrent correlations were weak between growing season NDVI and soil moisture in the top 30 cm. Much higher correlations were found when soil moisture lagged NDVI by up to eight weeks. A separate study found NDVI was best correlated with root zone soil moisture 5-10 days prior (Schnur *et al*., 2010). Engstrom *et al*. (2008) compared data obtained by the Airborne Data Acquisition and Registration (ADAR) imaging system to ground-based soil moisture sensors in the Barrow Peninsula of Alaska. They noted areas having a substantial small-scale variation in topography were much more likely to show a significant relationship between NDVI and soil moisture.

The Palouse region of eastern Washington and northern Idaho is well known for its undulating landscape and high dryland wheat yields. The region has a seasonally dry climate in which ~60% of precipitation is received November through March (Kaiser, 1967). Local topography induces microclimates with unique patterns of wind, snowmelt, and sunlight exposure (Brooks *et al*., 2012). Soils also follow trends in topography such that distinct crop growth and yield patterns emerge at the field scale (see Figure 1). Multiple studies in the region have related wheat yield to terrain attributes (Ciha, 1984; Mulla *et al*., 1992; Fiez *et al*., 1994; Yang *et al.*, 1998) and have found significant effects of nitrogen fertilizer and growing season precipitation on yield. Their results have served to illustrate the high level of system complexity and yield uncertainty Palouse growers must manage.

1.2. Purpose and Objectives

This study assesses the key soil properties driving cropping patterns (crop type, crop growth, and crop development) observed with broadband VIs calculated from RapidEye™ satellite imagery. The study focuses on four agricultural fields located within the continuous dryland cereal production region of the Inland Pacific Northwest. RapidEye™ imagery is presented here primarily as a means of exploring the available field measurement and imagery datasets with the intention of determining

which of the available field data contribute most to a visible crop response. While it is not the goal of this particular study to build predictive models, it is hoped that results from this paper could be used to inform a more rigorous statistical analysis.

The objectives of the study were to: 1) identify statistically significant linear relationships between various soil measurements and broadband VIs derived from RapidEye^{TM} satellite imagery and 2) compare these relationships at fields located in the Palouse dryland cropping region that are distinct in terms of their precipitation, topography, and soils.

2. METHODS

2.1. Site Description

Data were collected in cooperation with growers at four fields located in eastern Washington and north Idaho as shown in Figure 2. Mean annual precipitation (MAP) ranges from 480 mm at the field located farthest west in Whitman County, near the town of Colfax, WA, to 720 mm at the field located farthest east in Latah County, just outside the town of Leland, ID. The remaining fields are located approximately 15 km southeast of Genesee, ID and 8 km south of Troy, ID where the MAP is 570 mm and 680 mm, respectively. The fields are aliased by nearest town, such that "Colfax" means the field near Colfax and likewise for the remaining sites. Colfax and Genesee fields have the most extreme topographies with maximum slopes of 45% and 36%, respectively, while the maximum slope at Troy is 32% and at Leland it is 18%.

Soil differences across the study area are driven by east-west gradients of temperature, elevation, and rainfall. The western-most field is located in a warmer, drier sub-region with soils of low clay content and deep topsoil relative to soils typically found farther east, where the climate is cooler and wetter. A key feature of soils in the intermediate (450-700 mm) and high (>700 mm) annual precipitation sub-regions of the Palouse is the presence of clay-rich, high bulk density (~1.65 g cm^{-3}) restrictive soil horizons (Brooks *et al.*, 2012). These argillic or fragipan horizons have low water permeability and impede root growth (Kramer and Boyer, 1995).

According to Soil Survey Geographic (SSURGO) data acquired for the four study areas, the Colfax field is composed of a single soil type, Palouse silt loam (fine-silty, mixed, mexic Pachic Ultic Haploxerolls), while the Genesee field is composed of a mixture of Palouse and Naff (fine-silty, mixed, mesic Ultic Argixerolls) silt loams. Major soils of the Troy field are Larkin silt loam (fine-silty, mixed, mesic Ultic Argixerolls), and Southwick silt loam (fine-silty, mixed mesic Boralfic Argixerolls). A Driscoll-Larkin complex and Latahco-Thatuna complex comprise the remaining field area of the Troy site. The Leland site is 100% Southwick silt loam by area (Soil Survey Staff). Both Troy and Leland

fields contain strong argillic horizons by virtue of the Southwick silt loam, resulting in seasonal formation of perched water tables (PWTs). These argillic horizons occur often within the first meter of soil and result in a typical profile in which both clay content and bulk density increase over a short vertical distance (Soil Survey Staff, 1999). Colfax and Genesee soils are deep by comparison; however, at Genesee the subsoil is a silty clay loam with moderate restricting properties that cause perched water to form in a few places.

2.2. Vegetation Indices Derived from RapidEye™ Satellite Imagery

Images were acquired at all four fields during the 2012-2014 growing seasons from the distributor, BlackBridge (BlackBridge, Berlin, Germany). The level 3A imagery product is delivered already orthorectified with sensor calibration, geometric, and terrain corrections. Post-processing of the data included atmospheric correction with the 6S radiative transfer model (Kotchenova *et al*., 2006; Kotchenova and Vermote, 2007), run as a module within the open-source geospatial analysis software GRASS, version 6.3 (GRASS Development Team, 2012). Inputs to the model were aerosol optical depth at 550 nm using data from the station in Rimrock, ID (46.49°N, 116.99°W) (Aerosol Robotic Network), spectral conditions given by waveband-specific filter functions (BlackBridge, 2012), and homogenous surface ground reflectance with no directional effect.

The RapidEye™ sensor collects data in five spectral bands: blue (440-510 nm), green (520-590 nm), red (630-685 nm), red-edge (690-730 nm), and near-infrared (760-850 nm). Four commonly-used VIs and two combined VIs were compared in this study for their strength of association with ground-based measurements obtained by manual soil sampling and from proximal soil sensors. These VIs, their equations, and corresponding references are provided in Table I. The red-edge band of RapidEye™ is featured in both the normalized difference red-edge (NDRE) (Barnes *et al.*, 2000) and modified chlorophyll in absorption (MCARI) (Daughtry *et al.*, 2000) indices. An advantage to these indices is that they are sensitive to chlorophyll over a wider range of chlorophyll contents than the more traditional near-infrared (NIR) and red band indices like NDVI (Gamon *et al.*, 1995; Mutanga and Skidmore, 2004; Eitel *et al.*, 2011).

Since agricultural fields are composed of both soil and vegetation, the signal received at sensor is responsive to variability in soil background, particularly early in the season when vegetation cover is minimal. Extensive studies of soil spectra have discovered a linear relationship between reflectance in the NIR and visible light regions (e.g. Huete, 1988; Baret and Guyot, 1991; Qi *et al.*, 1994). Rondeaux *et al*. (1996) used this concept to formulate the “optimized” soil-adjusted vegetation index (OSAVI). In addition to NDVI, NDRE, MCARI, and OSAVI, the ratios NDRE/NDVI

(Barnes *et al.*, 2000) and MCARI/OSAVI (Daughtry *et al.*, 2000) were calculated. Work by Rodriguez *et al*. (2006), Fitzgerald *et al.* (2010), and Eitel *et al.* (2009) have all shown that by using combined indices, the confounding influence of soil background can be significantly diminished while retaining high sensitivity to leaf chlorophyll.

The 2013 growing season offered the most complete set of images across all fields and therefore the best opportunity for a regional study of drivers of cropping patterns. In comparison, few images were acquired in 2012, and crop failure occurred at one of the fields in 2014. Crop rotations for 2012-2014 are indicated in Table II alongside the 2013 satellite overpass dates and corresponding stages of crop development. Field-wide averages and coefficient of variation for all six VIs computed for all 2013 RapidEye^{TM} images are provided in Appendix B, Table B-I.

2.3. Dataset Description

Data related to soil, crop, and hydrologic variability were collected in four agricultural fields located in distinct Palouse climate sub-regions as part of the Site-Specific Climate-Friendly Farming project sponsored by the U.S. Department of Agriculture's National Institute of Food and Agriculture. Within each field, measurements were acquired at twelve locations, distributed across different landscape positions. These measurement locations will be referred to hereafter as microsites. The data presented in this study, as well as attributes derived from the data have been divided into three categories as follows: 1) simple, field-measured variables, 2) compound variables, and 3) spatially-continuous variables. The methods for each are discussed below.

2.3a. Simple, Field-Measured Variables

Soil cores for bulk density (BD) measurements were extracted at 30 cm increments down to 150 cm. Dry season bulk density samples were taken following harvest for each of the 2012 and 2013 growing seasons using a 2.7 cm-diameter Giddings probe (Giddings Machine Company, Windsor, CO). Wet season samples were taken Jan/Feb 2014 at two fields (Leland and Troy) and May 2013 at the Genesee field. A lumped, static BD value (g cm^{-3}) was obtained by averaging datasets, excluding observations more than two standard deviations from the mean difference. This averaging and exclusion procedure was used as a means of filtering questionable data. Clay, sand, and silt fractions (% by mass) were determined from soil samples collected fall 2011. Total nitrogen (TN) and total carbon (TC) (% by mass, g C per g dry soil) were determined fall 2011 and fall 2012. Samples were air-dried, ground to 2 mm, and subsequently analyzed using a LECO TruSpec combustion analyzer (LECO Corporation, St. Joseph, MI) for TC and TN concentrations. Although individual measurements were sometimes significantly different with regard to year, the datasets were not significantly different,

and so both TC and TN were treated as static variables. Total inorganic nitrogen (IN), represented as the sum of ammonia and nitrate, was determined once in spring and once post-harvest for each of the 2012-2014 growing seasons. Samples were extracted with 0.1 M KCL solution and subsequently analyzed using a Lachat flow injection analyzer (Lachat Instruments, Milwaukie, WI) for nitrate and ammonia concentrations (mg L^{-1}, mg IN per 0.025 L of extract). These concentrations were subsequently determined on a mass per area basis using known BD (g IN per g dry soil x BD per m).

2.3b. Compound Variables

Available water content AWC (cm cm^{-1}) was calculated from field observations in combination with the pedo-transfer function described by Rawls and Brakensiek (1985). The definition of AWC adopted here is the difference between field capacity θ_{fc} and wilting point θ_{wp} where θ_{fc} and θ_{wp} are the volumetric water contents (cm cm^{-1}) at tensions of 33 kPa and 1500 kPa, respectively. Porosity ϵ was determined from BD, assuming a particle density of 2.65 g cm^{-3} ($\epsilon = 1 - BD/2.65$). Values for θ_{fc} and θ_{wp} were estimated based on the moisture-tension model of Brooks and Corey (1964), reproduced here as Equation (1).

$$\frac{\theta-\theta_{\mathrm{r}}}{\epsilon-\theta_{\mathrm{r}}} = \left(\frac{\psi_{\mathrm{b}}}{\psi}\right)^{\lambda} \quad (1)$$

where ψ_{b}, λ, and θ_{r} are the bubbling pressure, pore size index, and residual moisture content, respectively. These parameters were estimated from clay, sand, and porosity, and using the regression coefficients of Rawls and Brakensiek (1985). Re-arranging Equation (1) and setting ψ = 1500 kPa for wilting point and ψ = 33 kPa for field capacity gives:

$$\theta_{\mathrm{wp}} = \theta_{\mathrm{r}} + (\epsilon - \theta_{\mathrm{r}})\left(\frac{\psi_{\mathrm{b}}}{1500}\right)^{\lambda} \quad (2)$$

$$\theta_{\mathrm{fc}} = \theta_{\mathrm{r}} + (\epsilon - \theta_{\mathrm{r}})\left(\frac{\psi_{\mathrm{b}}}{33}\right)^{\lambda} \quad (3)$$

Similarly, total available water TAW is the available water storage capacity of the soil between the soil surface and a root-restricting layer (soil depth). It is the product of soil depth and AWC averaged over that depth. Multiple methods were used to determine soil depth, including approximations from clay content and BD, plots of change in soil moisture with time, and depth to E or Bt horizon. These methods are each discussed below.

Low-permeability argillic horizons are characterized by high BD in combination with high clay content (Soil Survey Staff). Accordingly, minimum cut-off values for BD (1.60-1.70 g cm^{-3}) and for clay (32-37%) were implemented and the depth at which these values were exceeded assumed to be the soil depth to within 30 cm precision. Depth to a restrictive layer was also inferred from high

frequency soil moisture measurements using 5TM/5TE soil moisture sensors (Decagon Devices, Pullman, WA). A sensor reading saturation (near-constant water content) for long periods of time relative to the sensors above it was assumed to be under the influence of a nearby water table. The soil depth was taken as the minimum depth at which these sustained saturation periods were observed. Soil depth and TAW computed from BD only, clay only, BD and clay together, and approximated from the moisture sensors were lumped into a single predictor of soil depth or TAW and are denoted with the $_{AVG.}$ subscript. In argillic soils, the restrictive Bt horizon resides beneath a low-clay E horizon of ~20 cm thickness (Soil Survey Staff, 1999). Three of the four fields have soils with a Bt horizon; however, depth to Bt horizon was recorded at all 12 microsites for only the Leland field, while depth to E rather than Bt horizon was reported consistently at the Troy site. The soils of Colfax field lack a Bt horizon, and at the Genesee field, depth to Bt horizon was reported at only a few microsites where a Bt horizon could be distinguished. A soil depth of 150 cm was assumed at microsites lacking a Bt horizon in order to match the range of soil measurements. The TAW and soil depth determined from observed depth to an E or Bt horizon are subscripted $_{OBS.}$ for this analysis.

2.3c. Spatially-Continuous Variables

The relationships between maps of the topographic wetness index TWI (Beven and Kirkby, 1979; Moore *et al.*, 1991) and VIs and between kriged maps of apparent electrical conductivity (ECa) and VIs were also investigated. Spatially-continuous maps of both TWI and ECa were converted to point data in order to give them the same support (sampling volume) as the other field measurements. This was accomplished by extracting values from a grid map with cells centered on each of the 12 microsites. The TWI uses hillslope attributes computed from a digital elevation model (DEM) in order to predict soil moisture patterns driven by upslope redistribution of water under wet conditions. It is a function of A_S and β where A_S is the upslope area contributing flow through a point per unit length of contour ($m^2\ m^{-1}$) and β is the slope angle: $TWI = ln(A_S/tan\beta)$**.** Elevation data obtained from the U.S. Geological Survey's National Elevation Dataset was input to the Geographic Resources Analysis Support System (GRASS) version 6.3 (GRASS Development Team, 2012) for calculating TWI. Soil ECa ($mS\ m^{-1}$) was measured spring 2012, fall 2013, and spring 2013 using an EM38-MK2 instrument (Geonics Limited, Mississauga, Ontario). The ECa surfaces were created on a 10 m grid using either ordinary kriging or regression kriging.

2.4. Statistical Methods

The term "data", as it is used in this chapter, refers to all categories of data: simple, compound, and spatially-continuous data as a collective while "variable" or "attribute" is used to

indicate a particular measured or computed quantity such as BD or TWI. Variables are divided further by depth (if applicable) and field in which they were measured/calculated. Use of the name RapidEye™ applies generally to any VI computed from any RapidEye™ image, while the term "RapidEye™ image" will be used when we wish to refer to a particular date and a specific field.

The following procedure for identifying significant linear relationships between data and VIs was followed. Variables were paired with VIs for each RapidEye™ image and the sample Pearson product-moment correlation coefficient r calculated for all pairs. For each variable, the highest-correlating RapidEye™ image and VI was selected so long as r was significant at the p=0.05 level, assessed using the t-test for significance with null hypothesis of zero correlation. The best-correlated pairs were subsequently checked for satisfaction of the underlying assumptions of the Pearson correlation, which state that the variables are random, independent, and come from a bivariate normal distribution (Devore, 2008). The normality of each variable and VI was assessed by normal quantile-quantile plotting and the Shapiro-Wilkes test using the statistical open-source software, R, version 3.0.2 (R Core Team, 2013). Regression diagnostics were run using the "stats" package of R, the diagnostics routine of which includes as standard output a plot of residuals vs. fitted values (independence in residuals), a normal quantile-quantile plot (normality of residuals), and a plot of Cook's distance (influence, regression outliers). In the final step, correlations passing diagnostics were tabulated for each field.

3. RESULTS

3.1. Effect of Crop Development Stage, VI, and Aggregation Depth on Correlations

The correlations between field attributes and RapidEye™ were generally more affected by crop growth stage than by the specific index (MCARI, NDRE, etc.). This was due to the dependence of VIs on crop growth stage (see Table B-I of Appendix B) as well as the high degree of correlation among VIs computed for the same image (see Table B-VI of Appendix B). The development-stage effect, though noticeable in all cases, was less pronounced for static soil attributes (e.g. texture and BD) than for dynamic attributes (e.g. IN and GWC). With the exception of the Leland site, for which early season images were not available, relationships between IN and RapidEye™ were strongest early in the season, prior to heading. In contrast, correlations of RapidEye™ with GWC and of RapidEye™ with ECa were greatest for images taken later in the season, during the period from grain-filling through ripening (refer to Table III and Table A-I of Appendix A).

The VI primarily affected correlations with IN and ECa. With the exception of Colfax and to some extent Genesee, VIs featuring the red-edge band (MCARI and NDRE) were generally better

correlated than NDVI and OSAVI with IN. The combined indices NDRE/NDVI and MCARI/OSAVI typically were better correlated with ECa than the single indices. The effect of aggregation depth was also considered, but no general trends could be deduced, as these were highly dependent on crop development stage.

3.2. Regional Trends in Top Correlations

A complete list of the best correlations between field attributes and RapidEye™ can be viewed in Appendix A, Table A-I. Correlation matrices for these variables are provided in Tables B-II through B-V of Appendix B . Table III is an abbreviated form of Table A-I in which variables are only included if they are not correlated at the p=0.01 significance level. The highest correlations between RapidEye™ and TC were observed at Colfax between 8 July $NDRE$ and 0-60 cm TC (r=0.92, N=12, p<0.001) and at Genesee between 15 July $NDRE$ and 0-120 cm TC (r=0.83, N=12, p<0.001). In contrast, TC was not significantly correlated with RapidEye™ at either of the Troy or Leland sites. Field measurements indicate that the subsoil (below 30 cm) TC is more variable at the Colfax and Genesee fields than at either of the Leland or Troy fields (Appendix A, Figure A-3). Furthermore, the correlations between TC and RapidEye™ at Colfax and Genesee were significant regardless of image date or aggregation depth (see Appendix A, Table A-II).

Yield was significantly correlated with RapidEye™ at all fields except for Leland, with the strongest relationship occurring at Colfax between 8 July $OSAVI$ and $Yield$ (r=0.94, N=12, p<0.001). A significant, negative relationship was detected between clay content and RapidEye™ at all fields except for Colfax. The best correlation was observed at Genesee between 15 July $NDVI$ and 0-30 cm $clay$ (r= -0.89, N=12, p<0.001). The TAW, which combines the effects of soil depth and AWC, was significant at Leland and Troy but not at the other two fields. At Leland the best correlation occurred between 27 June $OSAVI$ and TAW based on depth to Bt horizon, $TAW_{\mathrm{OBS.}}$ (r=0.94, N=12, p<0.001) and at Troy between 16 July $OSAVI$ and TAW determined from BD, clay, and water table measurements, $TAW_{\mathrm{AVG.}}$ (r=0.65, N=12, p=0.022). With the exception of the Troy site, ΔGWC was significantly correlated with RapidEye™ at all fields. The variables: AWC, $IN_{\mathrm{SPR.}}$, and ΔIN were each significantly correlated with RapidEye™ at all four fields. The only field where TWI was significantly correlated with RapidEye™ was at Colfax, using 27 July $OSAVI$ (r=0.79, N=11, p=0.003).

4. DISCUSSION

4.1. Correlations of field measurements with RapidEye™ Imagery: Regional Trends

The crop canopy was least dense at the Colfax field due to a different crop type (spring wheat rather than winter wheat) and perhaps also due to the drier climatic conditions compared

with the other three sites. It has been reported in the literature that indices based on NIR and red wavelengths saturate at high canopy cover (Sellers, 1985; Mutanga and Skidmore, 2004). So, while NDVI saturated at the other three fields with denser canopies, it may not have saturated at the Colfax field. A comparison of LAI by field over the 2013 growing season can be viewed in Appendix A, Table A-III.

The high correlation of TC with RapidEye™ at the Colfax and Genesee fields is likely due to the impact topsoil erosion has had on agricultural productivity in the Palouse. The origin and early history of erosion in the region was described in detail by Horner *et al*. (1944). Kok *et al.* (2009) have reported substantial progress in erosion control over the last four decades as a result of the widespread adoption of conservation tillage practices. Prior to the 1980s, the Colfax field had a history of management under conventional tillage, which leaves little residue cover after planting. Lack of surface residue severely limits water infiltration capacity and exposes soil to raindrop impact. This leads to a condition that is conducive to Hortonian overland (infiltration excess) runoff and the subsequent removal of topsoil. Indeed, the Colfax grower tells stories of witnessing firsthand as a child the devastating effects of tillage and water erosion in the area (Aeschliman, J., personal communication).

Both Colfax and Genesee fields are presently under no-till management, but loss of organic matter (determined as approximately 1.72 x TC%) in years past from ridgetops and summits has made an imprint on the landscape. Figure 3 shows an RGB color composite of the Genesee and Colfax catchments from RapidEye™ satellite imagery, with measured organic matter content in the top 90 cm at the 12 microsites superimposed. It is hypothesized here that SOM is affecting crop growth in the Colfax and Genesee catchments primarily through its effect on PAW. This hypothesis is supported by the work of Hudson (1994) who studied the effects of SOM on soils of different textures and found that in silt loam soils, a 1% by weight increase in SOM resulted in a 3.6% by volume increase in available water. The range of SOM measured at Colfax within the top 60 cm was 1-3%, which converts to ~4.3 cm additional water (2 x 0.036 cm cm^{-1} x 60 cm). The measurable effect on grain yield at Colfax was striking. The two microsites with lowest SOM both had yields ~30 % of the field-wide average of 2890 lb/ac (N=12) (data not shown).

Restrictive soil horizons at Leland and Troy impose a limit on the amount of water available to the crop by restricting crop rooting depth. Additionally, impeded drainage above these clay-rich Bt horizons leads to frequent waterlogging in the spring, mainly in the draws, which deprives young plant roots of oxygen (Gregory, 2006). Waterlogging can lead to yellowing and delayed crop

development (Steffens et al., 2005). Figure 4 shows the effects of waterlogging on winter wheat development at the Troy site.

4.2. Opportunities for RapidEye™ Imagery in Field-Scale Management

Satellite imagery is a potentially useful tool for studying the fine-scale interactions between crops, soil, and water. When combined with additional information from *in-situ* soil and hydrological measurements, it can be used for hypothesis testing as well. The null hypothesis in dryland agriculture is that differences in PAW drive crop response. In this framework, a VI is chosen as the proxy for crop response, while hydrologic modeling provides spatially-continuous predictions of PAW-- the hypothesized driver of the crop response. In those areas of the field where errors were sufficiently large, the null hypothesis would be rejected in favor of an alternative, such as that soil N primarily drives crop response.

In precision agriculture, zone maps generated with the aid of satellite imagery could be designed to capture variability in one or two features of the field (such as SOM or soil depth) that produce a visible crop response. Field management zones based on satellite imagery are much easier to develop in theory and less labor-intensive than those requiring grid-based soil sampling. Furthermore, it is possible to survey large swathes of land with a single image, making transition from field-scale to farm-scale a non-issue, assuming the important soil features are not field-dependent. Images acquired during the growing season could then provide instant feedback on crop performance within the zones established, or they could be used to modify zone boundaries and/or farm practices within existing zones.

4.3. Limitations and Recommendations for Future Work

The Pearson correlation coefficient is limited to relationships that are linear; however, relationships between soil properties and the response of a crop need not be linear. In addition, a number of the variables and VIs in this study were too highly skewed for the Pearson correlation coefficient to be an appropriate metric of association. It may be beneficial to explore nonlinear data transformations and/or non-parametric modeling approaches to address this issue.

The foregoing analysis considered relationships for which the correlations were highly empirical because the object being sensed (the plant) was not the object for which inferences were being drawn (the soil). In terms of future work, the next, simplest step would be multiple regression with the significant variables identified by this study as covariates and a VI as the response variable. Additional work requiring more effort would be to build a spatially-explicit, predictive model. In this

approach, image classification could be used to direct soil sampling and the data could be analyzed by appropriate statistical methods.

5. CONCLUSION

This paper presented a synthesis of field measurements with satellite imagery in four fields distributed across distinct soil, topography, and climate sub-regions of the Palouse. Key linear relationships between data collected at these sites and VIs computed from the RapidEye™ wavebands were identified. The most important for the two drier and more topographically variable fields was found to be TC. The working hypothesis is that TC is the primary contributor to variable productivity and grain yield in these two fields through its influence on available water. The TC distributions are likely legacy effects from excessive soil erosion that occurred in these fields before conversion to conservation tillage practices. Meanwhile the two fields of the higher precipitation sub-region exhibited a strong correlation between soil depth and RapidEye™. Restrictive soil horizons influence the amount of water the soil is able to hold within the crop rooting zone. Shallow soils are prone to saturation in spring and rapid moisture depletion late in the growing season. Both features, soil depth in the wet sub-region and TC in the dry sub-region, should be taken into account whenever site-specific farm-management strategies are considered.

6. REFERENCES

Aase JK, Siddoway FH. 1981. Assessing winter wheat dry matter production via spectral reflectance measurements. *Remote Sensing of Environment* **11**(4): 267-277. DOI: 10.1016/0034-4257(81)90025-0

Aerosol Robotic Network. National Aeronautics and Space Administration—Goddard Space Flight Center, Holben B (Principle Investigator), Rimrock, ID. URL http://aeronet.gsfc .nasa.gov.

Ahmed Z, Iqbal J. 2014. Evaluation of Landsat TM5 multispectral data for automated mapping of surface soil texture and organic matter in GIS. *European Journal of Remote Sensing* **47**: 557-573. DOI: 10.5721/EuJRS20144731

Allbed A, Kumar L, Sinha P. 2014. Mapping and modelling spatial variation in soil salinity in the Al Hassa Oasis based on remote sensing indicators and regression techniques. *Remote Sensing* **6**(2): 1137-1157. DOI: 10.3390/rs6021137

Adegoke JO, Carleton AM. 2002. Relations between soil moisture and satellite vegetation indices in the US Corn Belt. *Journal of Hydrometeorology* **3**(4): 395-405. DOI: 10.1175/1525-7541(2002)003<0395:RBSMAS>2.0.CO;2

Ballabio C, Panagos P, Montanarella L. 2014. Predicting soil organic carbon content in Cyprus using remote sensing and Earth observation data. In *Second International Conference on Remote Sensing and Geoinformation of the Environment (RSCy2014),* Hadjimitsis DG, Themistocleous K, Michaelides S, Papadavid G (eds). *Proceedings of the SPIE* **9229**: 92290F-(1-9).

Baret F, Guyot G. 1991. Potentials and limits of vegetation indices for LAI and APAR assessment. *Remote Sensing of Environment* **35**(2-3): 161-173. DOI: 10.1016/0034-4257(91)90009-U

Barnes EM, Clarke TR, Richards SE, Colaizzi PD, Haberland J, Kostrzewski M, Waller P, Choi C, Riley E, Thompson T, Lascano RJ, Li H, Moran MS. 2000. Coincident detection of crop water stress, nitrogen status and canopy density using ground-based multispectral data. In *Proceedings of the Fifth International Conference on Precision Agriculture, Bloomington, Minnesota, USA, 16-10 July, 2000*, Robert PC, Rust RH, Larson WE (eds). American Society of Agronomy: Madison, WI; 1-15.

Barnes EM, Baker MG. 2000. Multispectral data for mapping soil texture: possibilities and limitations. *Applied Engineering In Agriculture* **16**(6): 731-741.

Bauer ME, Daughtry CST, Biehl LL, Kanemasu ET, Hall FG. 1986. Field spectroscopy of agricultural crops. *IEEE Transactions on Geoscience and Remote Sensing* **24**(1): 65-75. DOI: 10.1109/TGRS.1986.289589

Ben-Dor E. 2002. Quantitative remote sensing of soil properties. In *Advances in Agronomy, Vol. 75*, Sparks DL (ed). Elsevier Academic Press Inc.: San Diego, CA; 173-243. DOI: 10.1016/S0065-2113(02)75005-0

Beven KJ, Kirkby MJ. 1979. A physically based, variable contributing area model of basin hydrology. *Hydrological Sciences-Bulletin* **24**(1): 43-69. DOI: 10.1080/02626667909491834

Bishop TFA, McBratney AB. 2001. A comparison of prediction methods for the creation of field-extent soil property maps. *Geoderma* **103**(1-2): 149-160. DOI: 10.1016/S0016-7061(01)00074-X

BlackBridge. 2012. Spectral response curves of the RapidEye sensor, 31pp. Accessed December 20, 2015 at http://blackbridge.com/rapideye/upload/Spectral_Response_Curves.pdf.

Brooks ES, Boll J, McDaniel PA. 2012. (Chapter 10) Hydropedology in seasonally dry landscapes: the Palouse region of the Pacific Northwest, USA. In *Hydropedology: Synergistic Integration of Soil Science and Hydrology*, Lin H (ed). Academic Press: Elesevier B.V.; 329-350.

Brooks RH, Corey AT. 1964. Hydraulic properties of porous media, Hydrology Papers No. 3, 37pp. Corey AT, Dils RE, Yevdjevich VM (eds). Colorado State University, Fort Collins, CO.

Carlson TN, Gillies RR, Schmugge TJ. 1995. An interpretation of methodologies for indirect measurement of soil water content. *Agricultural and Forest Meteorology* **77**(3-4): 191-205. DOI: 10.1016/0168-1923(95)02261-U

Carlson TN, Ripley DA. On the relation between NDVI, fractional vegetation cover, and leaf area index. *Remote Sensing of Environment* **62**(3): 241-252. DOI: 10.1016/S0034-4257(97)00104-1

Carter GA. 1993. Response of leaf spectral reflectance to plant stress. *American Journal of Botany* **80**: 239-243.

Carter GA. 1994. Ratios of leaf reflectances in narrow wavebands as indicators of plant stress. *International Journal of Remote Sensing* **15**(3): 697-703.

Carter GA, Knapp AK. 2001. Leaf optical properties in higher plants: linking spectral characteristics to stress and chlorophyll concentration. *American Journal of Botany* **88**(4): 677-684. DOI: 10.2307/2657068

Chang CW, Laird DA. 2002. Near-infrared reflectance spectroscopic analysis of soil C and N. *Soil Science* **167**(2): 110-116. DOI: 10.1097/00010694-200202000-00003

Chen F, Kissel DE, West LT, Adkins W. 2000. Field-scale mapping of surface soil organic carbon using remotely sensed imagery. *Soil Science Society of America Journal* **64**(2): 746-753.

Cho MA, Skidmore AK. 2006. A new technique for extracting the red edge position from hyperspectral data: The linear extrapolation method. *Remote Sensing of Environment* **101**(2): 181-193. DOI: 10.1016/j.rse.2005.12.011

Ciha AJ. 1984. Slope position and grain yield of soft white winter wheat. *Agronomy Journal* **76**(2): 193-196.

Clevers JGPW, De Jong SM, Epema GF, Addink EA, Van Der Meer F, Bakker WH, Skidmore AK. 2000. MERIS and the red-edge index. In *Second EARSeL Workshop on Imaging Spectroscopy*, *Enschede, The Netherlands, 11-13 July 2000* [online], 16pp. Accessed December 13, 2015 at http://www.earsel.org/workshops/imaging-spectroscopy-2000/papers/Clevers43.pdf.

Daughtry CST, Walthall CL, Kim MS, Brown de Colstoun E, McMurtrey III JE. 2000. Estimating corn leaf chlorophyll concentration from leaf and canopy reflectance. *Remote Sensing of Environment* **74**(2): 229-239. DOI: 10.1016/S0034-4257(00)00113-9

Dematte JAM, Dematte JLI, Camargo WP, Fiorio PR, Nanni MR. 2001. Remote sensing in the recognition and mapping of tropical soils developed on topographic sequences. *Mapping Sciences and Remote Sensing* **38**(2): 79-102.

Dematte JAM, Toledo AMA, Simoes MS. 2004. Methodology for the recognition of three soils by using laboratory and orbital sensors [translated from Portuguese]. *Brazillian Journal of Soil Science* **28**(5): 877-889. DOI: 10.1590/S0100-06832004000500010

Dematte JAM, Moreti D, de Vasconcelos ACF, Genu AM. 2005. Satellite images on the discrimination of soils developed from basalt and sandstone of Paraguacu Paulista region [translated from Portuguese]. *Brazilian Journal of Agricultural Research* **40**(7): 697-706. DOI: 10.1590/S0100-204X2005000700011

Devore JL. 2008. *Probability and Statistics for Engineering and the Sciences*, *Seventh Edition*, 720pp. Thomas Higher Education: Belmont, CA.

Dutta D, Goodwell AE, Kumar P, Garvey JE, Darmody RG, Berretta DP, Greenberg JA. 2015. On the feasibility of characterizing soil properties from AVIRIS data. *IEEE Transactions on Geoscience and Remote Sensing* **53**(9): 5133-5147. DOI: 10.1109/TGRS.2015.2417547

Eitel JUH, Long DS, Gessler PE, Hunt Jr. ER, Brown DJ. 2009. Sensitivity of ground-based remote sensing estimates of wheat chlorophyll content to variation in soil reflectance. *Soil Science Society of America Journal* **73**(5): 1715-1723. DOI: 10.2136/sssaj2008.0288

Eitel JUH, Vierling LA, Litvak ME, Long DS, Schulthess U, Ager AA, Krofcheck DJ, Stoscheck L. 2011. Broadband, red-edge information from satellites improves early stress detection in a New Mexico conifer woodland. *Remote Sensing of Environment* **115**(12): 3640-3646. DIO: 10.1016/j.rse.2011.09.002

Eldeiry AA, Garcia LA. 2010. Comparison of ordinary kriging, regression kriging, and cokriging techniques to estimate soil salinity using LANDSAT images. *Journal of Irrigation and Drainage Engineering-ASCE* **136**(6): 355-364. DOI: 10.1061/(ASCE)IR.1943-4774.0000208

Engstrom R, Hope A, Kwon H, Stow D. 2008. The relationship between soil moisture and NDVI near Barrow, Alaska. *Physical Geography* **29**(1): 38-53. DOI: 10.2747/0272-3646.29.1.38

Fiez TE, Miller BC, Pan WL. 1994. Winter wheat yield and grain protein across varied landscape positions. *Agronomy Journal* **86**(6): 1026-1032.

Fitzgerald G, Rodriguez D, O'Leary G. 2010. Measuring and predicting canopy nitrogen nutrition in wheat using a spectral index—the canopy chlorophyll content index (CCCI). *Field Crops Research* **116**: 318-324. DOI: 10.1016/j.fcr.2010.01.010

Gamon JA, Field CB, Goulden ML, Griffen KL, Hartley AE, Joel G, Penuelas J, Valentini R. 1995. Relationships between NDVI, canopy structure, and photosynthesis in three California vegetation types. *Ecological Applications* **5**(1): 28-41.

Gan SS, Amasino RM. 1997. Making sense of senescence. *Plant Physiology* **113**(2): 313-319.

Gillies RR, Carlson TN, Cui J, Kustas WP, Humes KS. 1997. A verification of the `triangle' method for obtaining surface soil water content and energy fluxes from remote measurements of the Normalized Difference Vegetation Index (NDVI) and surface radiant temperature. *International Journal of Remote Sensing* **18**(15): 3145-3166. DOI: 10.1080/014311697217026

Gomez C, Rossel RAV, McBratney AB. 2008. Soil organic carbon prediction by hyperspectral remote sensing and field vis-NIR spectroscopy: an Australian case study. *Geoderma* **146**(3-4): 403-411. DOI: 10.1016/j.geoderma.2008.06.011

GRASS Development Team. 2012. Geographic Resources Analysis Support System (GRASS) Software. Open Source Geospatial Foundation Project. URL http://grass.osgeo.org.

Gregory PJ. 2006. *Plant Roots: Growth, Activity and Interactions with the Soil*, 328pp. Blackwell Publishing Ltd.

Horler DNH, Dockray M, Barber J. 1983. The red edge of plant leaf reflectance. *International Journal of Remote Sensing* **4**(2): 273–288.

Horner G, McCall AG, Bell FG. 1944. Investigations in erosion control and the reclamation of eroded land at the Palouse Conservation Experiment Station, Pullman, Wash. 1931-42, Technical Bulletin No. 860, 83pp. U.S. Department of Agriculture, Washington, DC.

Hudson BD. 1994. Soil organic matter and available water capacity. *Journal of Soil and Water Conservation* **49**(2): 189-194.

Huete AR. 1988. A soil-adjusted vegetation index (SAVI). *Remote Sensing of Environment* **25**(3): 295-309. DOI: 10.1016/0034-4257(88)90106-X

Jaber SM, Lant CL, Al-Qinna MI. 2011. Estimating spatial variations in soil organic carbon using satellite hyperspectral data and map algebra. *International Journal of Remote Sensing* **32**(18): 5077-5103. DOI: 10.1080/01431161.2010.494637

Jordan CF. 1969. Derivation of leaf-area index from quality of light on the forest floor. *Ecology* **50**(4): 663-666. DOI: 10.2307/1936256

Kaiser VG. 1967. Soil erosion and wheat yield in Whitman County, Washington. *Northwest Science* **41**(2): 86-91.

Kok H, Papendick RI, Saxton KE. 2009. STEEP: Impact of long-term conservation farming research and education in Pacific Northwest Wheatlands. *Journal of Soil and Water Conservation* **64**(4): 253-264. DOI: 10.2489/jswc.64.4.253

Kotchenova SY, Vermote EF, Matarrese R, Klemm FJ. 2006. Validation of a vector version of the 6S radiative transfer code for atmospheric correction of satellite data. Part I. Path radiance. *Applied Optics* **45**(26): 6762-6774. DOI: 10.1364/AO.45.006762

Kotchenova SY, Vermote EF. 2007. Validation of a vector version of the 6S radiative transfer code for atmospheric correction of satellite data. Part II. Homogeneous Lambertian and anisotropic surfaces. *Applied Optics* **46**(20): 4455-4464. DOI: 10.1364/AO.46.004455

Kramer PJ, Boyer JS. 1995. (Chapter 5) Roots and root systems. In *Water Relations of Plants and Soils*. Academic Press, Inc.: San Diego, CA; 115-166.

Liao K, Xu S, Wu J, Zhu Q. 2013. Spatial estimation of surface soil texture using remote sensing data. *Soil Science and Plant Nutrition* **59**(4): 488-500. DOI: 10.1080/00380768.2013.802643

Lopez-Grenados F, Jurado-Exposito M, Atenciano S, Garcia-Ferrer A, de la Orden MS, Garcia-Torres L. 2002. Spatial variability of agricultural soil parameters in southern Spain. *Plant and Soil* **246**(1): 97-105. DOI: 10.1023/A:1021568415380

Lopez-Grenados F, Jurado-Exposito M, Pena-Barragan JM, Garcia-Torres L. 2005. Using geostatistical and remote sensing approaches for mapping soil properties. *European Journal of Agronomy* **23**(3): 279-289. DOI: 10.1016/j.eja.2004.12.003

Moore ID, Grayson RB, Ladson AR. 1991. Digital terrain modeling—a review of hydrological, geomorphological, and biological applications. *Hydrological Processes* **5**(1): 3-30. DOI: 10.1002/hyp.3360050103

Moore ID, Gessler PE, Nielsen GA, Peterson GA. 1993. Soil attribute prediction using terrain analysis. *Soil Science Society of America Journal* **57**: 443-452.

Moran MS, Clarke TR, Inoue Y, Vidal A. 1994. Estimating crop water deficit using the relation between surface-air temperature and spectral vegetation index. *Remote Sensing of Environment* **49**(3): 246-263. DOI: 10.1016/0034-4257(94)90020-5

Mulla DJ, Bhatti AU, Hammond MW, Benson JA. 1992. A comparison of winter wheat yield and quality under uniform versus spatially-variable fertilizer management. *Agriculture Ecosystems & Environment* **38**(4): 301-311. DOI: 10.1016/0167-8809(92)90152-2

Mutanga O, Skidmore AK. 2004. Narrow band vegetation indices overcome the saturation problem in biomass estimation. *International Journal of Remote Sensing* **25**(19): 3999-4014. DOI: 10.1080/01431160310001654923

Perry EM, Fitzgerald GJ, Nuttall JG, O'Leary GJ, Schulthess U, Whitlock A. 2012. *Field Crops Research* **134**: 158-164. DOI: 10.1016/j.fcr.2012.06.003

Pinter PJ, Hatfield JL, Schepers JS, Barnes EM, Moran MS, Daughtry CST, Upchurch DR. 2003. Remote sensing for crop management. *Photogrammetric Engineering and Remote Sensing* **69**(6): 647-664.

Qi J, Chehbouni A, Huete AR, Kerr YH, Sorooshian S. 1994. A modified soil adjusted vegetation index. Remote Sensing of Environment 48(2): 119-126. DOI: 10.1016/0034-4257(94)90134-1

Ramoelo A, Skidmore AK, Cho MA, Schlerf M, Mathieu R, Heitkonig IMA. 2012. Regional estimation of savanna grass nitrogen using the red-edge band of the spaceborne RapidEye sensor. *International Journal of Applied Earth Observation and Geoinformation* **19**: 151-162. DOI: 10.1016/j.jag.2012.05.009

Rasmussen. 1992. Assessment of millet yields and production in Burkina Faso using integrated NDVI from the AVHRR. *International Journal of Remote Sensing* **13**(8): 3431-3442. DOI: 10.1080/01431169208904132

Raun WR, Solie JB, Johnson GV, Stone ML, Lukina EV, Thomason WE, Schepers JS. 2001. In-Season prediction of potential grain yield in winter wheat using canopy reflectance. *Agronomy Journal* **93**: 131-138.

Rawls WJ, Brakensiek DL. 1985. Prediction of soil water properties for hydrologic modeling. In *Watershed Management in the Eighties*, Jones EB, Ward TJ (eds). *Proc. Symp., 30 April--1 May, 1985, Denver, CO*. American Society of Civil Engineers: New York, NY; 293-299.

R Core Team. 2013. R: A language and environment for statistical computing. R Foundation for Statistical Computing , Vienna, Austria. URL http://www.R-project.org/.

Rodriguez D, Fitzgerald GJ, Belford R, Christensen LK. 2006. Detection of nitrogen deficiency in wheat from spectral reflectance indices and basic crop eco-physiological concept. *Australian Journal of Agricultural Research* **57**: 781-789. DOI: 10.1071/AR05361

Rondeaux G, Steven M, Baret F. 1996. Optimization of soil-adjusted vegetation indices. *Remote Sensing of Environment* **55**(2): 95-107. DOI: 10.1016/0034-4257(95)00186-7

Rouse Jr. JW, Haas RH, Schell JA, Deering DW. 1974. Montoring the vernal advancement and retrogradation (greenwave effect) of natural vegetation, Type III Final Report, 164pp. National Aeronautics and Space Administration—Goddard Space Flight Center: Greenbelt, MD.

Sadler EJ, Jones JW, Sudduth KA. 2007. Modeling for precision agriculture: how good is good enough, and how can we tell?. In *Precision Agriculture '07,* Stafford JV (ed). Papers presented at the 6th European Conference on Precision Agriculure, Skiathos, Greece, 3-6 June 2007. Wageningen Academic Publishers: the Netherlands; 241-248.

Sandholt I, Rasmussen K, Andersen J. 2002. A simple interpretation of the surface temperature/vegetation index space for assessment of surface moisture status. *Remote Sensing of Environment* **79**(2-3): 213-224. DOI: 10.1016/S0034-4257(01)00274-7

Schnur MT, Xie H, Wang X. 2010. Estimating root zone soil moisture at distant sites using MODIS NDVI and EVI in a semi-arid region of southwestern USA. *Ecological Informatics* **5**: 400-409. DOI: 10.1016/j.ecoinf.2010.05.001

Sellers PJ. 1985. Canopy reflectance, photosynthesis and transpiration. *International Journal of Remote Sensing* **6**(8): 1335-1372.

Soil Survey Staff. U.S. Department of Agriculture-Natural Resources Conservation Service, Web Soil Survey. Accessed December 13, 2015 at http://websoilsurvey.nrcs.usda.gov/.

Soil Survey Staff. 1999. *Soil Taxonomy—A Basic System of Soil Classification for Making and Interpreting Soil Surveys, Second Edition*. U.S. Depart of Agriculture--Natural Resources Conservation Service, Agricultural Handbook No. 436. U.S. Government Printing Office: Washington, DC.

Steffens D, Hutsch BW, Eschholz T, Losak T, Schubert S. 2005. Water logging may inhibit plant growth primarily by nutrient deficiency rather than nutrient toxicity. *Plant Soil and Environment* **51**(12): 545-552.

Stoner ER, Baumgardner MF. 1981. Characteristic variations in reflectance of surface soils. *Soil Science Society of America Journal* **45**(6): 1161-1165.

Sudduth KA, Kitchen NR, Wiebold WJ, Batchelor WD, Bollero GA, Bullock DG, Clay DE, Palm HL, Pierce FJ, Schuler RT, Thelen KD. 2005. Relating apparent electrical conductivity to soil properties across the north-central USA. *Computers and Electronics in Agriculture* **46**(1-3): 263-283. DOI: 10.1016/j.compag.2004.11.010

Sullivan DG, Shaw JN, Rickman D. 2005. IKONOS imagery to estimate surface soil property variability in two Alabama physiographies. *Soil Science Society of America Journal* **69**(6): 1789 -1798. DOI: 10.2136/sssaj2005.0071

Sultana SR, Ali A, Ahmad A, Mubeen M, Zia-Ul-Haq M, Ahmad S, Ercisli S, Jaafar HZE. 2014. Normalized difference vegetation index as a tool for wheat yield estimation: a case study from Faisalabad, Pakistan. *Scientific World Journal* Article No. 725326. DOI: 10.1155/2014/725326

Temimi M, Leconte R, Chaouch N, Sukumal P, Khanbilvardi R, Brissette F. 2010. A combination of remote sensing data and topographic attributes for the spatial and temporal monitoring of soil wetness. *Journal of Hydrology* **388**: 28-40. DOI: 10.1016/j.jhydrol.2010.04.021

Tucker CJ. 1979. Red and photographic infrared linear combinations for monitoring vegetation. *Remote Sensing of Environment* **8**(2): 127-150.

Tucker CJ, Elgin Jr. GH, McMurtrey III JE. 1980. Relationship of spectral data to grain yield variation. *Photogrammetric Engineering and Remote Sensing* **46**: 657-666.

Wilcox CH, Frazier BE, Ball ST. 1994. Relationship between soil organic-carbon and Landsat TM data in eastern Washington. *Photogrammetric Engineering and Remote Sensing* **60**(6): 771-781.

Yang C, Peterson CL, Shropshire GJ, Otawa T. 1998. Spatial variability of field topography and wheat yield in the Palouse Region of the Pacific Northwest. *Transactions of the ASAE* **41**(1): 17-27.

Zhang R, Warrick AW, Myers DE. 1992. Improvement of the prediction of soil particle size fraction using spectral properties. *Geoderma* **52**(3-4): 223-234. DOI: 10.1016/0016-7061(92)90038-9

7. TABLES

Table I. Equations and references for vegetation indices

Vegetation Index	Equation	Reference
Normalized Difference Red Edge (NDRE)	$NDRE = (\rho_{\mathrm{NIR}} - \rho_{\mathrm{R.E.}})/(\rho_{\mathrm{NIR}} + \rho_{\mathrm{R.E.}})$	Barnes *et al.* (2000)
Normalized Difference Vegetation Index (NDVI)	$NDVI = (\rho_{\mathrm{NIR}} - \rho_{\mathrm{RED}})/(\rho_{\mathrm{NIR}} + \rho_{\mathrm{RED}})$	Rouse *et al.* (1973)
Modified Chlorophyll Absorption in Reflectance Index (MCARI)	$MCARI = [(\rho_{\mathrm{R.E.}} - \rho_{\mathrm{RED}}) - 0.2(\rho_{\mathrm{R.E.}} - \rho_{\mathrm{GREEN}})]\,(\rho_{\mathrm{R.E.}}/\rho_{\mathrm{RED}})$	Daughtry *et al.* (2000)
Optimized Soil-Adjusted Vegetation Index (OSAVI)	$OSAVI = (1 + 0.16)[(\rho_{\mathrm{NIR}} - \rho_{\mathrm{RED}})/(\rho_{\mathrm{NIR}} + \rho_{\mathrm{RED}} + 0.16)]$	Rondeaux *et al.* (1996)

Table II. Crop type, image acquisition date, and crop development stage for the 2013 growing season

Field	Crop Rotation[a] (2012-2013-2014)	Date of 2013 Image	Development Stage
Colfax	WW-SW-SW	8 June	Stem Extension
		15 June	Stem Extension
		29 June	Heading/Anthesis
		8 July	Heading/Anthesis
		27 July	Grain Fill/Ripening
Genesee	SW-SB-Can	15 June	Stem Extension
		27 June	Heading
		15 July	Heading/Anthesis
		24 July	Grain Fill/Ripening
Leland	GBS-WW-SW	6 June	Heading/Anthesis
		15 June	Heading/Anthesis
		27 June	Heading/Anthesis
		9 July	Grain Fill/Ripening
Troy	GBS-WW-GBS	6 June	Stem Extension
		15 June	Heading
		29 June	Heading/Anthesis
		16 July	Grain Fill/Ripening

[a]GBS=garbanzos, WW=winter wheat, SW=spring wheat, Can=canola, SB=spring barley

Table III. Abbreviated table of top correlations between field measurements and vegetation indices from RapidEye™ imagery

Field	Variable	Depth (cm)	Index	Image Date	r^2	N	p-value	r
Colfax	$GWC_{SPR.}$	0-90	OSAVI	27 July	0.88	11	<.001	0.94
	TC_{2011}	0-60	NDRE	8 July	0.85	12	<.001	0.92
	Δ*IN*	0-90	NDVI	15 June	0.77	12	<.001	0.88
	Δ*GWC*	0-90	NDVI	8 July	0.64	12	0.002	0.80
	TWI	NA	OSAVI	27 July	0.62	11	0.003	0.79
	VWC_{FALL}	0-90	MCARI	8 June	0.58	12	0.004	-0.76
	$ECa_{SPR.}$	NA	OSAVI	27 July	0.49	11	0.016	-0.70
	Sand	0-90	OSAVI	15 June	0.44	12	0.019	-0.66
Genesee	*Sand*	0-60	OSAVI	15 July	0.86	12	<.001	0.93
	$ECa_{FALL.}$	NA	MCARI	15 July	0.85	12	<.001	-0.92
	TN_{2012}	0-90	NDRE	15 July	0.75	12	<.001	0.86
	Δ*IN*	0-120	MCARI	15 July	0.58	11	0.007	0.76
	Δ*GWC*	0-30	NDRE/NDVI	27 June	0.67	8	0.012	-0.82
	Yield	NA	NDRE	15 July	0.44	12	0.018	0.66
Leland	$IN_{SPR.}$	0-120	NDRE	9 July	0.94[a]	11	<.001	0.97
	$TAW_{OBS.}$	NA	OSAVI	27 June	0.88	12	<.001	0.94
	$D_{OBS.}$	NA	OSAVI	27 June	0.81	12	<.001	0.90
	Δ*GWC*	0-60	OSAVI	15 June	0.72	12	<.001	0.85
	Silt	0-90	NDVI	15 June	0.69	12	<.001	0.83
	$ECa_{SPR.}$	NA	MCARI/OSAVI	27 June	0.61	12	0.003	0.78
	TN_{2011}	0-120	OSAVI	15 June	0.56	12	0.005	0.75
	Δ*EC*a	NA	MCARI/OSAVI	27 June	0.38	12	0.032	0.62
Troy	*Yield*	NA	OSAVI	29 June	0.72	12	<.001	0.85
	Δ*EC*a	NA	MCARI/OSAVI	29 June	0.53	12	0.007	0.73
	$IN_{SPR.}$	0-60	NDRE/NDVI	15 June	0.50	12	0.009	-0.71
	IN_{FALL}	0-150	NDRE/NDVI	6 June	0.46	12	0.015	-0.68
	$TAW_{OBS.}$	NA	OSAVI	16 July	0.42	12	0.022	0.65
	$GWC_{SPR.}$	0-30	NDVI	16 July	0.36	12	0.041	0.60

[a]Obtained with outlier point removed. With outlier included r^2=0.64.

8. FIGURES

Figure 1. Photo of the Colfax field planted to winter wheat. Taken 19 June 2015, looking east

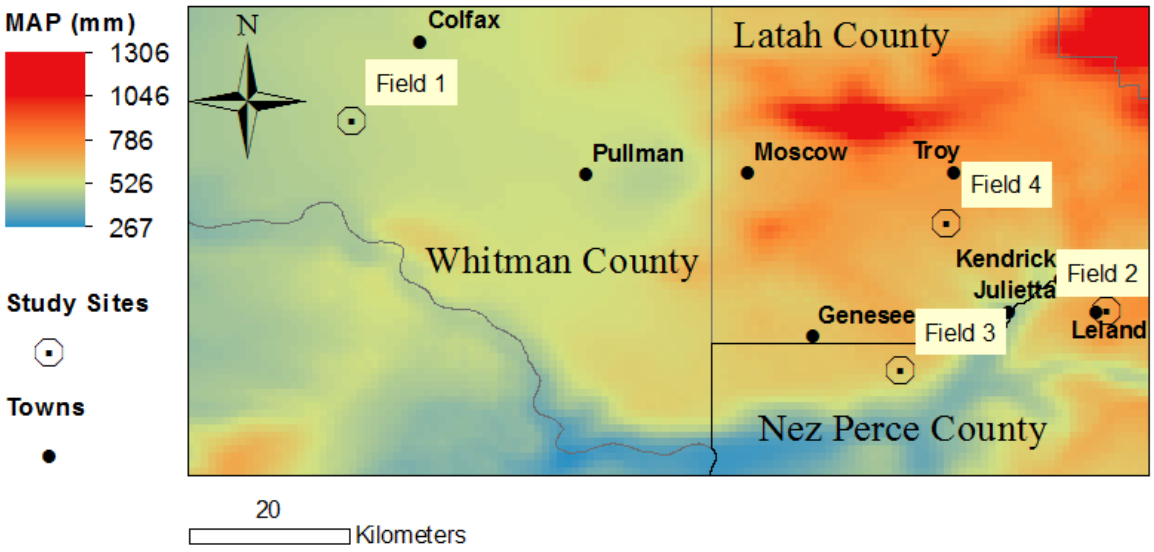

Figure 2. Field locations across the southeastern Palouse climate gradient. The basemap layer is mean annual precipitation (MAP) obtained from the parameter-elevation regressions on independent slopes (PRISM) climate model, 30-yr precipitation normals (PRISM ClimateGroup, Oregon State University, http://prism.oregonstate.edu, created 10 July 2012).

Genesee

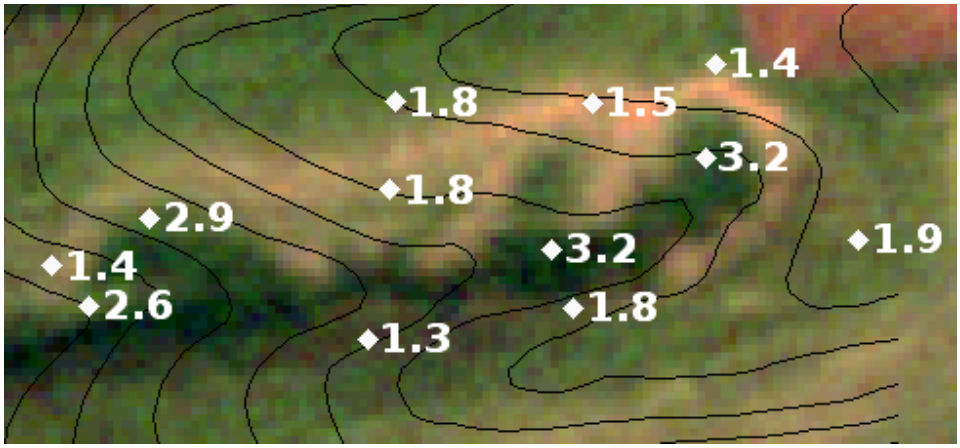

Colfax

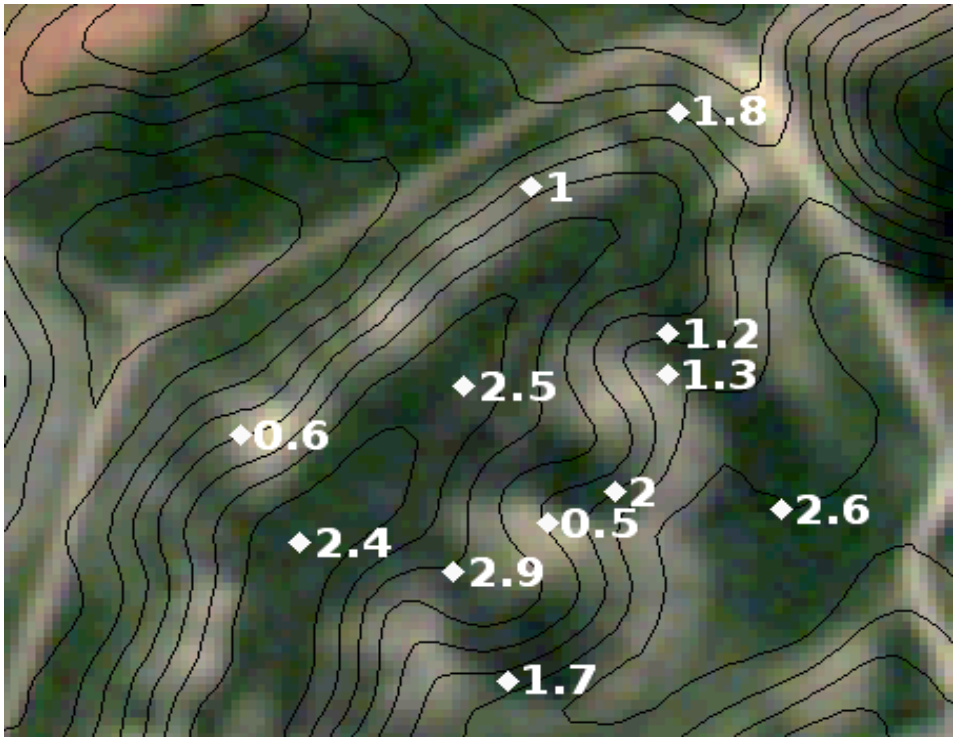

Figure 3. Spatial distribution of organic matter at the Genesee and Colfax fields. The background is a RGB color composite from RapidEye™. Numbers represent organic matter approximated as 1.72 x TC (% by mass) in the top 90 cm.

Figure 4. Effects of waterlogging on winter wheat at the Troy field. Image taken 6 May 2013, looking east. Lower elevations are frequently saturated in the spring leading to delayed crop development.

CHAPTER 3: CAPTURING FIELD-SCALE HYDROLOGIC VARIABILITY ACROSS THE PALOUSE CLIMOSEQUENCE USING PROXIMAL SOIL SENSING AND DISTRIBUTED HYDROLOGIC MODELLING

1. INTRODUCTION

1.1. Background

Water management issues brought to light during the International Hydrological Decade (Nace, 1980) spurred an era of computer modelling, beginning with Freeze (1974), that sought ways of simulating the physical mechanisms by which rainfall becomes streamflow (see also Beven and Kirbky, 1979; Beven, 1980, 1987; Quinn *et al.*, 1991; Grayson *et al*., 1992a; Calver and Wood, 1995; Refsgaard and Storm, 1995). Although these "bottom-up" models, which aimed to extrapolate small-scale physics to the catchment scale, could provide fundamental representations of important flow processes in a landscape, it was quickly recognized that key challenges in applying these models were: 1) limited availability of spatially-detailed soils data for model parameterization and 2) lack of hydrologic data measured at an appropriate scale to assess model predictions (Grayson *et al*., 1992b; Dunne, 1982; James and Burges, 1982; Wood *et al*., 1988, 1990). In the absence of spatially-detailed validation data, models were being calibrated and assessed using streamflow measurements alone. This led to a condition of "equifinality" (Beven, 1996) among models in which simulated streamflow could be fit to match observed streamflow using multiple combinations of input parameters. There was a problem: the model might "work well" for "the wrong reasons" (Klemes, 1986). Some questioned whether it was even possible to develop reliable, spatially-explicit hydrologic models (Beven, 1989; Grayson *et al*., 1992b). Without the ability to capture spatial variability in soil input parameters such as depth to a hydraulic restricting horizon (e.g. bedrock or fragipan) and soil texture, and without the ability to capture soil moisture patterns throughout a catchment, the hydrologic community directed its focus onto 'top down' approaches (Kirchner, 2006). These efforts attempted to capture the hydrologic functioning of a catchment as a unit using a wide range of hydrologic as well as isotopic measurements (Kirchner, 2003; McDonnell and Woods, 2004; Weiler and McDonnell, 2007).

Significant progress over the last decade in the areas of remote sensing (RS), proximal soil sensing, and geographic information systems (GIS) has renewed interest in spatially-explicit hydrologic modeling. RS data is now widely available for most of the world at high spatial resolutions (<10 m) with repeat coverages of less than six days thanks to satellites such as RapidEye^{TM}, IKONOS, and the recently launched Worldview-2 and Sentinel-2 satellites. These multispectral imagers provide

a wealth of information on spatial vegetation patterns, and in turn they can reveal much about the hydrology of a landscape. For example, different water regimes of a landscape resulting from topography-induced microclimates and soil hydraulic properties have been inferred from vegetation cover (Gomez-Plaza *et al.*, 2000; Qiu *et al.*, 2001; Western *et al.*, 2002; Canton *et al.*, 2004). In one application, Temimi *et al.* (2010) combined multispectral imagery from the MODIS satellite with passive microwave data and terrain attributes to develop a dynamic topographic wetness index. In agriculture, RS of vegetation reveals, to some extent, the time-integrated effect of water supply on crop growth patterns, especially within dryland agricultural systems of semi-arid regions where fields often exhibit significant variability in stored soil water (Pan *et al.*, 2007; Ibrahim and Huggins, 2011).

Proximal soil sensing and RS technologies have enabled rapid measurement and mapping of soils and elevation data to support model parameterization and assessment. Studies incorporating high resolution RS and proximal sensing data have had mixed success. For example, Shi *et al*. (2015) used a coupled, surface energy-hydrology model (Flux-PIHM) with different soils and bedrock maps to illustrate the advantage of detailed mapping. They observed a poor correlation (r= -0.02) between simulated and observed moisture patterns when using a soils map obtained from the Soil Survey Geographic (SSURGO) database but reported a large improvement (r= 0.63) with model results using a detailed field survey map. In another study, Noh *et al*. (2015) noted that despite one-meter resolution elevation data and field-measured hydraulic conductivity, their mechanistic model made large errors in soil moisture prediction. They had more success matching simulated and observed moisture patterns when applying a stochastic model to the same hillslope.

Most hydrologic models that have been applied to agricultural systems are fundamentally one-dimensional models that cannot capture the lateral redistribution of water in topographically-complex landscapes, e.g. the hydrology components of: EPIC (Sharpley and Williams, 1990), AGNPS (Young *et al*., 1989), CREAMS (Knisel, 1980), ANSWERS (Beasley *et al*., 1980), RZWQM (RZWQM Development Team, 1992), CERES (Ritchie, 1998), SWAP (Van Dam *et al*., 1997), WOFOST (Supit *et al*., 1994), CropSyst (Stockle *et al*., 2003), and DSSAT (Jones *et al*., 2003) fit this category. Others are large-scale models that were not developed to capture sub-field scale variability, e.g. SWAT (Arnold *et al*., 1998). Recent examples of hydrologic models developed for simulating soil water storage and transport at spatial scales useful for cropping decisions in actively-managed agricultural fields include PALMS (Molling *et al.*, 2005) and PROMET (Hank *et al.*, 2015). Nelson *et al*. (2013) evaluated the PALMS model in fields of the semi-arid Texas High Plains region planted to corn, cotton, and sorghum. They reported overall good performance in seasonal soil moisture patterns but reported

some discrepancies between observed and predicted moisture content, which they attributed to incorrect parameterization of soil hydraulic properties. In the second study, Hank *et al.* (2015) extended the original PROMET model of Mauser and Bach (2009) and coupled it with a land surface process model to simulate growth and yield of winter wheat in two Central European agricultural areas. The PROMET model, having originally been developed for watersheds of mountainous regions, has a process-based representation of subsurface lateral flow along hillslopes, while the PALMS model distributes shallow groundwater evenly among connected grid cells without explicitly modeling the subsurface flow process.

Topography greatly affects the redistribution of soil water in steep-sloping, convergent landscapes (Beven and Kirkby, 1979), especially those having shallow, hydraulically-restrictive soil horizons that support perched water tables (McDaniel *et al*., 2008). Therefore, hydrologic models applied to these landscapes need to simulate subsurface lateral flow in order to capture spatial variability in soil moisture and runoff generation (Brooks *et al*., 2007). In hillslopes containing a hydraulic restricting layer, upslope drainage has potential to rapidly move solutes downslope (Mallawatantri *et al.*, 1996; Reuter *et al.*, 1998; Needelman *et al*., 2004), which has important implications for agrichemical fate and transport modeling.

Brooks *et al.*, (2004), adopting the formulation of Childs (1971) for groundwater flow above a sloping permeable bed, demonstrated with a hillslope plot experiment conducted in Troy, ID that the hydraulic gradient above a sloping fragipan layer parallel to the ground surface is approximately equal to landslope. This hydraulic gradient is conducive to accumulation of water in convergent downslope areas (Hammermeister *et al*., 1982; Brooks *et al*., 2004, 2007; Needelman *et al*., 2004; Gburek *et al.*, 2006) and subsequent generation of saturation excess runoff. The area contributing runoff expands in response to storm events and contracts as the catchment drains, a concept called variable source area (VSA) hydrology (Hewlett and Hibbert, 1967; Dunne and Black, 1970; Dunne *et al*., 1975).

Two distributed hydrologic models well-adapted for VSA hydrology are the DHSVM (Wigmosta *et al*., 1994) and SMR (Frankenberger *et al*., 1999) models. DHSVM has been primarily applied in forested, mountainous regions, while SMR has been used in both the Catskill Mountains of New York (Frankenberger *et al*., 1999) and in the gently-rolling landscape of the Palouse region (Brooks, 2003). Neither model has been applied to agricultural land under cereal grain production, an obstacle this research is meant to address. A distinct advantage of both DHSVM and SMR is that both use open-source software. For example, the SMR program is tightly coupled to the Geographic

Resources Analysis Support System (GRASS) (GRASS Development Team, 2012) and runs as a scripted sequence of commands issued to and executed by GRASS. New algorithms can be added to the script as needed to meet the needs of the intended application. This feature of SMR makes it a very attractive option for watershed modeling in annually-cropped watersheds of the Palouse region.

1.2. Research Overview and Objectives

In this study, we assess the ability of a modified version of the soil moisture routing (SMR) model to capture field-scale (10 m resolution) variability in water storage and distribution within four actively managed field sites in the low-to-high precipitation zones of the eastern Palouse dryland cereal production region. SMR was chosen because it had the greatest potential to be adapted for use in Palouse dryland cropping systems, and because it has had success simulating spatial moisture patterns at a perennial grassland catchment in the region (Brooks *et al*., 2007). The location of the study sites were chosen to represent the regional variability in climate, topography, and soils. At each of these sites we acquired detailed soil maps using electromagnetic induction surveys and a novel, visible and near-infrared (VNIR) proximal sensor, and we documented spatial crop senescence patterns using 5 m resolution RapidEye^{TM} satellite imagery acquired up to five times during the growing season. Extensive monitoring networks were installed over a three year period to capture the export and redistribution of water at each of these field sites.

The objectives of this study were to: 1) modify and extend the existing SMR code to more effectively capture spatially-explicit patterns of soil moisture in agricultural catchments of the Palouse, 2) parameterize the model in four agricultural, Palouse region fields using detailed soil mapping 3) assess the ability of the model to capture field-scale soil water storage and transport, and 4) quantify the percentage of variability in the normalized difference vegetation index (NDVI) explained by modelled predictions of plant available water and cumulative evapotranspiration.

1.3. SMR Model Overview

SMR is a distributed, grid-based water balance model well adapted to regions with steep-sloping land and shallow soils. It is simple, with few parameters and requires little calibration (Boll *et al.*, 1998; Frankenberger *et al*., 1999). Its original application was to inform management decisions addressing nonpoint source (NPS) pollution from agriculture in the Catskill Mountains of New York (Frankenberger *et al*., 1996; Walter *et al.*, 2000). A distinguishing feature of SMR is its ability to predict variable source areas (VSAs) that generate runoff at any point in the watershed using publically-available data. SMR does not simulate overland flow because infiltration excess has not been deemed an important runoff mechanism in the watersheds for which it was developed, i.e.

forested watersheds located in humid/sub-humid regions with low intensity rainfall (Boll *et al.*, 1998; Frankenberger *et al.*, 1999; Mehta *et al.,* 2004). The model simulates inputs from precipitation and lateral inflow in addition to losses via evapotranspiration, percolation through a restrictive layer, lateral outflow, and runoff. Soil water storage is updated at the end of each time step (hourly or daily) for each grid cell. Runoff is generated from a grid cell whenever the net inputs for a time step exceed the total storage capacity of the soil. Model structure and algorithms have been provided by Frankenberger *et al*. (1999). Past modifications have included a mass and energy budget approach to snowmelt simulation (Brooks and Boll, 2005), distribution of saturated lateral hydraulic conductivity with depth based on hillslope measurements (Brooks *et al.*, 2004), and a representation of soil water storage as a function of perched water depth (Brooks *et al.*, 2007). In the present work, we retain these modifications and further adapt the SMR model for use in continuously-cropped watersheds by specifying a root zone layer that increases with days after planting.

2. METHODS

2.1. Site Description

The Palouse region of the inland Pacific Northwest USA is famous for its rolling, loess-formed hills that support remarkable yields of soft white winter wheat (Washington Wheat Commission, 2009). The moisture regime of the Palouse region is dominated by low-intensity storms (Klages, 1942) distributed evenly between the fall, winter, and spring months (United States Department of Agriculture, Natural Resources Conservation Service, 2006). Mean annual precipitation (MAP) ranges from <450 mm in the western part of Whitman County (Donaldson, 1980) to more than 800 mm in the eastern part of Latah County (Barker, 1981).

Land relief and climate are predominant soil-forming factors in the Palouse region (Brooks *et* al., 2012). Soils in the intermediate precipitation (450-700 mm) and high (>700 mm) annual precipitation zones show visible signs of carbonate leaching and clay eluviation with subsequent illuviation in argillic and fragipan layers. Vertical drainage of water through these layers is restricted such that seasonal perched water tables develop (Reuter *et al*., 1998). Soils to the west, in the low precipitation zone (< 450 mm), tend to be deeper and bear little evidence of carbonate leaching or illuviation of clays in the subsoil (Busacca, 1989; Soil Survey Staff, 2006). At the hillslope scale, soils on northeast-facing slopes tend to be more developed (e.g. have greater clay eluviation/illuviation and carbonate leaching) than on southwest-facing slopes owing to topography-induced differences in effective precipitation (Brooks *et al.*, 2012). The influence soil pedology has on hydrologic functionality in a landscape is a topic that has been discussed in detail by Lin *et al.* (2008).

Four fields in the dryland cropping region of eastern Washington and northern Idaho were selected for intensive hydrologic monitoring in cooperation with four private growers located near the towns of Colfax, WA; Genesee, ID; Troy, ID; and Leland, ID, respectively (Figure 5). For simplicity, the field located near Colfax will be called Colfax field or just Colfax, and likewise for the other study sites. Each field is part of a well-defined catchment delineated in ArcGIS using a 10-m resolution digital elevation model (DEM) obtained from the United States Geological Survey (USGS) National Elevation Dataset. The Colfax and Genesee fields are under no-till, continuous cereal management while the Troy and Leland fields are managed with minimal tillage and a wheat-pulse-wheat rotation. Study sites capture a steep climate gradient across the southeastern part of the Palouse River Basin and its immediate vicinity--from the drier, slightly warmer western part to the wetter and slightly cooler eastern part. Figure 5 shows 30-year MAP normals estimated from the parameter-elevation regressions on independent slopes model (PRISM Climate Group, 2012) for the region. MAP is also tabulated for the four study sites in Table IV using the same PRISM dataset. Topographic variability is most pronounced at the Colfax field where slopes up to 45% are observed and mean slope is 21%. In addition to MAP and slope, Table IV reports mean elevation and catchment area for the four fields.

According to the SSURGO database, the Colfax site (46.79°N, 117.44°W) is composed of a Palouse silt loam (fine-silty, mixed, mexic Pachic Ultic Haploxerolls) with typical A, AB horizonation (Soil Survey Staff). The Genesee field (46.55°N, 116.92°W) is composed of a mixture of Palouse silt loam and Naff silt loam (fine-silty, mixed, mesic Ultic Argixerolls). Naff soils have a Bt horizon beneath the AB horizon which restricts vertical drainage somewhat. This site has a tile line to improve subsurface drainage at lower elevations in the watershed. The predominant soil types at the Troy field (46.68°N, 116.77°W) are Larkin silt loam (fine-silty, mixed, mesic Ultic Argixerolls), comprising 41% of the field by area, and Southwick silt loam (fine-silty, mixed mesic Boralfic Argixerolls), comprising 33% of the field by area. Southwick silt loam has a water-restricting layer, classified as argillic, within the first meter. Soils with an argillic layer exhibit a sharp increase in clay content (> 5% by mass) over a small depth increment (<15 cm) (Soil Survey Staff, 1999). A Driscoll-Larkin complex and a Latahco-Thatuna complex make up the remaining 20% and 7% of the field by area, respectively. The Leland field (46.58°N, 116.60°W) is composed entirely of Southwick silt loam. At each field the topsoil (A, AB horizon) is silt loam, while for series other than Palouse silt loam the subsoil (Bt horizon) is a silty clay loam (Soil Survey Staff).

2.2. Soil Property, Hydrological, and Meteorological Measurements

2.2a. Soil Properties

The SSURGO database, while providing soil data of finer spatial detail than the state survey geographic (STATSGO) database, is still of limited value to distributed modeling where the parameters in question may change considerably over distances of only a few meters; therefore, site-specific measurements of bulk density (BD), and texture (sand, silt, and clay contents) were acquired for each field. Soil cores for BD determination were extracted at 36 locations per field at depth increments (cm) of 0-10, 10-20, 20-30, 30-60, 60-90, 90-120, and 120-150 cm using a Giddings Probe core extraction device (Giddings Machine Company, Windsor, CO). Samples were oven-dried and the initial volume of the extracted core used to calculate dry bulk density (g cm^{-3}). Two-dimensional BD surfaces were generated using automated 3D regression-kriging (Hengl *et al.*, 2014) at depths of 30 cm, 60 cm, 90 cm, 120 cm, and 150 cm using elevation, slope, curvature, and apparent electrical conductivity (ECa) as covariates. The kriged BD maps were used for distributing surface-soil porosity, in addition to the restricting-layer depth and porosity values. Soil texture (sand, silt, and clay contents) was measured fall of 2011 at 0-10, 10-20, 20-30, 30-60, 60-90, 90-120, and 120-150 cm depth increments at 12 sampling locations (microsites) within each of the four fields. For two of the fields, clay content was also measured on a 30-m grid to a depth of 70 cm using a VNIR sensor housed within a cone penetrometer (Poggio *et al*., 2015). Maps of clay content were generated for the Colfax and Leland fields, again using automated regression-kriging. If clay maps were not available, the field-wide average clay content, calculated from measurements made at the 12 microsites, was applied uniformly over the entire catchment.

Dense soil layers impede root extension (Kramer and Boyer, 1995) and are often associated with poor drainage in soils containing a fragipan or argillic layer. This was the rationale behind determining soil depth from a threshold BD value BD_{C} . In this method, a value for BD_{C} was chosen based on recommendations by the Natural Resources Conservation Service (2008) and the soil depth interpolated between the depth at which this critical value was exceeded and the above layer. Restrictive horizons at the study sites are high-clay argillic horizons. An argillic layer is present if the clay content of the underlying illuvial horizon (high-clay) is at least 1.2 times that of the overlying elluvial (low-clay) layer, and this increase normally occurs over a depth of 15 cm or less (Soil Survey Staff, 1999).

2.2b. Hydrological Instrumentation and Measurements

Hydrological and meteorological measurements were made at each of the four catchments during the 2012-2014 water years. Each field has twelve instrumented microsites equipped with 5TE or 5TM soil moisture sensors (Decagon Devices Inc., Pullman, WA) installed at 30 cm depth intervals ranging from 30 to 150 cm and connected to Em50R Data Loggers (Decagon Devices Inc., Pullman, WA). The 5TM sensor measures moisture and temperature, while the 5TE sensor also measures electrical conductivity. Drain gauges were installed at two or three locations per field for percolation monitoring and soil water sampling. Shallow groundwater monitoring wells for water sampling and manual perched water depth (PWD) readings were installed at microsites above hydraulically-restrictive horizons. PWD in each well was recorded every site visit. In addition, continuous water level measurements with the WT-HR sensor and datalogger (Intech Instruments Ltd, Christchurch, New Zealand) were used to measure PWD at 15 minute intervals. The pressure sensors were typically installed at two monitoring wells over the wet season at Genesee, Leland, and Troy catchments (no seasonal water tables were observed at Colfax). Surface runoff was measured at the catchment outlet of Troy by a single, 9-inch H-flume and at Genesee and Leland catchments using a 6-inch Parshall flume. Periodic snow depth and density measurements were made at all fields if snow was present. Surface saturation patterns were also mapped with hand-held GPS on a few events.

2.2c. Continuous *In-Situ* Monitoring of Soil Moisture with Field-Calibrated Sensors

The 5TE/5TM soil moisture sensor from Decagon Devices directly measures the dielectric permittivity of the soil, which is converted to volumetric water content (VWC) via the Topp equation (Topp *et al*., 1980). Sensors come with a factory calibration that provides accurate soil moisture measurements (±0.03 cm cm^{-1}) for a wide variety of soils. However, Decagon Devices encourages soil-specific calibrations to increase reliability of the measurements. We found accuracy using the factory calibration was poor and attempted to improve the accuracy through in-season soil sampling. Refer to Appendix C for more details on this method. Following calibration, sensor accuracy improved from ±0.084 cm cm^{-1} (RMSE=0.084 cm cm^{-1}, N=753) to ±0.047 cm cm^{-1} (RMSE=0.047 cm cm^{-1}, N=753).

2.2d. Meteorological Measurements

All four fields are equipped with a weather station that collects hourly precipitation, air temperature, wind speed, and wind direction. The Leland field weather station also records hourly solar radiation and relative humidity. Since neither Colfax, Troy, nor Genesee stations record these data, an arithmetic average was taken of solar radiation or relative humidity from the Leland

catchment and three AgWeatherNet stations (Pullman, 46.7°N, 117.15°W; Pullman NE, 46.78°N, 117.09°W; and Lacrosse, 46.86°N, 117.85°W) operated by the Washington State University's automated weather station network (*http://weather.wsu.edu*).

2.3. Acquisition and Post-Processing of Satellite Imagery

The RapidEye™ constellation of five identical satellites provides imagery at high spatial resolutions (6.5 m ground sampling distance, orthorectified and re-sampled to 5 m pixels) and temporal resolution (5.5 day revisit time). The on-board multispectral imager collects data in five wave bands: blue (440-510 nm), green (520-590 nm), red (630-685 nm), red-edge (690-730 nm), and near-infrared (760-850 nm) (BlackBridge, 2012). Images were obtained from the commercial vendor, BlackBridge (BlackBridge, Berlin, Germany), with radiometric, sensor and geometric corrections applied to the data. Post-processing of the data consisted of atmospheric correction using the 6S radiative transfer model (Kotchenova *et al*., 2006; Kotchenova and Vermote, 2007) implemented by the GRASS module, *i.atcorr*. More detail on *i.atcorr* module input is provided in Appendix C. The corrected atmospheric reflectance in red and near-infrared NIR wavelengths were used to compute the normalized difference vegetation index (NDVI) (Tucker, 1979).

2.4. Modifications to SMR

2.4a. Root zone and Deep Soil Layers

In order to track soil water uptake in a growing crop, the single soil profile approach used in the Brooks *et al*. (2007) version of SMR was replaced by a two layer profile where the top soil layer thickness is dynamic and dependent upon the increasing rooting depth of the crop as it matures. The lower soil layer extends from the bottom of the root zone (top layer) to the top of the hydraulic restricting layer. Root zone depth increases linearly with time after planting to a maximum rooting depth at maturity, which is crop dependent. Because it is assumed that plant roots do not penetrate the hydraulic restricting layer, the profile is modeled as a single soil layer once rooting depth equals soil depth. Over the non-growing season, top layer thickness is fixed at 30 cm. The choice of 30 cm facilitates comparison of model output with the 30-cm sensor VWC measurement and the VWC measured for the 0-30 cm depth soil sample. A capillary fringe for near-surface water tables was incorporated into the model following the approach of Brooks *et al*. (2007) which defines a linear relationship between moisture content and vertical distance from the water table. The published slope (Brooks *et al*., 2007) of this relationship was applied uniformly across all four fields.

The depth of water held in each soil layer at field capacity is apportioned according to layer thickness. As with the Brooks *et al*. (2007) model, percolation of water through the restricting layer

begins once field capacity of the lower soil layer is exceeded, and percolation ceases once the soil of the lower layer has drained to its field capacity. Percolation is assumed to occur as saturated flow at a rate equal to the saturated hydraulic conductivity (Ksat) based on a hydraulic gradient of unity. It is assumed that a perched water table develops first in the lower soil layer whenever the total storage exceeds field capacity and only rises into the upper soil layer if the lower layer is saturated. Vertical drainage from the top to the lower soil layer is controlled by field capacity of the top layer (root zone field capacity). Unless the lower soil layer is saturated, any moisture above field capacity in the upper layer moves into the lower layer within a single time step (i.e. wetting fronts are not simulated within a single soil layer). Additionally, upward movement of water into the root zone via unsaturated flow is neglected. Transmissivity, which is the water table thickness multiplied by average Ksat, is apportioned between root zone and deep layers based on water table thickness and root zone depth.

2.4b. Net Solar Radiation and Actual Evapotranspiration

Net solar radiation algorithms are implemented in SMR to better capture the influence of topography on direct, diffuse, and reflected solar radiation and are required as input for the evapotranspiration (ET) and snowmelt algorithms. Reference ET is calculated using the FAO-Penman-Montieth method (Allen *et al.*, 1998) and scaled to actual ET using the single crop coefficient approach described by Allen *et al.* (1998) in FAO Irrigation and Drainage Paper No. 56, hereafter referred to as FAO-56. The primary departure from FAO-56 is in the method used to approximate net solar radiation. SMR computes global (total) short-wave radiation through the GRASS module *R.sun* (Hofierka and Suri, 2002). The *R.sun* module predicts clear-sky (cloud free) irradiance (beam, diffuse, and reflected) on horizontal and sloping surfaces with user-input atmospheric turbidity, day of year, and time of day. The effects of cloud cover were factored into model predictions by calibrating the beam and diffuse radiation coefficients. For a complete description of how *R.sun* radiation coefficients were calibrated, see Appendix C.

Under stress-free conditions, ET occurs at the potential rate given by the reference evapotranspiration ET_0 multiplied by a crop coefficient K_{C}. However, environmental stress can induce stomatal closure and significantly reduce the actual rate at which leaves transpire. As with Brooks *et al*. (2007) the only stress condition considered in SMR is shortage of plant available water PAW, defined in Equation (4) in terms of root depth D_{r} and available water capacity AWC.

$$PAW = D_{\mathrm{r}} \cdot AWC \quad \text{and} \quad AWC = \min(fc, VWC_{\mathrm{rz}}) - wp \tag{4}$$

where VWC_{rz} is volumetric water content in the root zone (cm cm^{-1}), and fc and wp are the field capacity and wilting point moisture contents (cm cm^{-1}) at tension values of 33 kPa and 1500 kPa, respectively. Values for fc and wp were estimated using the pedo-transfer function of Rawls and Brakensiek (1985) to determine the Brooks and Corey (1964) moisture-tension parameters. We adopted the Campbell and Norman (1998) approach to account for the effects of water stress on ET which is an exponential relationship rather than the linear relationship used in the Brooks *et al*. (2007) and Frankenberger *et al*. (1999) versions of SMR. When the root zone water content is below fc, ET is assumed to decline as a function of AWC and a soil-specific shape parameter B as described by Campbell and Norman (1998). This is incorporated into the model as a stress coefficient K_{S}, defined in Equation (5).

$$K_{\mathrm{S}} = 1 - (1 + 1.3 \cdot AWC)^{-B} \quad (5)$$

The B parameter is used to convert between moisture contents and tension values in the derivation of K_{S}. The resulting equation (6) for actual evapotranspiration ET_{A}, upon consideration of water stress and crop development stage is:

$$ET_{\mathrm{A}} = K_{\mathrm{C}} \cdot K_{\mathrm{S}} \cdot ET_0 \quad (6)$$

During the initial stages of growth, from emergence to early tillering, the majority of ET_{A} comes as a result of water evaporating from the top 10-15 cm of soil. In the FAO-56 single crop coefficient approach, K_{C} during the initial stage of crop growth (~10% cover) is adjusted for frequency of wetting. Transpiration is assumed to be zero when no live crop is present and ET_{A} is fully attributed to evaporation from the soil surface. Over the non-growing season, a thin top soil layer of 15 cm thickness is added to the model in order to simulate soil evaporation, with ET_{A} calculated using the initial stage K_{C} value adjusted for wetting frequency over the non-growing period. Water-limited soil evaporation assumes a linear decline after a readily evaporable fraction is exceeded, according to the FAO-56 method. After planting, the thin top soil layer is removed and all ET_{A} occurs from the root zone.

2.5. Water Balance Approximation from Observed Data

The ability of the model to replicate catchment-scale water fluxes was assessed with the catchment water balance shown in Equation (7). The observed precipitation P, runoff RO, tile line drainage TL, and sensor-approximated soil water storage ΔS terms are placed on the left-hand side, and the estimated residual terms, deep percolation DP and ET_{A} are placed on the right-hand side of Equation (7).

$$P - \Delta S - RO - TL = ET_{\mathrm{A}} + DP \quad \text{(mm)} \quad (7)$$

Approximations for ΔS were made at microsites using the calibrated Decagon moisture sensors at depths of 30 cm, 60 cm, and 90 cm and determined as the average change in moisture content for the three depths combined, multiplied by 900 mm for conversion to mm water held within a 90 cm profile. Due to intermittent failure of the sensors, it was often not possible to obtain corrected sensor values at all microsites such that the actual sample size (N) used to calculate changes in water storage in each catchment was less than 12 (N=8 for Colfax, N=8 for Genesee, N=7 for Troy, and N=3 for Leland). Mean catchment ΔS was approximated as the average of ΔS from each microsite. Loss by lateral flow across the catchment boundary was considered negligible.

2.6. Model Spatial and Temporal Assessment

2.6a. Surface Runoff

Surface runoff is an integrated response of the catchment to precipitation, and its prediction is required for satisfactory modeling of the catchment water balance. The definition of "satisfactory" adopted here is the one given by Moriasi *et al*. (2007) as Nash-Sutcliffe efficiency NSE greater than 0.5, percent bias $PBIAS$ within ± 25%, and ratio of root mean square error to the standard deviation of measured data RSR less than 0.70. The NSE is a ratio of error variance "noise" to data variance "information" while $PBIAS$ indicates the tendency of a model to overestimate (+) or underestimate (-) the flow relative to observed flow magnitude. The NSE, $PBIAS$, and RSR are calculated according to Equation (8), where Q_{obs} is observed discharge (mm d^{-1}), Q_{sim} is simulated discharge (mm d^{-1}), and $\bar{Q}_{\mathrm{obs}}$ is mean observed discharge (mm d^{-1}).

(a) $NSE = 1 - \frac{\sum(Q_{\mathrm{obs}} - Q_{\mathrm{sim}})^2}{\sum(Q_{\mathrm{obs}} - \bar{Q}_{\mathrm{obs}})^2}$

(b) $PBIAS = 100\ \frac{\sum(Q_{\mathrm{sim}} - Q_{\mathrm{obs}})}{\sum Q_{\mathrm{obs}}}$ (8)

(c) $RSR = \sqrt{\frac{\sum(Q_{\mathrm{obs}} - Q_{\mathrm{sim}})^2}{\sum(Q_{\mathrm{obs}} - \bar{Q}_{\mathrm{obs}})^2}}$

2.6b. Soil Moisture

Simulated root zone water content VWC_{SIM} (cm cm^{-1}) was compared with water content determined from soil samples VWC_{SAMP} over the same depth range used by the model. For example, if the modeled root zone depth on the date of soil sampling was 90 cm, then the 0-30 cm, 30-60 cm, and 60-90 cm soil samples were averaged to obtain VWC_{SAMP} . During the non-growing season, defined as the time from harvest of one crop to sowing of the next crop, the root zone layer was replaced with a 0-30 cm "root zone" layer. Moisture in this layer was compared to 0-30 cm VWC_{SAMP} . The majority (77%) of samples were taken during the non-growing season while the

remaining samples were taken typically once or twice during the growing season. Agreement between VWC_{SAMP} and VWC_{SIM} was assessed with the root mean square error $RMSE$ calculated according to Equation (9) as:

$$RMSE = \sqrt{\frac{1}{N}\sum(VWC_{\mathrm{SIM}} - VWC_{\mathrm{SAMP}})^2} \quad (9)$$

Equation (9) was also used to assess the accuracy of corrected 5TM/5TE sensor readings. For comparison of VWC during the growing season (including winter dormancy), water contents were aggregated according to the simulated rooting depth, so that for the example above using a rooting depth of 90 cm, the 0-30 cm, 30-60 cm, and 60-90 cm soil samples were averaged and compared to the average of 30 cm, 60 cm, and 90 cm 5TM/5TE sensor readings. Over the non-growing season, the 30 cm sensor was compared to 0-30 cm soil samples.

Field-calibrated moisture sensors were used to assess the model's ability to capture both fine-scale (hourly) fluctuations and long term (seasonal) changes in soil moisture. Since there was little variability in soil moisture at the sub-day time scale, average daily moisture content from the Decagon sensors was compared to the simulated water content at noon each day. The seasonal trends of particular interest were the dry-down period (May through July) and the wetting-up period (typically late October through early March). Good visual agreement in simulated and sensor dry-down curves was interpreted as indication of satisfactory ET_{A} predictions, while VWC over the wetting-up period was important for assessing DP predictions.

2.6c. Perched Water Tables (PWTs) and Saturation Patterns

The spatial distribution of PWTs was modelled by calculating the average number of days per year in which perched water depth (PWD) was less than 30 cm. The PWD is determined as depth measured from the soil surface to the surface of the water table. The term "saturation" used in the context of saturation patterns refers a PWD less than 30 cm, not necessarily total profile saturation. The Decagon moisture sensors (uncorrected) installed at the 30 cm depth mark at each microsite were used for determining the observed number of days per year in which PWD was less than 30 cm. By this method, presence of a nearby water table was discerned from time-series plots of moisture as nearly constant, high water content. Small changes in water content indicate the sensor is within the capillary fringe layer where water content is at or very near saturation. Manual water table measurements taken from an observation well or data from a pressure sensor installed in a few wells were used to confirm the actual water table level. An example of this method is shown in Appendix C.

2.7. Model Calibration

The SMR model was calibrated at each of the catchments for the combined 2012-2014 water years. The three calibration parameters were a spatially-variable soil depth, saturated hydraulic conductivity of restricting layer $Ksat_{\mathrm{R}}$, and a maximum rooting depth Dr_{MAX} that depends on crop type and local soil depth. Soil depth determines total profile storage capacity and $Ksat_{\mathrm{R}}$ controls drainage rate through the restricting layer. These two parameters directly influence percolation, surface runoff, and subsurface lateral flow, while Dr_{MAX} does so indirectly.

Crop rooting depth influences the rate of soil water depletion over the growing season through its control of the fraction of soil depth in which root water uptake occurs. Root growth was partitioned into four stages corresponding with the four stages of crop growth outlined in FAO-56. The four stages include an initial stage from sowing to ~10% cover, a development stage from 10% cover to effective full cover, a mid-season stage from effective full cover to the beginning of maturity, and a late-season stage from maturity to harvest. Root depths were specified at the beginning and end of each stage and assumed to increase linearly between stages, with Dr_{MAX} being reached at the beginning of the late-season stage, or earlier if soil depth imposed a limitation, and assumed constant thereafter to harvest.

Maximum rooting depth was adjusted from FAO-56 tabulated values by crop. By assuming that plant roots do not penetrate the restricting layer, a local Dr_{MAX} was determined as the minimum of soil depth and the Dr_{MAX} in deep soil. The initial approximation of BD_{C} was 1.65 g cm^{-3} as suggested by the Natural Resources Conservation Service (2008) for silt loam soils. The initial $Ksat_{\mathrm{R}}$ estimate was equal to the soil survey value $Ksat_{\mathrm{SS}}$ divided by 100. It has been found in previous modeling efforts (Brooks *et al.*, 2007; Dijksma *et al*., 2011) that Ksat estimates based on soil core measurements in the restrictive horizon, such as those provided by the SSURGO database, are typically between one and two orders of magnitude larger than the drainage rate through these layers observed in the field. Presumably this is due to the fact that restrictive soil horizons can often be much thicker than individual soil cores used in laboratory analysis.

Soil depth and $Ksat_{\mathrm{R}}$ were manually calibrated through a structured iterative process. Individual model runs were evaluated by first comparing the simulated runoff hydrograph to observed flow (if measured) at the outlet. Simulated runoff was checked against the observed runoff hydrograph in all measurement years (2013-2014 for Troy and 2012-2014 for Leland). Following the guidelines of Moriasi *et al*. (2007), a trial was considered successful if $NSE > 0.5$ over the period of simulation. Additional adjustments were made to $Ksat_{\mathrm{R}}$ and BD_{C} (i.e. soil depth) to improve the

accuracy of PWD predictions. For the sub-regions where runoff is small or negligible, and where seasonal water tables are sparse or non-occurring, $Ksat_{\mathrm{R}}$ and BD_{C} were calibrated to soil moisture data and tile flow (Genesee) or soil moisture alone (Colfax). Secondarily, Dr_{MAX} was adjusted to influence onset of runoff following the fall and early winter recharge of the soil. Rooting depth influences the depth to which soil water depletion occurs via plant transpiration over the growing season, which in turn affects the volume of water the soil is able to absorb during the recharge period before runoff is generated.

2.8. Spatial Comparison of Model Output with RapidEye™ Satellite Imagery

NDVI computed from a July 2013 (corresponding with crop senescence) RapidEye™ satellite image was compared pixel-by-pixel with modeled PAW and cumulative evapotranspiration ET_{CUM} at each of the four fields. The change in correlation coefficient (Pearson) with time over the 2013 growing season was plotted for both daily ET_{A} and PAW in order to determine the optimal time (highest correlation) for comparing ET_{A} and PAW with NDVI. A single day was selected for PAW based on its strength of correlation with NDVI, as well as the corresponding stage of crop development. An effort was made to capture the critical period of crop senescence with the PAW comparison and to capture the late vegetative growth stage through ripening with the ET_{CUM} comparison.

3. RESULTS

3.1. Calibration Parameters

The calibrated BD_{C} values for determining a spatially-variable soil depth were 1.64, 1.69, and 1.65 g cm^{-3} for Genesee, Leland, and Troy catchments, respectively. The restricting layers (if existent) at Colfax are not well defined; therefore, rather than BD_{C} , a boundary layer BD value was set at a uniform depth of 150 cm based on the field-wide average BD at 150 cm as determined from the kriged BD map. The boundary layer BD was 1.52 g cm^{-3} with a calibrated hydraulic conductivity equal to $Ksat_{\mathrm{SS}}$/100 (0.144 mm h^{-1}). In the remaining three catchments, the calibrated $Ksat_{\mathrm{R}}$ values were 0.051 mm h^{-1} ($Ksat_{\mathrm{SS}}$/300), 0.031 mm h^{-1} ($Ksat_{\mathrm{SS}}$/60), and 0.013 mm h^{-1} ($Ksat_{\mathrm{SS}}$/300) for Genesee, Leland and Troy, respectively. Maximum rooting depth for various crops had a notable effect on annual water yields, and indirectly on runoff generation. Initially using default rooting depths from FAO-56 at Leland and Troy, runoff was under-predicted the year following garbanzos or spring wheat and over-predicted following winter wheat. It was reasoned that the under-prediction following spring wheat or garbanzos was due in part to over-prediction of water uptake in deep soils. FAO-56 reports maximum rooting depths of 100-150 cm for spring wheat and 60-100 cm for garbanzos.

Decreasing the maximum rooting depth of garbanzos from 90 cm to 75 cm and spring wheat from 150 to 115 cm decreased the volume of winter precipitation and snowmelt that could be stored over the non-growing season and ultimately resulted in better hydrograph fits. The maximum rooting depths used for winter wheat, spring barley, and canola were 150 cm, 115 cm, and 115 cm, respectively.

3.2. Surface Runoff and Tile Drainage

The timing and magnitude of runoff simulated by SMR generally agreed well with observations when flow data for a given catchment were analyzed as a single time series; however, when data were divided into individual water years, the agreement was poor at Leland for both the 2013 and 2014 water years. The hydrograph fit by water year improved considerably when weekly rather than daily totals were analyzed (see Table V). Hydrographs for the daily surface discharge are shown in Figure 6. Runoff was observed at Genesee only in 2012 (1.24 mm total); however, the tile line at Genesee was observed to run nearly year-round, with a cumulative tile flow of 97 mm over the period from 27 February 2012 to 11 August 2014. The effect of the tile drain on saturation and surface runoff at the Genesee catchment was assessed by running the model first without the tile and then with the tile. Inclusion of the tile line resulted in measurable improvement of predicted surface runoff and saturation patterns. Surface runoff decreased from 50 mm without the tile to 15 mm with the tile over the three-year simulation period, compared to 1 mm observed runoff.

3.3. Root Zone Volumetric Water Content

The spatio-temporal patterns of soil moisture were better captured by the model during periods when no crop was present. The $RMSE$ between VWC_{SAMP} and VWC_{SIM} for all fields and all years was 0.040 cm cm^{-1} (N=294) over all non-growing seasons. However, model $RMSE$ increased to 0.048 cm cm^{-1} (N=103) for growing-season predictions (see Figure 7a). Model simulations actually performed slightly better than calibrated sensors during non-crop periods, but the opposite was true during individual crop growing seasons. Table VI shows a comparison of $RMSE$ calculated for VWC_{SIM} and for VWC_{SENS}.

The time-series plots of VWC_{SIM} and VWC_{SENS} show generally good agreement with regards to the rate of dry-down over each growing season (see Figure 8). An exception was the 2012 season at both Leland (planted to garbanzos) and Colfax (planted to winter wheat), in which the simulated root zone water depletion occurred more rapidly than reported by the sensors. The modest decline in dry-season soil moisture at the Troy field in the 2014 crop year came as a result of crop failure, which was not simulated by the model.

3.4. Simulated and Approximated Water Balance

Simulated water balance totals generally agreed well with water balance components approximated from the observed precipitation, surface runoff, and tile line data. The sum $ET_{\mathrm{A}} + DP$ calculated as residual water from the Equation (7) catchment water balance is shown in Table VII alongside measured precipitation, surface runoff, and outflow from the Genesee tile drain. Separated ET_{A} and DP components predicted by the model are presented in Table VIII with totals by field and water year (1 October-30 September). The cumulatively plotted sums: $P - \Delta\mathrm{S} = ET_{\mathrm{A}} + DP + TL + RO$ for model simulations and the water balance calculated from observed P and approximated $\Delta\mathrm{S}$ (Figure 9) show close agreement for all fields except Troy.

3.5. Frequency of Saturation

The SMR model was able to match the frequency and spatial patterns of soil saturation within each field reasonably well. Saturation maps are shown along with maps of topographic wetness index (Beven and Kirkby, 1979) and soil depth in Figures 10-12 for Genesee, Leland, and Troy, respectively. Only three of twelve microsites at Genesee were seasonally saturated during the three-year observation period. Two of these microsites are located in the main draw while the third is situated on a south-facing slope with a restrictive horizon at 90-120 cm. Annual days of saturation at the wettest microsite decreased from 39 d yr^{-1} (days per year) with tile drain removed to 26 d yr^{-1} with tile drain included in the simulation. Overall, the model over-predicted seasonal saturation at Genesee (*PBIAS* = +55%, *RMSE*=3 d yr^{-1}, N=12) and under-predicted frequency of saturation at Leland (*PBIAS*= -35%, *RMSE*= 25 d yr^{-1}, N=12) and Troy (*PBIAS*= -24%, *RMSE*=28 d yr^{-1}, N=12).

3.6. Comparison of ET_{CUM}, PAW, and NDVI

The spatial patterns revealed by NDVI images most closely matched PAW and ET_{CUM} patterns at the wetter fields (Leland and Troy). Figures 13-16 show maps of simulated ET_{CUM}, PAW, and calculated July 2013 NDVI at each catchment. The best results were obtained at the Leland field where PAW simulated on 19 June 2013 explained 20% of the variability in an NDVI image captured 9 July 2013. Correlations were comparatively poor at the drier locations (Genesee and Colfax). The goodness-of-fit statistics by field are provided in Table IX. Results in both Figure 15 and Table IX for the Genesee catchment apply to the no-tile simulation, as the correlations were weaker when modeling the tile line (data not shown).

4. DISCUSSION

4.1. Regional Trends in Catchment Hydrology

The SMR model was able to simulate the unique landscape hydrology of each catchment, especially in fields with a well-defined hydraulic restricting layer. The combination of deep soils and low MAP at the Colfax site make lateral flow negligible despite steep catchment topography. Simulations at the site with intermediate precipitation and soil depth showed lateral flow occurring along backslopes with a hydraulic restricting layer and subsequent accumulation of water in toeslopes. Farther east at the Troy and Leland catchments, field observations confirm, in support of the SSURGO soil survey, that restrictive layers are more widespread. At the Leland catchment, north-facing slopes and flat areas tend to be the shallowest and wettest while south-facing slopes have the deepest soils and saturate very infrequently. At the Troy site, toeslopes and draws tend to have relatively deep soils while both north and south-facing slopes have relatively shallow soils, except at higher elevations where Larkin silt loam is the predominant soil type. Observed saturation patterns, to a large degree, reflect trends in soil depth, with shallow soils tending to be the first to generate runoff and also the first to drain when situated on upper hillslopes. Generation of runoff from deeper soils is delayed until lateral inflow from upslope drainage is sufficient to bring the water table to the surface. Once the saturation-excess process begins, these deep soils make a sustained contribution to catchment outflow.

The model under-predicted saturation on backslopes and over-predicted saturation in toeslopes and draws. The most likely explanation is that lateral Ksat was set too high, and saturation was driven too much by topography and upslope drainage (wetness index) and too little by soil depth (refer to Figures 10-12) . The observed surface runoff for the combined 2013 and 2014 water years was three times greater and saturation more sustained at the Troy catchment than at Leland despite similar precipitation and soil depths. This suggests either that deep percolation through the restricting layer occurred more rapidly or that there was more evaporation of water detained at the surface at the Leland catchment. In other words, the model assumption that all saturation-excess water reaches the catchment outlet within a single time step may not be valid in the Leland catchment where the detention time of excess water in certain parts of the watershed may be sufficiently long to permit re-infiltration or evaporation of ponded water.

4.2. Possible Discontinuity in Restricting Layers

In 2014, at both Troy and Leland catchments, the model predicted runoff between one and two months longer into the spring than observed. This suggests either that ET_{A} or DP were under-

predicted. In fragipans and argillic horizons, cracks can form as a result of dry conditions (Saether and de Caritat, 1997). These cracks and fissures provide preferential flow pathways for percolating water (Bruggeman, 1997; Western and Grayson, 2000; Western *et al.*, 2002) and limited root penetration (Soil Survey Staff, 1999). Plant roots tend to clump in the openings of high impedance soil layers, resulting in severely-restricted water uptake from the deeper subsoil (Gregory, 2006), so it would seem unlikely that the presence of deep macropores would lead to any considerable increase in ET. A more likely scenario is given by Brooks *et al*. (2007) who speculated that cracks in the fragipan were leading to possible recharge sites on their hillslope in Troy, ID. It is therefore possible that percolation in the Leland and Troy catchments was enhanced by deep macropores in the argillic layers. Without knowledge of discontinuities in the argillic horizon, model simulations were limited to a uniform $Ksat_{\mathrm{R}}$.

4.3. Catchment Water Balance

From the cumulative water balance plots in Figure 9, all catchments other than Troy exhibited reasonably good agreement with the temporal trends and magnitude in cumulative total losses ($ET + DP + RO + TL$). Uniquely at Troy, the 2012 simulated losses were less than the losses determined using the observed data. A possible explanation is that percolated water from upland areas hits a confining layer and ultimately re-surfaces farther downslope. The upper-elevation south-facing slopes of the Troy catchment are predominately in Larkin Silt loam soil, which is considerably deeper than the Southwick silt loam of lowland areas. Midway through the south-facing slope at Troy we observed a large seep or spring that remained wet well into the growing season (see Figure 17). This saturated area often produced little to no crop. Although we do not know the source, we speculate that a deep restrictive layer beneath these Larkin soils may be directing subsurface flow to downslope seep locations, where once this water emerges, it either evaporates or becomes surface runoff. No attempt was made in the model to track the percolated water, and therefore re-emergent spring flow was not simulated.

4.4. Spatial Patterns of ET_{CUM}, PAW, and NDVI

At all catchments, ET_{A} patterns matched best with NDVI after the biomass peaked in May-June. A likely reason is that early in the season before full canopy cover, a significant fraction of ET comes from soil evaporation. Soil moisture distribution and cumulative ET mapping with the model explained at least some (maximum of 20%) of the spatial variability in crop senescence observed with RapidEye™ satellite imagery. The fact that not more variability could be explained is due either to errors in model estimates or else complex, and frequently nonlinear interactions between nitrogen,

PAW, crop biomass, and the spectral response of the crop. Multiple studies point to the influence of vegetation and topography on the spatial organization of soil moisture (Ladson and Moore, 1992; Qiu *et al*., 2001; Western *et al*., 2002). Topography has also been shown to contribute greatly to variability in soil fertility and crop yield (Bhatti *et al*., 1991; Mulla, 1993) as well as nitrogen use efficiency (Fiez *et al.*, 1994, 1995) and soil organic carbon (Huggins and Uberuaga, 2010) in the Palouse region. These studies would suggest additional variability in senescence patterns could be explained by integrating terrain attributes with remotely-sensed imagery as in (Ladson and Moore, 1992; Temimi *et al*., 2010). The potential is also great for combining remote sensing with geostatistical analysis for mapping soil properties such as texture and organic matter (Mulla, 2013) that have a measurable effect on crop productivity.

The simulated PAW, ET_{A}, ET_{CUM}, and calculated NDVI all appeared to be heavily influenced by soil depth at the Troy and Leland catchments. This result is not surprising since shallow soils can hold less water and dry-up more rapidly than deep soils. It is speculated that simulated PAW at the two drier, steeper-sloping catchments was less able to capture observed senescence patterns because of greater variability in organic matter (which was not captured by the model) with landscape position (see Figure A-3 of Appendix A). This variability is likely leftover from many years of soil erosion, a well-documented, historical problem for the Palouse region (Frazier *et al*., 1983; Pimentel *et al*., 1995; Kok *et al.*, 2009). The importance of soil organic matter (SOM) in determining available water capacity (AWC) has been stressed notably by Hudson (1994). It is speculated that an important source of error in simulated PAW was failure by the model to capture differences in AWC arising from changes in SOM. This model deficiency can be addressed by choosing a pedo-transfer function that accounts for SOM such as that of Rawls *et al*. (1982). The better correlations between PAW and NDVI at the two wetter field sites with more restrictive soils reflects the close relationship between soil depth and water dynamics in the root zone, which the model was able to capture quite effectively.

5. SUMMARY AND CONCLUSION

Rapid advances in remote and proximal sensing technologies, together with powerful methods of spatial interpolation, are providing the type of spatial data layers required for parameterizing and validating distributed hydrologic models. In this study, parameterization of the distributed model, SMR was improved with high-resolution bulk density maps, while *in-situ* measurements of PWD and manual soil moisture sampling at 12 monitoring locations within each catchment improved model spatial assessment. Model temporal assessment was improved with

continuous (hourly) moisture monitoring using Decagon 5TM/5TE moisture sensors that tracked root zone VWC fluctuations at five depths. This study also used model predictions of PAW and ET_{CUM} to help explain crop senescence patterns observed with the RapidEye™ satellite.

We recommend the SMR model as a tool for capturing spatial moisture patterns and surface runoff in dryland cereal systems of the Palouse region. Its effectiveness has been demonstrated in four catchments with unique soils, climate, and topography. While a few opportunities for improvement have been noted, the SMR model framework, using open-source tools and detailed spatial input, is a very hopeful way forward to distributed hydrologic modelling applications in precision agriculture, water quality management, and similar endeavors.

6. REFERENCES

Allen RG, Pereira LS, Raes D, Smith M. 1998. Crop evapotranspiration--guidelines for computing crop water requirements, Irrigation and Drainage Paper 56, 174pp. Food and Agriculture Organization of the United Nations: Rome, Italy.

Arnold JG, Srinivasan R, Muttiah RS, Williams JR. 1998. Large area hydrologic modeling and assessment part I: model development. *Journal of the American Water Resources Association* **34**(1): 73-89. DOI: 10.1111/j.1752-1688.1998.tb05961.x

Barker RJ. 1981. Soil survey of Latah County Area, Idaho, 166pp. U.S. Department of Agriculture—Soil Conservation Service (Natural Resources Conservation Service). U.S. Government Printing Office, Washington, DC. Accessed December 25, 2015 at http://www.nrcs.usda.gov/Internet/FSE_ MANUSCRIPTS/idaho/LatahID1981/latahID1981.pdf.

Beasley DB, Huggins LF, Monke EJ. 1980. ANSWERS: a model for watershed planning. *Transactions of the ASAE* **23**(4): 938-944.

Beven KJ. 1989. Changing ideas in hydrology: the case of physically-based models. *Journal of Hydrology* **105**(1-2): 157-172. DOI: 10.1016/0022-1694(89)90101-7

Beven KJ. 1996. (Chapter 13A) A discussion of distributed hydrologic modeling. In *Distributed Hydrological Modelling*, Abbot MB, Refsgaard (eds). Kluwer Academic Publishers: Netherlands; 255-278.

Beven KJ, Calver A, Morris EM. 1987. The Institute of Hydrology distributed model, Institute of Hydrology Report No. 98 (unpublished), 33pp. Wallingford, Institute of Hydrology. Accessed December 13, 2015 at http://nora.nerc.ac.uk/5977/1/IH_098.pdf.

Beven KJ, Kirkby MJ. 1979. A physically based, variable contributing area model of basin hydrology. *Hydrological Sciences-Bulletin* **24**(1): 43-69. DOI: 10.1080/02626667909491834

Beven K, Warren R, Zaoui J. 1980. SHE: towards a methodology for physically-based distributed forecasting in hydrology. In *Hydrological Forecasting—(Proceedings of the Oxford Symposium, April 1980)*, IAHS Publication No. 129; 133-137.

Bhatti AU, Mulla DJ, Frazier BE. 1991. Estimation of soil properties and wheat yields on complex eroded hills using geostatistics and Thematic Mapper images. *Remote Sensing of Environment* **37**(3): 181-191. DOI: 10.1016/0034-4257(91)90080-P

Blackbridge, 2012. Satellite Imagery Product Specifications version 6.1, 48pp. Accessed December 13, 2015 at http://blackbridge.com/rapideye/upload/RE_Product_Specifications_ENG.pdf.

Boll J, Brooks ES, Campbell CR, Stockle CO, Young SK, Hammel JE, McDaniel PA. 1998. Progress toward development of a GIS based water quality management tool for small rural watersheds: modification and application of a distributed model. In *1998 ASAE Annual International Meeting in Orlando, Florida, July 12-16*. ASAE: St Joseph, MI; paper 982230.

Brooks ES. 2003. *Distributed hydrologic modeling of the eastern Palouse*, PhD dissertation, 158pp. University of Idaho, Moscow, ID.

Brooks ES, Boll J. 2005. A simple GIS-based snow accumulation and melt model. In *Proceedings of the 2005 Western Snow Conference, 11-14 April, Great Falls, MT*, McGurk B, (ed). Western Snow Conference; 123-129.

Brooks ES, Boll J, McDaniel PA. 2004. A hillslope-scale experiment to measure lateral saturated hydraulic conductivity. *Water Resources Research* **40**: W04208. DOI: 10.1029/2003WR002858

Brooks ES, Boll J, McDaniel PA. 2007. Distributed and integrated response of a geographic information system-based hydrologic model in the eastern Palouse region, Idaho. *Hydrological Processes* **21**: 110-122. DOI: 10.1002/hyp.6230

Brooks ES, Boll J, McDaniel PA. 2012. (Chapter 10) Hydropedology in seasonally dry landscapes: the Palouse region of the Pacific Northwest, USA. In *Hydropedology: Synergistic Integration of Soil Science and Hydrology*, Lin H (ed). Academic Press: Elsevier B.V.; 329-350.

Brooks RH, Corey AT. 1964. Hydraulic properties of porous media, Hydrology Papers No. 3, 37pp. Corey AT, Dils RE, Yevdjevich VM (eds). Colorado State University, Fort Collins, CO.

Bruggeman AC. 1997. *Preferential Movement of Solutes Through Soils*, PhD Dissertation, 323pp. Virginia Polytechnic Institute and State University, Blacksburg, VA.

Busacca AJ. 1989. Long quaternary record in eastern Washington, U.S.A., interpreted from multiple buried paleosols in loess. *Geoderma* **45**(2): 105–122. DOI: 10.1016/0016-7061(89)90045-1

Calver A, Wood WL. 1995. The Institute of Hydrology distributed model. In *Computer Models of Watershed Hydrology*, Singh VP (ed). Water Resources Publications: Colorado, USA; 809-846.

Campbell GS, Norman JM. 1998. *An Introduction to Environmental Biophysics*, *Second Edition*, 286pp. Springer: New York, NY.

Canton Y, Sole-Benet A, Domingo F. 2004. Temporal and spatial patterns of soil moisture in semiarid badlands of SE Spain. *Journal of Hydrology* **285**(1-4): 199-214. DOI: 10.1016/j.jhydrol.2003.08.018

Childs EC. 1971. Drainage of groundwater resting on a sloping bed. *Water Resources Research* **7**(5): 1256-1263. DOI: 10.1029/WR007i005p01256

Dijksma R, Brooks ES, Boll J. 2011. Groundwater recharge in Pleistocene sediments overlying basalt aquifers in the Palouse Basin, USA: modeling of distributed recharge potential and identifying water pathways. *Hydrogeology Journal* **19**(2): 489-500. DOI: 10.1007/s10040-010-0695-9

Donaldson NC. 1980. Soil survey of Whitman County, Washington. U.S. Department of Agriculture—Natural Resources Conservation Service. U.S. Government Printing Office, Washington, DC. Accessed December 25, 2015 at http://www.nrcs.usda.gov/Internet/FSE_MANUSCRIPTS/washington/WA075/0/wa075_text.pdf.

Dunne T. 1982. Models of runoff processes and their significance. In *Scientific Basis of Water Resource Management*. National Academy Press: Washington, DC; 17-30.

Dunne T, Black RD. 1970. An experimental investigation of runoff production in permeable soils. *Water Resources Research* **6**(2): 478-499. DOI: 10.1029/WR006i002p00478

Dunne T, Moore TR, Taylor CH. 1975. Recognition and prediction of runoff-producing zones in humid regions. *Hydrological Sciences—Bulletin* **20**(3): 305-327.

Fiez TE, Miller BC, Pan WL. 1994. Winter wheat yield and grain protein across varied landscape positions. *Agronomy Journal* **86**(6): 1026-1032.

Fiez TE, Pan WL, Miller BC. 1995. Nitrogen use efficiency of winter wheat among landscape positions. *Soil Science Society of America Journal* **59**(6): 1666-1671.

Frankenberger JR, Boll J, Walter MF. 1996. Identification of runoff generating areas for farm planning in the New York City watershed. In *Watershed Restoration Management: Physical, Chemical and Biological Considerations, Proceedings of the AWRA Annual Symposium, July 14-17,1996 in Syracuse, NY*, McDonnel J (ed). American Water Resources Association; 7-16.

Frankenberger JR, Brooks ES, Walter MT, Walter MF, Steenhuis TS. 1999. A GIS-based variable source area hydrology model. *Hydrological Processes* **13**(6)**:** 805-822. DOI: 10.1002/(SICI)1099-1085(19990430)13:6<805::AID-HYP754>3.0.CO;2-M

Frazier BE, McCool DK, Engle CF. 1983. Soil erosion in the Palouse: an aerial perspective. *Journal of Soil and Water Conservation* **38**(2): 70-74.

Freeze AR. 1974. Streamflow generation. *Reviews of Geophysics and Space Physics* **12**(4): 627-647.

Gburek WJ, Needelman BA, Srinivasan MS. 2006. Fragipan controls on runoff generation: Hydropedological implications at landscape and watershed scales. *Geoderma* **131**(3-4): 330-344. DOI: 10.1016/j.geoderma.2005.03.021

Gomez-Plaza A, Alvarez-Rogel J, Albaladejo J, Castillo VM. 2000. Spatial patterns and temporal stability of soil moisture across a range of scales in a semi-arid environment. *Hydrological Processes* **14**(7): 1261-1277. DOI: 10.1002/(SICI)1099-1085(200005)14:7<1261::AID-HYP40>3.0.CO;2-D

GRASS Development Team. 2012. Geographic Resources Analysis Support System (GRASS) Software. Open Source Geospatial Foundation Project. URL http://grass.osgeo.org.

Grayson RB, Moore ID, McMahon TA. 1992a. Physically based hydrologic modeling 1. A terrain-based model for investigative purposes. *Water Resources Research* **28**(10): 2639-2658. DOI: 10.1029/92WR01258

Grayson RB, Moore ID, McMahon TA. 1992b. Physically based hydrologic modeling 2. Is the concept realistic? *Water Resources Research* **28**(10): 2659-2666. DOI: 10.1029/92WR01259

Gregory PJ. 2006. *Plant Roots: Growth, Activity and Interactions with the Soil*, 328pp. Blackwell Publishing Ltd.

Hammermeister DP, Kling GF, Vomocil JA. 1982. Perched water tables on hillsides in western Oregon I: some factors affecting their development and longevity. *Soil Science Society of America Journal* **46**(4): 811–818.

Hank TB, Bach H, Mauser W. 2015. Using a remote sensing-supported hydro-agroecological model for field-scale simulation of heterogeneous crop growth and yield: application for wheat in Central Europe. *Remote Sensing* **7**: 3934-3965. DIO: 10.3390/rs70403934

Hengl T, Mendes de Jesus J, MacMillan RA, Batjes NH, Heuvelink GBM, Ribeiro E, Samuel-Rosa A, Kempen B, Leenaars JGB, Walsh MG, Gonzalez MR. 2014. SoilGrids1km—Global soil information based on automated mapping. *PLOS ONE* **9**(8), Article No. e105992. DOI: 10.1371/journal.pone.0105992

Hofierka J, Suri M. 2002. The solar radiation model for open source GIS: implementation and applications. In *Proceedings of the Open source GIS-GRASS Users Conference, 2002—Trento, Italy, 11-13 September 2002* [online], Ciolli M, Zatelli P (eds). Accessed December 13, 2015 at http://www.ing.unitn.it/~grass/conferences/GRASS2002/proceedings/proceedings/pdfs/Hofierka_Jaroslav.pdf.

Hudson BD. 1994. Soil organic matter and available water capacity. *Journal of Soil and Water Conservation* **49**(2): 189-194.

Huggins D, Uberuaga D. 2010. (Chapter 14) Field heterogeneity of soil organic carbon and relationships to soil properties and terrain attributes. In *Climate Friendly Farming—Final Report*, CSANR Research Report 2010-001, 23pp. Washington State University Center for Sustaining Agriculture and Natural Resources. Accessed December 14, 2015 at http://csanr.wsu.edu/wp-content/uploads/2013/02/CSANR2010-001.Ch14.pdf.

Ibrahim HM, Huggins DR. 2011. Spatio-temporal patterns of soil water storage under dryland agriculture at the watershed scale. *Journal of Hydrology* **404**(3-4): 186-197. DOI: 10.1016/j.jhydrol.2011.04.029

James LD, Burges SJ. 1982. Selection, calibration and testing of hydrologic models. In *Hydrological Modeling of Small Watersheds*, Haan CT, Johnson P, Brakensiek DL (eds). ASAE Monograph Vol. 5. American Society of Agricultural Engineers: St. Joseph, MI; 435-472.

Jones JW, Hoogenboom G, Porter CH, Boote KJ, Batchelor WD, Hunt LA, Wilkens PW, Singh U, Gijsman AJ, Ritchie JT. 2003. DSSAT cropping system model. *European Journal of Agronomy* **18**: 235-265.

Kirchner JW. 2003. A double paradox in catchment hydrology and geochemistry. *Hydrological Processes* **17**(4): 871-874. DOI: 10.1002/hyp.5108

Kirchner JW. 2006. Getting right answers for the right reasons: linking measurements, analyses, and models to advance the science of hydrology. *Water Resources Research* **42**: W03S04.

DOI: 10.1029/2005WR004362
Klages KHW. 1942. Climate of the Palouse area of Idaho as indicated by fifty years of climatological data on the University farm, University of Idaho Agricultural Experiment Station Bulletin No. 245, 19pp. University of Idaho, Moscow, ID.
Klemes V. 1986. Dilettantism in hydrology: transition of destiny? *Water Resources Research* **22**(9): 177S-188S. DOI: 10.1029/WR022i09Sp0177S
Knisel WG (ed). 1980. CREAMS: a field-scale model for chemicals, runoff, and erosion from agricultural management systems, Conservation Research Report No. 26, 640 pp. U.S. Department of Agriculture—Science and Education Administration.
Kok H, Papendick RI, Saxton KE. 2009. STEEP: Impact of long-term conservation farming research and education in Pacific Northwest Wheatlands. *Journal of Soil and Water Conservation* **64**(4): 253-264. DOI: 10.2489/jswc.64.4.253
Kotchenova SY, Vermote EF. 2007. Validation of a vector version of the 6S radiative transfer code for atmospheric correction of satellite data. Part II. Homogeneous Lambertian and anisotropic surfaces. *Applied Optics* **46**(20): 4455-4464. DOI: 10.1364/AO.46.004455
Kotchenova SY, Vermote EF, Matarrese R, Klemm FJ. 2006. Validation of a vector version of the 6S radiative transfer code for atmospheric correction of satellite data. Part I. Path radiance. *Applied Optics* **45**(26): 6762-6774. DOI: 10.1364/AO.45.006762
Kramer PJ, Boyer JS. 1995. (Chapter 5) Roots and root systems. In *Water Relations of Plants and Soils*. Academic Press, Inc.: San Diego, CA; 115-166.
Ladson AR, Moore ID. 1992. Soil water prediction on the Konza Prairie by microwave remote sensing and topographic attributes. *Journal of Hydrology* **138**(3-4): 385-407. DOI: 10.1016/0022-1694(92)90127-H
Lin H, Brooks E, McDaniel PA, and Boll J. 2008. Hydropedology and surface/subsurface runoff processes. Part 10: Rainfall runoff processes, 25pp. In *Encyclopedia of Hydrological Sciences* [online], Anderson MG (ed). John Wiley & Sons. DOI: 10.1002/0470848944.hsa306
Mallawatantri AP, McConkey BG, Mulla DJ. 1996. Characterization of pesticide sorption and degradation in macropore linings and soil horizons of Thatuna silt loam. *Journal of Environmental Quality* **25**(2): 227-235.
Mauser W, Bach H. 2009. PROMET—large scale distributed hydrological modelling to study the impact of climate change on the water flows of mountain watersheds. *Journal of Hydrology* **376**(3-4): 362-377. DOI: 10.1016/j.jhydrol.2009.07.046
McDaniel PA, Gabehart RW, Falen AL, Hammel JE, Reuter RJ. 2001. Perched water tables on Argixeroll and Fragixeralf hillslopes. *Soil Science Society of America Journal* **65**: 805-810.
McDaniel PA, Regan MP, Brooks E, Boll J, Barndt S, Falen A, Young SK, Hammel JE. 2008. Linking fragipans, perched water tables, and catchment-scale hydrological processes. *Catena* **73**: 166-173. DOI: 10.1016/j.catena.2007.05.011
McDonnell JJ, Woods R. 2004. On the need for catchment classification. *Journal of Hydrology* **299**(1-2): 2-3. DOI: 10.1016/j.jhydrol.2004.09.003
Mehta VK, Walter MT, Brooks ES, Steenhuis TS, Walter MF, Johnson M, Boll J, Thongs D. 2004. Application of SMR to modeling watersheds in the Catskill Mountains. *Environmental Modeling and Assessment* **9**(2): 77-89. DOI: 10.1023/B:ENMO.0000032096.13649.92
Molling CC, Strikwerda JC, Norman JM, Rodgers CA, Wayne R, Morgan CLS, Diak GR, Mecikalski JR. 2005. Distributed runoff formulation designed for a precision agricultural landscape modeling system. *Journal of the American Water Resources Association* **41**(6): 1289-1313.
Moriasi DN, Arnold JG, Van Liew MW, Bingner RL, Harmel RD, Veith TL. 2007. Model evaluation guidelines for systematic quantification of accuracy in watershed simulations. *Transactions of the ASABE* **50**(3): 885-900.

Mulla DJ. 1993. Mapping and managing spatial patterns in soil fertility and crop yield. In *Soil Specific Crop Management*, Robert P, Larson W, Rust R (eds). American Society of Agronomy: Madison, WI; 15-26.

Mulla DJ. 2013. Twenty five years of remote sensing in precision agriculture: Key advances and remaining knowledge gaps. *Biosystems Engineering* **114**(4): 358-371. DOI: 10.1016/j.biosystemseng.2012.08.009

Nace RL. 1980. Hydrology comes of age: impact of the international hydrological decade. *Eos, Transactions of the American Geophysical Union* **61**(53): 1241.

Natural Resources Conservation Service. 2008. Soil health—bulk density/moisture/aeration, Guides for Educators, 11pp. Accessed December 23, 2015 at http://www.nrcs.usda.gov/Internet/FSE_DOCUMENTS/nrcs142p2_050936.pdf.

Needelman BA, Gburek WJ, Petersen GW, Sharpley AN, Kleinman PJA. 2004. Surface runoff along two agricultural hillslopes with contrasting soils. *Soil Science Society of America Journal* **68**: 914–923.

Nelson JR, Lascano RJ, Booker JD, Zartman RE, Goebel TS. 2013. Evaluation of the precision agricultural landscape modeling system (PALMS) in the Semiarid Texas Southern High Plains. *Open Journal of Soil Science* **3**: 169-181. DOI: 10.4236/ojss.2013.34020

Noh SJ, An H, Kim S, Kim H. 2015. Simulation of soil moisture on a hillslope using multiple hydrologic models in comparison to field measurements. *Journal of Hydrology* **523**: 342-355. DOI: 10.1016/j.jhydrol.2015.01.047

Pan W, Schillinger W, Huggins D, Koenig R, Burns J. 2007. (Chapter 10) Fifty years of predicting wheat nitrogen requirements in the Pacific Northwest USA, 6pp. In *Managing Crop Nitrogen for Weather*, Bruulsema T (ed). International Plant Nutrition Institute: Norcross, GA.

Pimentel D, Harvey C, Resosudarmo P, Sinclair K, Kurz D, McNair M, Crist S, Shpritz L, Fitton L, Saffouri R, Blair R. 1995. Environmental and economic costs of soil erosion and conservation benefits. *Science* **267**(5201): 1117-1123.

Poggio M, Brown DJ, Bricklemeyer RS. 2015. Laboratory-based evaluation of optical performance for a new soil penetrometer visible and near-infrared (VisNIR) foreoptic. *Computers and Electronics in Agriculture* **115**: 12-20. DOI: 10.1016/j.compag.2015.05.002

PRISM ClimateGroup. 2012. Oregon State University, http://prism.oregonstate.edu. Accessed December 25, 2015.

Qiu Y, Fu B, Wang J, Chen L. 2001. Soil moisture variation in relation to topography and land use in a hillslope catchment of the Loess Plateau, China. *Journal of Hydrology* **240**(3-4): 243-263. DOI: 10.1016/S0022-1694(00)00362-0

Quinn P, Beven K, Chevallier P, Planchon O. 1991. The prediction of hillslope flow paths for distributed hydrological modelling using digital terrain models. *Hydrologic Processes* **5**(1): 59-79. DOI: 10.1002/hyp.3360050106

Rawls WJ, Brakensiek DL. 1985. Prediction of soil water properties for hydrologic modeling. In *Watershed Management in the Eighties*, Jones EB, Ward TJ (eds). *Proc. Symp., 30 April--1 May, 1985, Denver, CO*. American Society of Civil Engineers: New York, NY; 293-299.

Rawls WJ, Brakensiek DL, Saxton KE. 1982. Estimation of soil water properties. *Transactions of the ASAE* **26**: 1747-1752.

Refsgaard JC, Storm B. 1995. MIKE SHE. In *Computer Models of Watershed Hydrology*, Singh VP (ed). Water Resources Publications: Colorado, USA; 809-846.

Reuter RJ, McDaniel PA, Hammel JE, Falen AL. 1998. Solute transport in seasonal perched water tables in loess-derived soilscapes. *Soil Science Society of America Journal* **62**(4): 977–983.

Ritchie JT. 1998. Soil water balance and plant water stress. In *Understanding Options for Agricultural Production*, Tsuji GY, Hoogenboom G, Thornton PK (eds). Kluwer Academic Publishers: Dordrecht, the Netherlands; 41–54.

RZWQM Development Team. 1992. RZWQM technical documentation, GPSR Technical Report No. 2. U.S. Department of Agriculture--Agricultural Research Service and Great Plains Systems Research: Fort Collins, CO.

Saether OM, de Caritat P (Eds.). 1997. Geochemical Processes, Weathering and Groundwater Recharge in Catchments, 440 pp. A.A. Balkema Publishers: Rotterdam, Netherlands.

Sharpley AN, Williams JR (eds). 1990. EPIC—erosion/productivity impact calculator: 1. Model documentation, Technical Bulletin No. 1768, 235pp. U.S. Department of Agriculture--Agricultural Research Service.

Shi Y, Baldwin DC, Davis KJ, Xuan Y, Duffy CJ, Lin H. 2015. Simulating high-resolution soil moisture patterns in the Shale Hills watershed using a land surface hydrologic model. *Hydrological Processes* **29**(21): 4624-4637. DOI: 10.1002/hyp.10593

Soil Survey Staff. U.S. Department of Agriculture--Natural Resources Conservation Service, Web Soil Survey. Accessed December 13, 2015 at http://websoilsurvey.nrcs.usda.gov/.

Soil Survey Staff. 1999. *Soil Taxonomy—A Basic System of Soil Classification for Making and Interpreting Soil Surveys, Second Edition*. U.S. Depart of Agriculture--Natural Resources Conservation Service. U.S. Government Printing Office: Washington, DC.

Soil Survey Staff. 2006. *Keys to Soil Taxonomy, Tenth Edition***.** U.S. Department of Agriculture--Natural Resources Conservation Service, Washington, DC.

Stockle CO, Donatelli M, Nelson R. 2003. CropSyst, a cropping systems simulation model. *European Journal of Agronomy* **18**(3-4): 289-307. DOI: 10.1016/S1161-0301(02)00109-0

Supit I, Hooijer AA, van Diepen CA (eds). 1994. System description of the WOFOST 6.0 crop simulation model implemented in CGMS, vol. 1: theory and algorithms, EUR 15956 EN, 146pp. Joint Research Centre, European Commission: Luxembourg.

Temimi M, Leconte R, Chaouch N, Sukumal P, Khanbilvardi R, Brissette F. 2010. A combination of remote sensing data and topographic attributes for the spatial and temporal monitoring of soil wetness. *Journal of Hydrology* **388**: 28-40. DOI: 10.1016/j.jhydrol.2010.04.021

Topp GC, Davis JL, Annan AP. 1980. Electromagnetic determination of soil water content: measurements in coaxial transmission lines. *Water Resources Research* **16**(3): 574-582. DOI: 10.1029/WR016i003p00574

Tucker CJ. 1979. Red and photographic infrared linear combinations for monitoring vegetation. *Remote Sensing of Environment* **8**(2): 127-150. DOI: 10.1016/0034-4257(79)90013-0

United States Department of Agriculture, Natural Resources Conservation Service. 2006. *Land Resource Regions and Major Land Resource Areas of the United States, the Carribbean, and the Pacific Basin*. U.S. Department of Agriculture Handbook 296.

Van Dam JC, Huygen J, Wesseling JG, Feddes RA, Kabat P, Van Walsum PEV, Groenendijk P, Van Diepen CA. 1997. Theory of SWAP Version 2.0: simulation of water flow, solute transport and plant growth in the soil-water-atmosphere-plant environment, Technical Document 45, 167pp. Department Water Resources, Wageningen Agricultural University and DLO Winand Staring Center.

Walter MT, Walter MF, Brooks ES, Steenhuis TS, Boll J, Weiler K. 2000. Hydrologically sensitive areas: implications for water quality risk assessment. *Journal of Soil and Water Conservation* **55**(3): 277-284.

Washington Wheat Commission. 2009. Washington wheat facts 2008-2009. Washington Wheat Commission. Accessed December 12, 2015 at http://admin.aghost.net/images/E0177801/2008WF4WebSmHomepage.pdf.

Weiler M, McDonnell JJ. 2007. Conceptualizing lateral preferential flow networks and simulating the effects on gauged and ungauged hillslopes. *Water Resources Research* **43**: W03403. DOI: 10.1029/2006WR004867

Western AW, Grayson RB. 2000. Soil moisture and runoff processes at Tarrawarra. In *Spatial Patterns in Catchment Hydrology--Observations and Modelling*, Grayson RB, Bloschl G (eds). Cambridge University Press: Cambridge; 209-246.

Western AW, Grayson RB, Gunter B. 2002. Scaling of soil moisture: a hydrologic perspective. *Annual Review of Earth and Planetary Sciences* **30**: 149-180. DOI: 10.1146/annurev.earth.30.091201.140434

Wigmosta MA, Vail LW, Lettenmaier DP. 1994. A distributed hydrology-vegetation model for complex terrain. *Water Resources Research* **30**(6): 1665-1679. DOI: 10.1029/94WR00436

Wood EF, Sivapalan M, Beven KJ. 1990. Similarity and scale in catchment storm response. *Reviews of Geophysics* **28**(1): 1-18. DOI: 10.1029/RG028i001p00001

Wood EF, Sivapalan M, Beven KJ, Band L. 1988. Effects of spatial variability and scale with implications to hydrologic modeling. *Journal of Hydrology* **102**(1-4): 29-47. DOI: 10.1016/0022-1694(88)90090-X

Young RA, Onstad CA, Bosch DD, Anderson WP. 1989. AGNPS: A nonpoint-source pollution model for evaluating agricultural watersheds. *Journal of Soil and Water Conservation* **44**(2): 168-173.

7. TABLES

Table IV. Mean annual precipitation (MAP), slope steepness, elevation, and watershed area of the study sites. The MAP is determined from a 800 m resolution regional map of 30-yr (1981-2010) precipitation normals accessed from the PRISM Climate Group, Oregon State University

Field	MAP (mm)	Mean Elevation (m)	Max Slope (%)	Mean Slope (%)	Watershed Area (ha)
Colfax	484	706	45	21	16
Leland	716	736	18	7	11
Genesee	568	821	36	13	12
Troy	675	815	32	11	25

Table V. Effect of time scale (daily or weekly) on the hydrograph fit statistics of Equation (8), shown for individual years, and all years combined (total), where subscripts (OBS.) and (SIM.) are for observed and simulated, respectively

Field	Water Year	Surface Runoff *RO* (mm)		Time Scale					
				Daily			Weekly		
		$RO_{OBS.}$	$RO_{SIM.}$	*NSE*	*RSR*	*PBIAS*	*NSE*	*RSR*	*PBIAS*
Leland	2012	92	80	0.84	0.4	-14%	0.92	0.28	-14%
	2013	20	28	-0.2	1.09	45%	0.26	0.85	45%
	2014	20	37	-1.1	1.45	97%	0.37	0.78	97%
Total		132	145	0.72	0.53	12%	0.88	0.35	12%
Troy	2013	87	89	0.76	0.49	2%	0.90	0.31	2%
	2014	39	70	0.55	0.67	81%	0.57	0.65	81%
Total		126	159	0.7	0.54	26%	0.83	0.41	26%

Table VI. Summary of 5TM/5TE sensor and model simulation accuracies for root zone water content, assessed with root mean square error as given by Equation (9)

Aggregation (all fields & all years)	Accuracy			
	5TM Sensor		Simulated	
	RMSE ($cm\ cm^{-1}$)	N	*RMSE* ($cm\ cm^{-1}$)	N
Growing Season	0.033	51	0.048	103
Non-Growing Season	0.041	219	0.040	294
Combined	0.039	270	0.042	397

Table VII. Simulated (Sim.) and observed (Obs.) water balance components where *P*=precipitation, *RO*=runoff, *TL*=tile line drainage, *DP*=deep percolation, and ET_A=actual evapotranspiration

				Water Balance Components					
Field	Crop[a]		Water Year	*P* (mm)	*RO* (mm)		*TL* (mm)		ET_A+ *DP* (mm)	
					Obs.	Sim.	Obs.	Sim.	Eq. (7)	Sim.
Colfax	WW		2012	423	0	0	NA	NA	432	462
	SW		2013	467	0	0	NA	NA	427	389
	SW		2014	315	0	0	NA	NA	371	337
		Total		1205	0	0	NA	NA	1230	1188
Genesee	SW		2012	529	1	13	(44+)[d]	42	545	531
	SB		2013	522	0	0	26	15	495	477
	Can		2014	443	0	2	30	21	493	464
		Total		1494	1	15	(100+)	78	1533	1472
Troy	GBS		2012	599	NA[b]	174	NA	NA	453	370
	WW		2013	572	87	89	NA	NA	478	518
	GBS		2014	470	39	70	NA	NA	382	380
		Total		1042	NA	333	NA	NA	1313	1268
Leland	GBS		2012	638	(92+)[c]	81	NA	NA	600	511
	WW		2013	604	20	28	NA	NA	616	589
	SW		2014	481	20	39	NA	NA	536	485
		Total		1723	(132+)	148	NA	NA	1752	1585

[a]WW=winter wheat, SW=spring wheat, SB=spring barley, GBS=garbanzos, Can=canola

[b]Surface runoff measurements did not begin at the Troy field until 30 November 2012.

[c]Incomplete water year, flume measurements did not begin until 2 February 2012

[d]Incomplete water year, tile line measurements did not begin until 27 February 2012

Table VIII. Modeled residual components of Equation (7) water balance for all four sites and all three simulation years where *DP*=deep percolation and ET_A=actual evapotranspiration

		Field Location							
		Colfax		Genesee		Troy		Leland	
Water Year		ET_A (mm)	*DP* (mm)	ET_A (mm)	*DP* (mm)	ET_A (mm)	*DP* (mm)	ET_A (mm)	*DP* (mm)
2012		462	0	367	164	303	67	385	126
2013		308	81	332	145	462	56	478	111
2014		313	24	345	119	317	63	395	90
	Total	1083	105	1044	428	1082	186	1258	327

Table IX. Correlation (R) and determination coefficient (R^2) between cumulative evapotranspiration ET_{CUM} and normalized difference vegetation index (NDVI) and between plant available water *PAW* and NDVI

Field	Map Date (Range)			Correlation with NDVI					
	ET_{CUM}	NDVI	*PAW*	ET_{CUM}			*PAW*		
				R	R^2	N	R	R^2	N
Colfax	11 June-17 June	27 July	31 May	0.39	0.15	1556	0.36	0.13	1556
Genesee	24 May-28 June	24 July	24 May	0.34	0.12	1110	0.38	0.14	1110
Troy	11 May-24 July	16 July	5 July	0.44	0.19	2360	0.43	0.18	2360
Leland	18 May-24 July	9 July	19 June	0.41	0.17	1097	0.45	0.20	1097

8. FIGURES

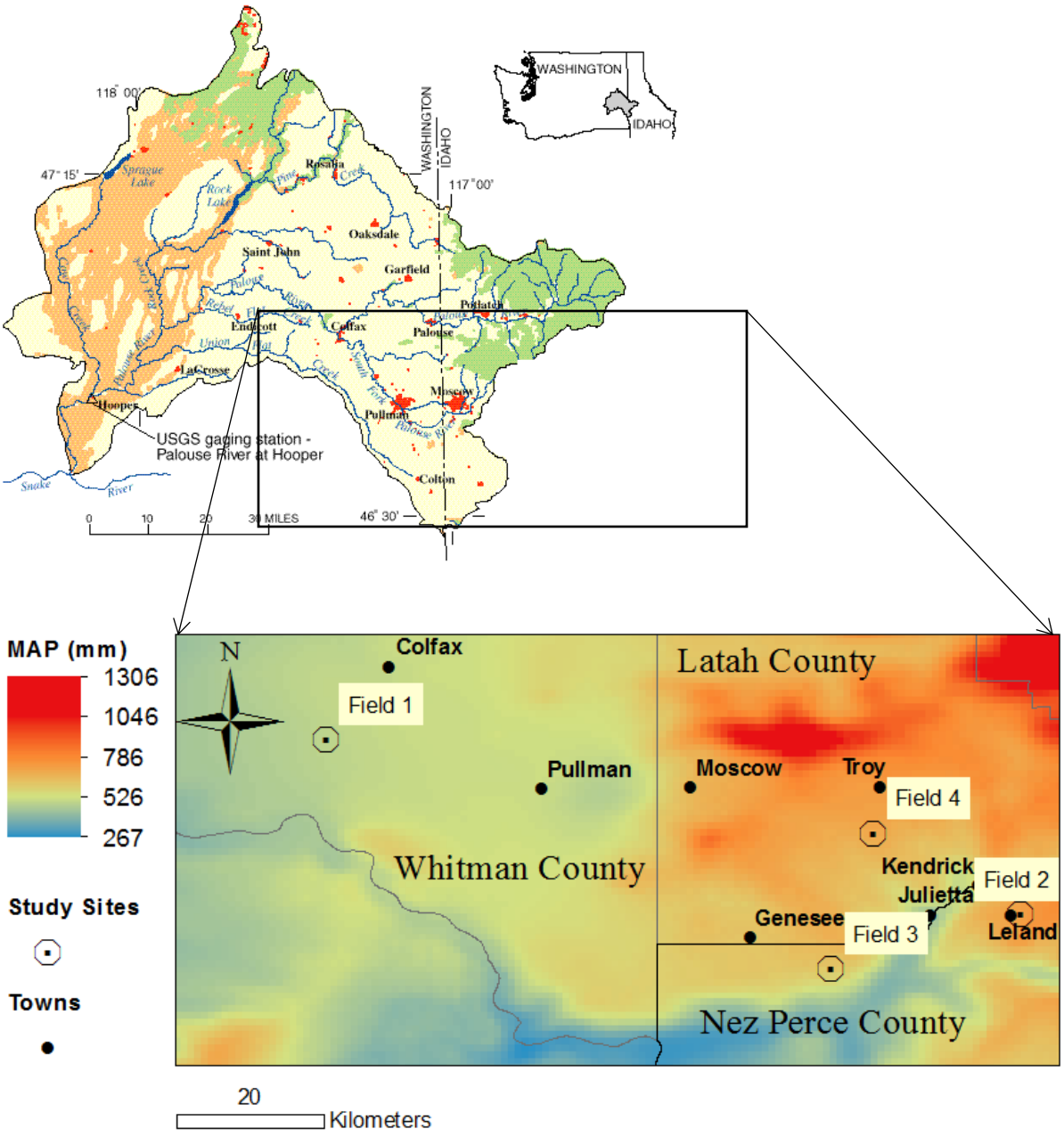

Figure 5. Field locations with color gradient showing regional variation in mean annual precipitation (MAP) determined according the PRISM climate model 30-yr precipitation normals (PRISM Climate Group, Oregon State University, http://prism.oregonstate.edu, map created 10 July 2012). The Troy and Leland sites are just east of the Palouse River Basin boundary as it has been mapped by Ebbert and Roe (top), 1998, map accessed December 12, 2015 at http://wa.water.usgs.gov/pubs/fs/fs069-98/.

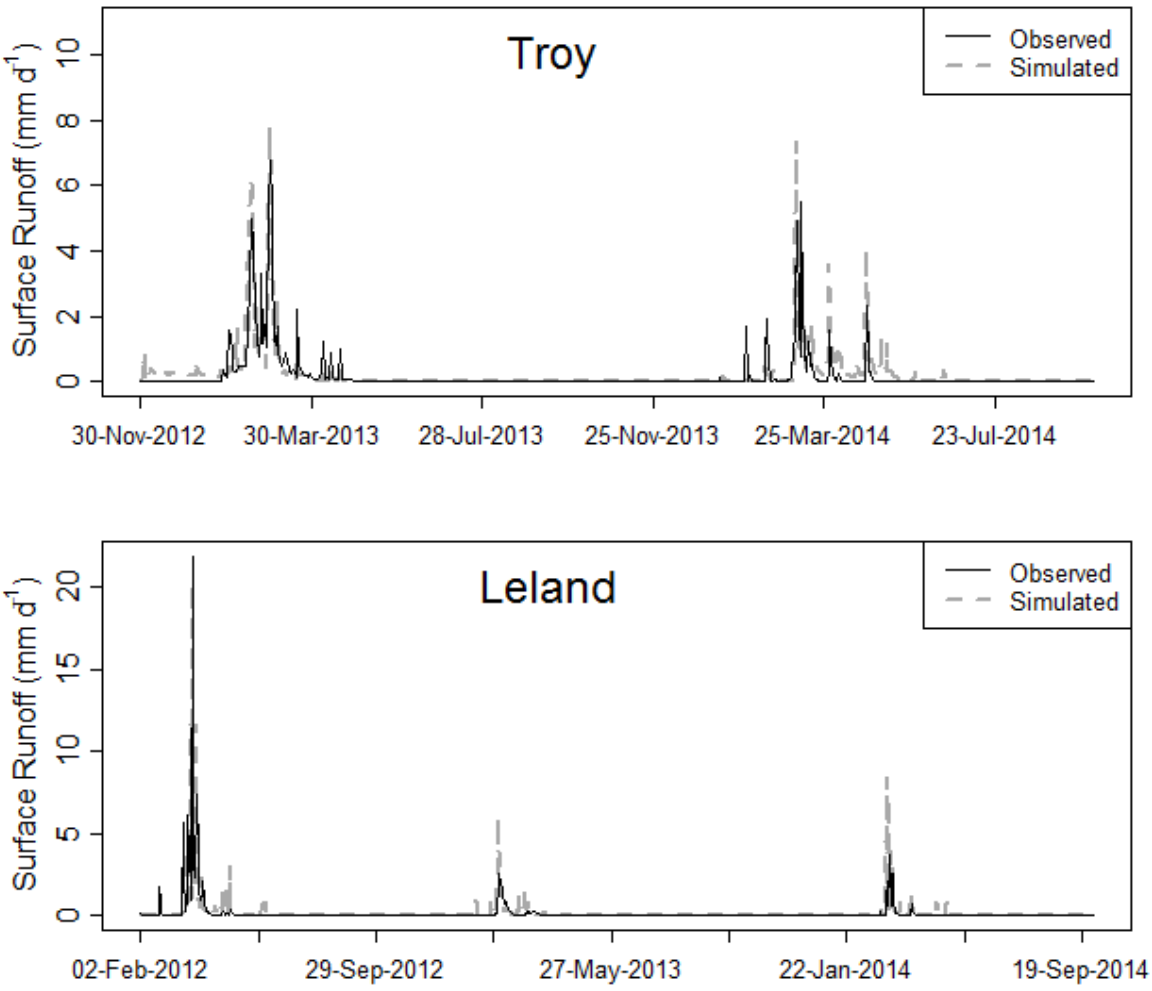

Figure 6. Daily runoff hydrographs for catchments in the high-precipitation zone

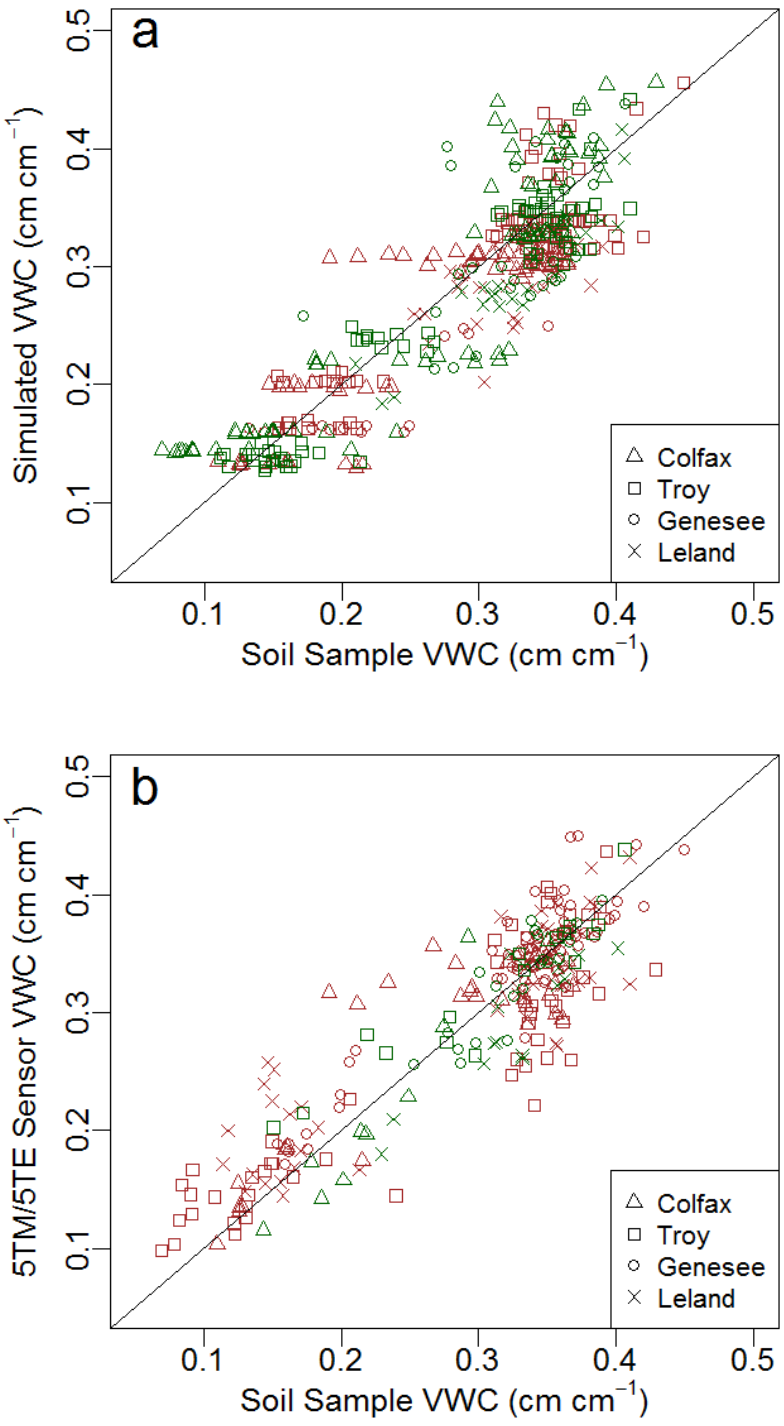

Figure 7. Spatio-temporal assessment of root zone soil moisture. Each point represents a sample collected during the three year (2012-2014) observation period. Brown color indicates no crop present and green indicates crop is present at the time of observation. Figure 3a shows the scatter for simulated moisture VWC_{SIM} and Figure 3b the scatter for 5TM/5TE sensor moisture VWC_{SIM}.

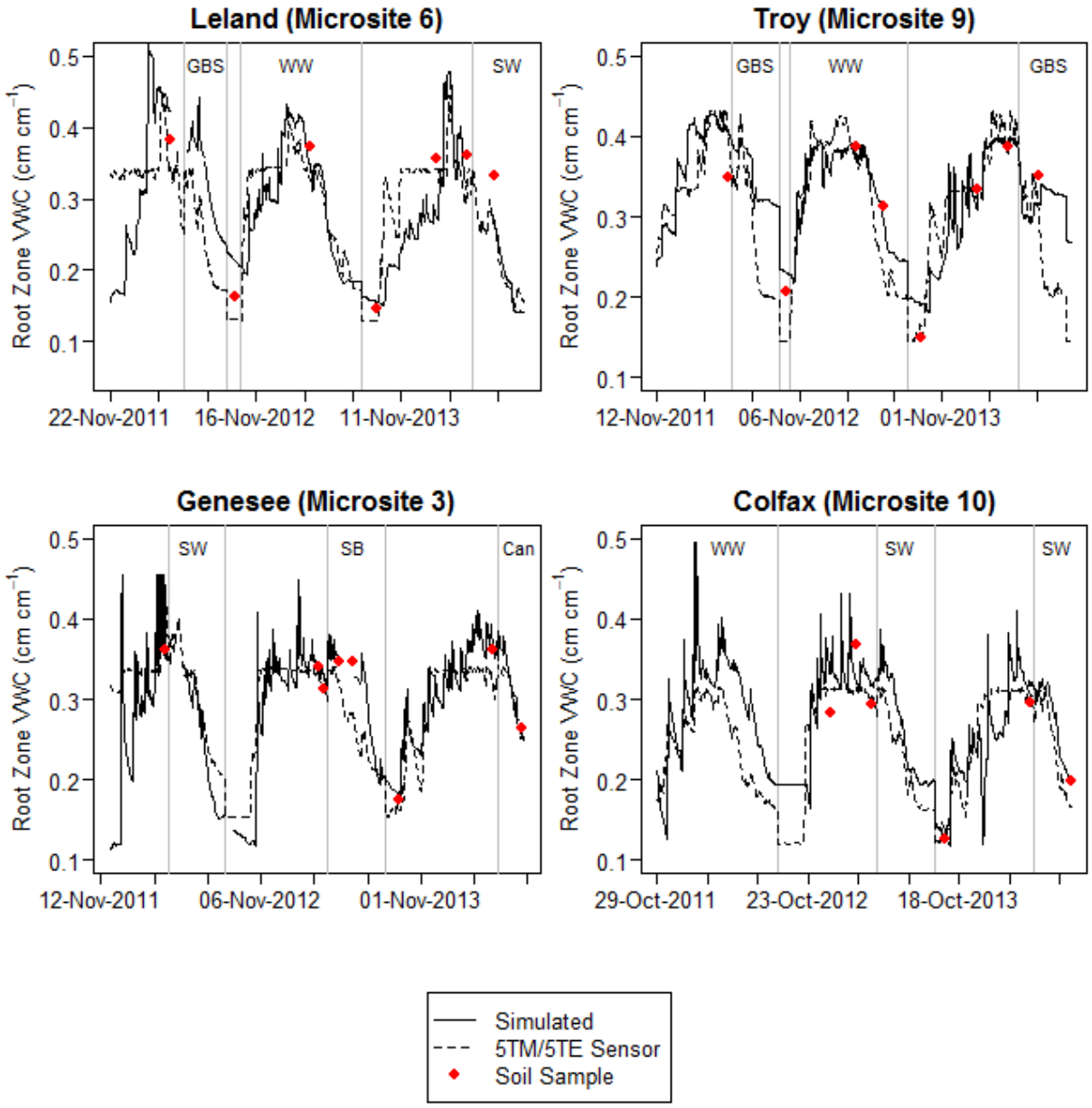

Figure 8. Temporal trends in root zone volumetric water content (VWC), shown for one microsite per field. The vertical grey lines divide the plotting region into crop and no-crop periods. GBS= garbanzos, WW=winter wheat, SW=spring wheat, SB=spring barley, Can=canola

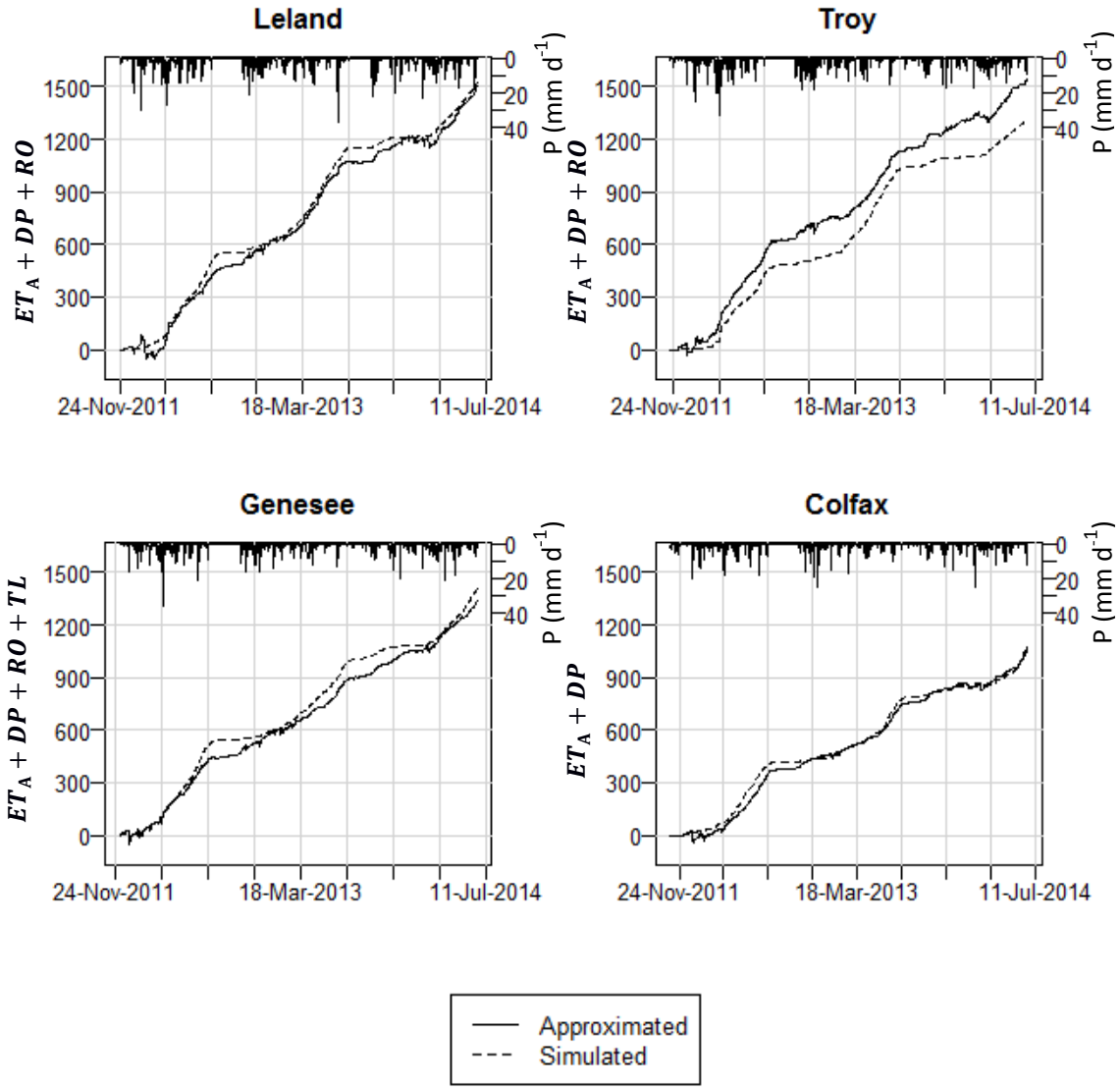

Figure 9. Cumulative water balance totals, approximated as *P*-Δ*S* from the Equation (7) catchment water balance, compared with simulated totals**.** ET_A= actual evapotranspiration, *DP*=deep percolation, *RO*=surface runoff, *TL*=tile line drainage, and *P*=precipitation

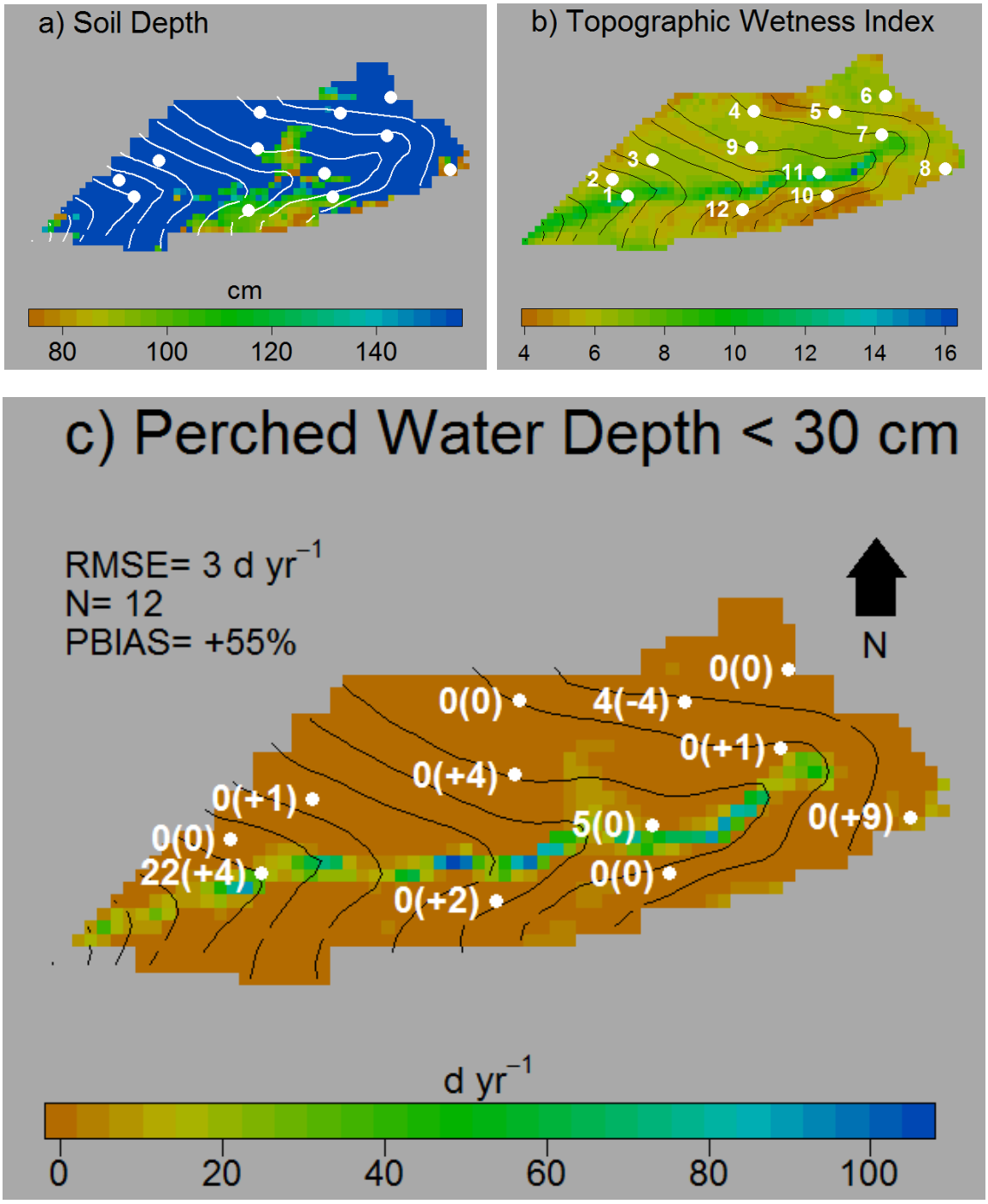

Figure 10. Frequency of saturation (perched water depths less than 30 cm) at the Genesee catchment (10c), compared with soil depth (10a) and topographic wetness index (10b). White text values in (10c) are observed saturation frequencies determined from the 5TM/5TE moisture sensors located at the 30 cm depth, with errors given in parenthesis. White dots mark the location of the 12 microsites, numbered in (10b).The color gradient in (10c) represents the simulated days per year (d yr^{-1}) of saturation.

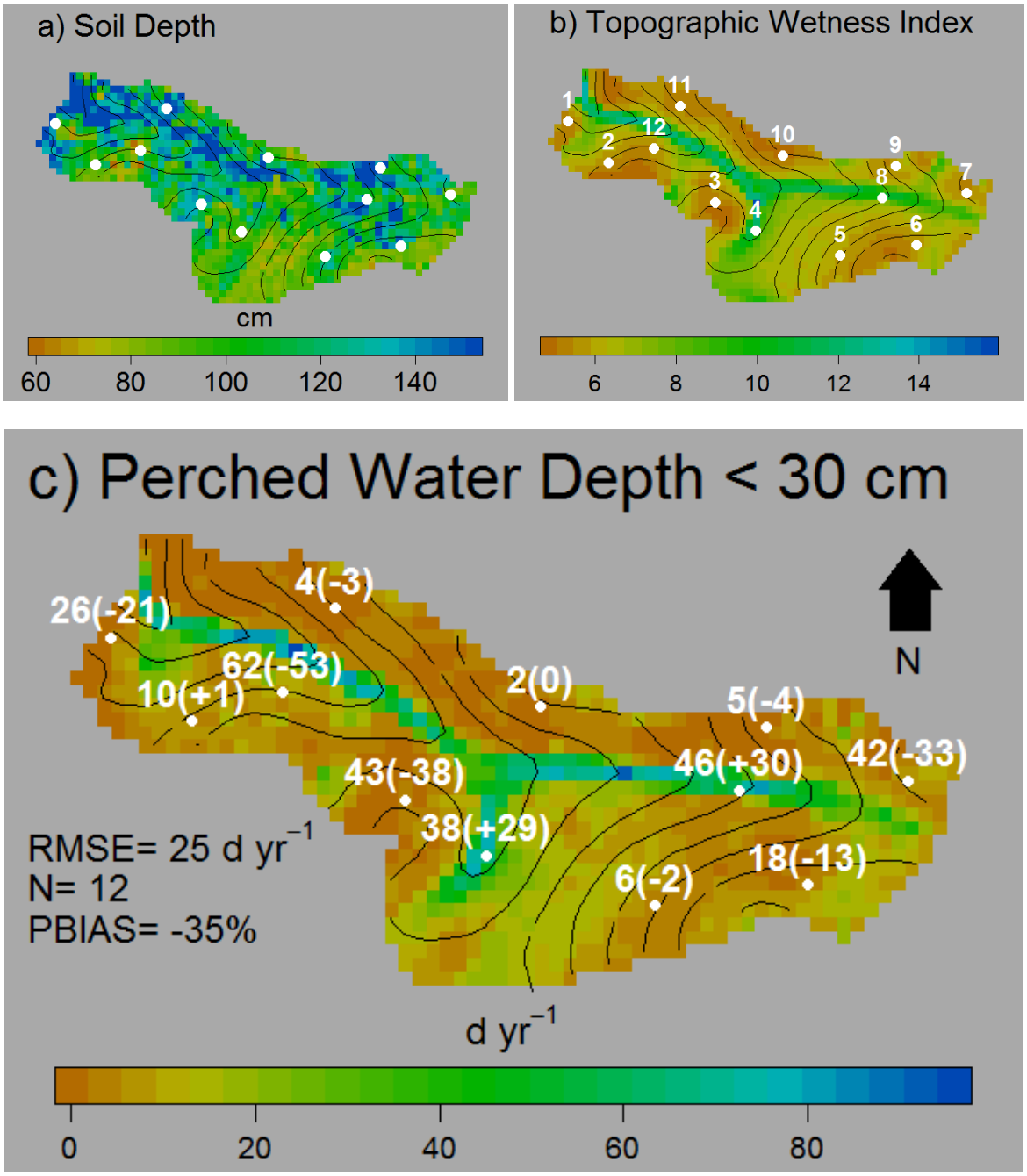

Figure 11. Frequency of saturation (perched water depths less than 30 cm) at the Leland catchment (11c), in comparison to soil depth (11a) and topographic wetness index (11b). White text shows the frequency of saturation determined from the 5TM/5TE moisture sensors installed at the 30 cm depth, with errors given in parenthesis. White points mark the 12 microsites, labeled in (11b). The color gradient of (11c) represents the simulated saturation frequency in days per year (d yr^{-1}).

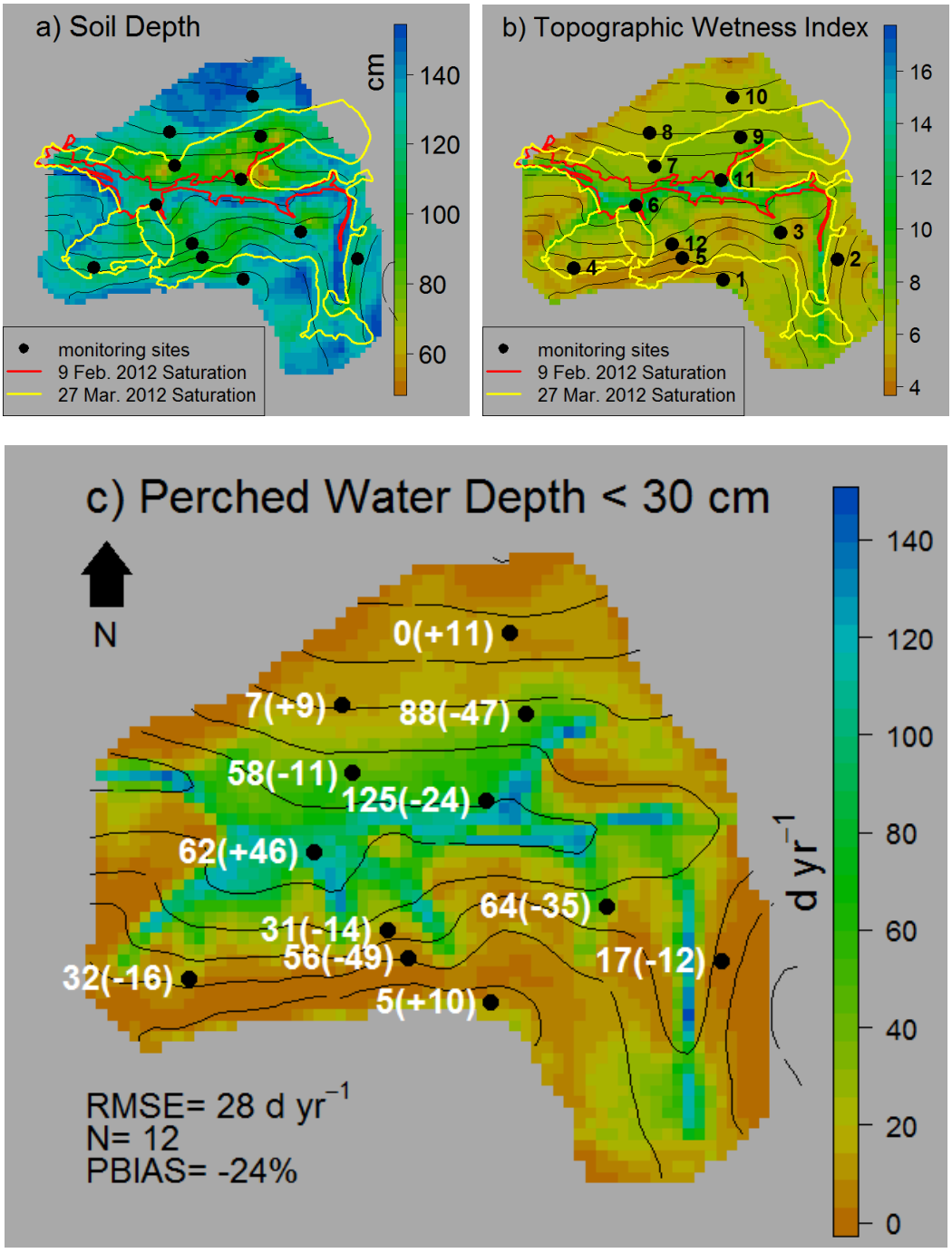

Figure 12. Frequency of saturation (perched water depths less than 30 cm) at theTroy catchment (12c), compared with soil depth (12a) and topographic wetness index (12b). The red and yellow outline in Figures 12a and 12b delineate the saturated zone as mapped with hand-held GPS on 9 Feb. 2012 (red) and 27 Mar. 2012 (yellow). White text in (12c) shows observed days per year (d yr^{-1})of saturation from the 5TM/5TE moisture sensors with errors given in parenthesis. Black dots mark the location of the 12 microsites, numbered in (12b). The color gradient in (12c) represents simulated days per year of saturation.

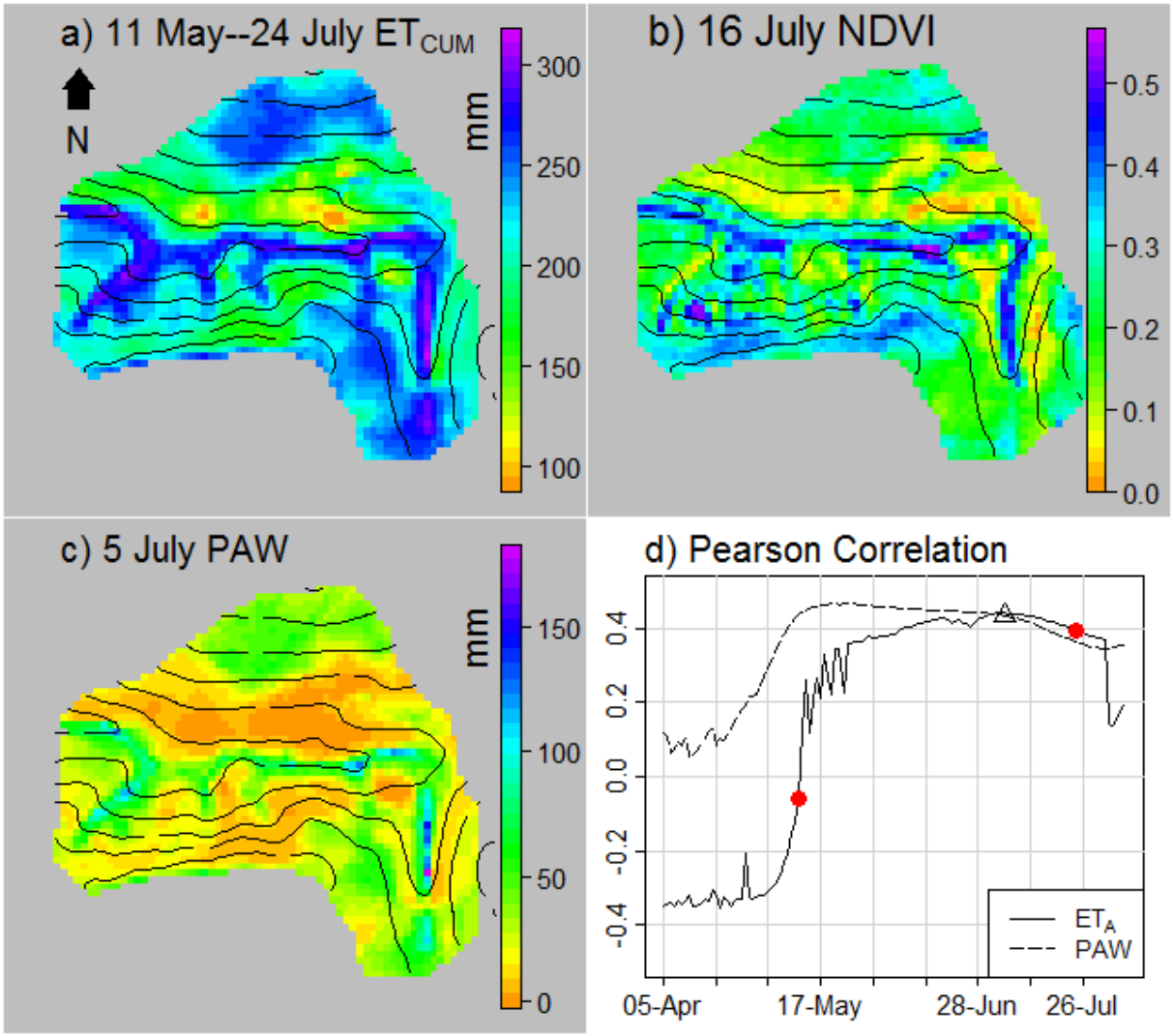

Figure 13. Mapped comparisons of ET_{CUM} (13a), NDVI (13b), and PAW (13c) at the Troy catchment for winter wheat, 2013**.** Shown in (13d) is a time series plot of the Pearson correlation between 16 July NDVI and daily sums of ET_A and between NDVI and end-of-day PAW simulated with the SMR model. Date ranges (5 April-6 August) correspond with the early stages of vegetative growth to the time of harvest. The pair of red dots in (13d) mark the start and end points of the cumulation period used to make the ET_{CUM} estimate. The open triangle indicates the day on which PAW was mapped.

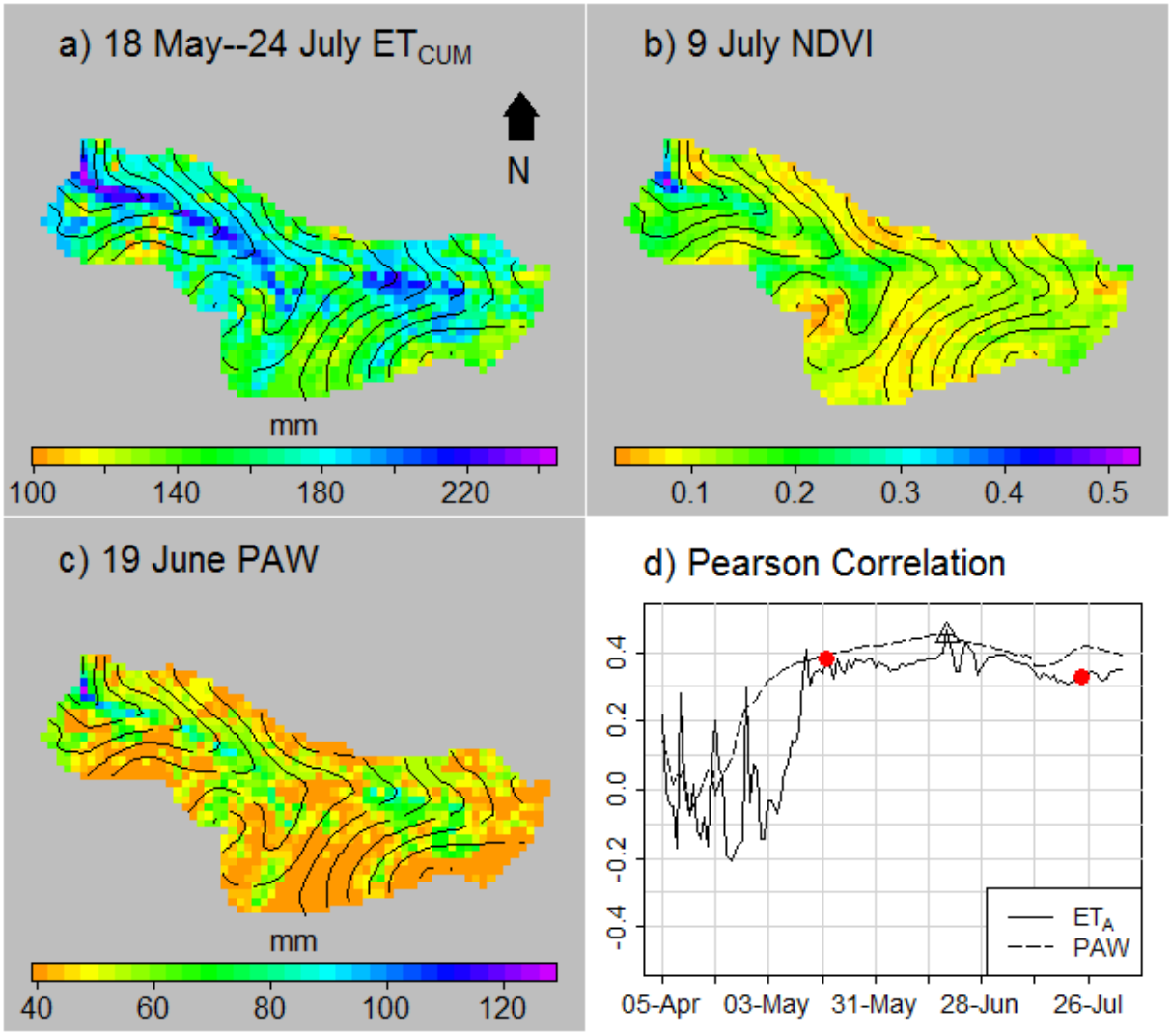

Figure 14. Mapped comparisons of ET_{CUM} (14a), NDVI (14b), and PAW (14c) at the Leland catchment for the 2013 growing season (winter wheat)**.** The time series plot (14d) of Pearson correlation coefficient is for 9 July NDVI with daily sums of ET_A and for NDVI with end-of-day PAW simulated with the SMR model. Date ranges (5 April-6 August) correspond with the early stages of vegetative growth to the time of harvest. The pair of red dots in (14d) mark the start and end points of the cumulation period used to make the ET_{CUM} estimate. The open triangle indicates the day on which PAW was mapped.

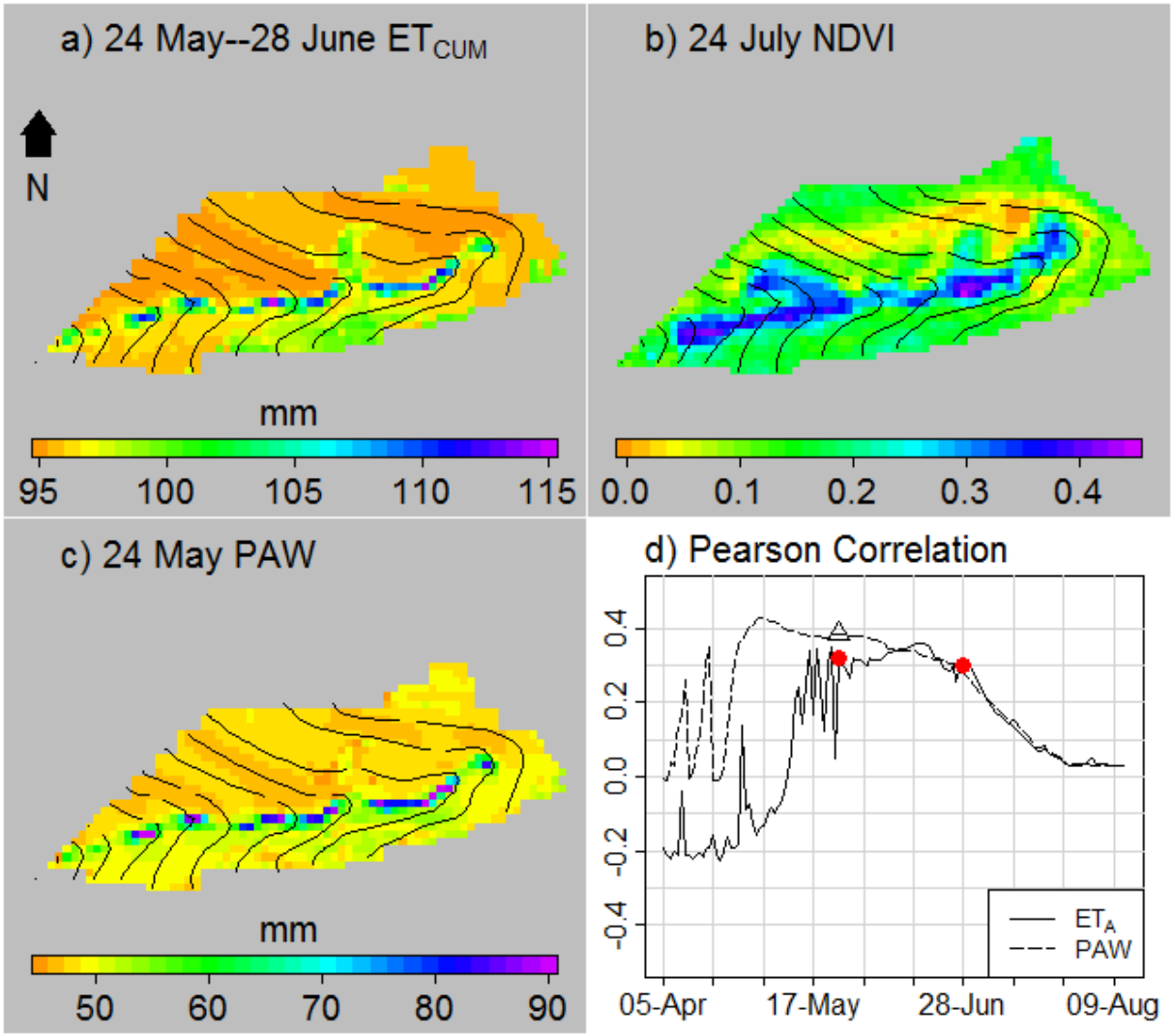

Figure 15. Mapped comparisons of ET_A (15a), NDVI (15b), and PAW (15c) at the Genesee catchment for spring barley, 2013. In (15d) is a time series plot of the Pearson correlation coefficient for 24 July NDVI with daily sums of ET_A and for NDVI with end-of-day PAW simulated with the SMR model (simulation without tile line). The date range (5 April-12 August) extends from sowing to harvest. The pair of red dots in (15d) mark the start and end points of the cumulation period used to make the ET_{CUM} estimate. The open triangle indicates the day on which PAW was mapped.

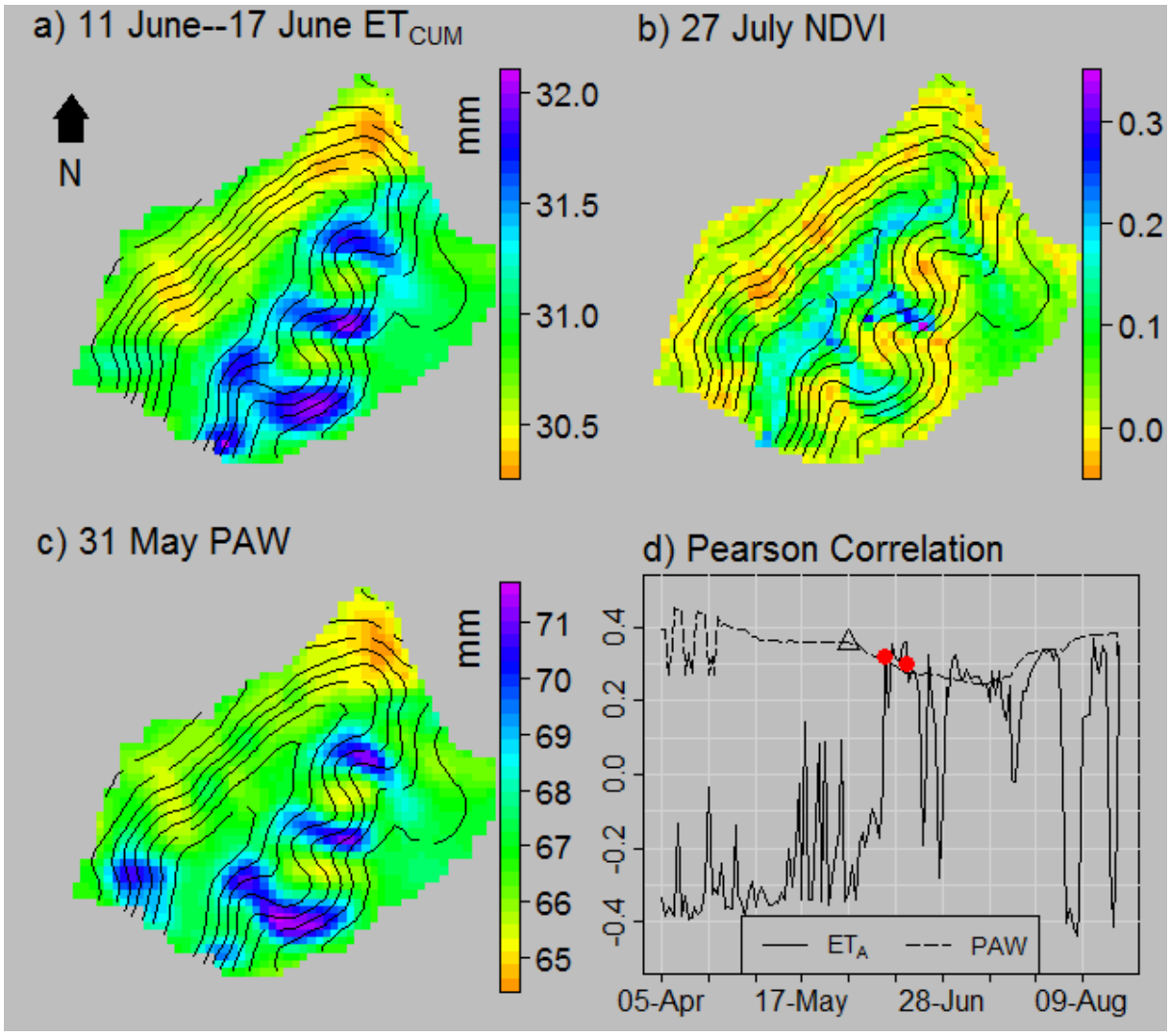

Figure 16. Mapped comparisons of ET_A (16a), NDVI (16b), and PAW (16c) at the Colfax catchment for the 2013 growing season (spring wheat). Shown in (16d) is a time series plot of the Pearson correlation between 27 July NDVI and daily sums of ET_A and between NDVI and end-of-day PAW simulated with the SMR model. Date ranges (5 April-19 August) extend from sewing to harvest. The pair of red dots in (16d) mark the start and end points of the cumulation period used to make the ET_{CUM} estimate. The open triangle indicates the day on which PAW was mapped.

Figure 17. Hillslope seep at the Troy catchment, looking northwest. Subsurface drainage emerges as return flow on this south-facing slope.

CHAPTER 4: CONCLUSION

1. IMPLICATIONS FOR PRECISION AGRICULTURE AND WATER QUALITY MANAGEMENT

Precipitation is the most uncertain input to dryland agricultural systems and is often the most critical. Managing uncertainty associated with moisture supply from stored soil water and growing-season precipitation can be achieved, in part, by setting realistic yield goals for different parts of a field and varying inputs of nitrogen fertilizer to meet site-specific yield goals (Rasmussen and Rhode, 1991; Gauer *et al.*, 1992; Mulla *et al*., 1992; Fiez *et al.*, 1994, 1995; Pan *et al.*, 2007; Huggins *et al.*, 2010). Within fields, available water, and hence water stress, usually follows patterns of topography and physical properties of the soil such as soil depth and available water content. Hydrologic models capable of simulating the spatio-temporal dynamics of plant available water (PAW) based on these sources of field heterogeneity can be valuable tools for developing management zones based on PAW patterns (Ibrahim and Huggins, 2011).

Besides managing for seasonal water stress, growers farming in the intermediate and high precipitation zones of the Palouse region face the additional challenge of managing for perched water tables. Subsurface flow is likely to be an important source of redistribution in these systems. Accordingly, growers may need to address lateral transport of mobile agrichemicals as a source of nonpoint pollution. They will more likely need to consider adopting erosion control practices that improve surface drainage or to consider installing subsurface drainage systems (Christen and Ayars, 2001). However, this latter option can greatly accelerate nitrate leaching (Randall et al., 1997). Timing and quantity of fertilizer application are crucial for ensuring nitrogen is used by the crop rather than leached or carried away by runoff.

Prolonged periods of saturation caused by underlying, low-permeability soil layers can delay spring planting, delay crop development, and depress yields (Cannell *et al.*, 1980; Steffens *et al.*, 2005; Gregory, 2006). Moreover, waterlogged soils promote denitrification and the release of the greenhouse gas, N_2O, to the atmosphere, especially in areas of a field where fertilizer is over-applied (Mosier *et al*., 2004; Allen *et al*., 2010). Shallow soils also hold less PAW and dry-up rapidly once evapotranspiration peaks. Water stress therefore becomes a concern at both ends of the growing season--in the spring from too much water and in the summer from too little water.

Growers in the drier, western parts of the Palouse region will likely need to consider management options that conserve soil water, including minimal-tillage and no-till, by increasing soil infiltration capacity and by reducing evaporative losses (Kok *et al*., 2009; Brooks *et al*., 2010). Management tools (e.g. crop growth simulation models) aimed at forecasting yield reduction as a

result of water stress can inform adjustments to fertilizer application rate from year to year while hydrologic modeling that accurately captures the spatial distribution of soil moisture can help to predict areas of a field that are more likely than others to develop water stress conditions or waterlogging.

The two fields of the dry and intermediate precipitation zones exhibited high correlations between total carbon (TC), i.e. organic matter, and NDVI computed from RapidEye™ imagery across most image dates. Examination of any one of the satellite images showed clear trends of early browning on the ridgetops and south-facing slopes, where the lowest organic matter was observed. This relationship between organic carbon and landscape position is similar to experimental results published in the literature (Moore *et al*., 1993; Gessler *et al*., 2000; Huggins and Uberuaga, 2010). Moreover, yield patterns followed similar trends to organic matter. Implications for growers in the dry sub-region are that N fertilizer applied on low organic matter soils will not be used efficiently by the crop owing to water constraints (Rasmussen and Rhode, 1991). Early season water stress may stunt root development (Kramer and Boyer, 1995) such that late in the season roots cannot access the nitrate leached earlier by spring rains.

2. CONCLUDING REMARKS

The focus of this thesis has been to relate soil moisture patterns to crop senescence patterns observed in fields of the southeastern section of the Palouse dryland cropping region by considering the linkage between soil properties, landscape hydrology, and crop water stress. The best-correlating soil properties with vegetation indices computed from the RapidEye™ wavebands were TC and soil depth, which both critically influence water availability. While the explanation is not exhaustive, this work strongly supports previous research in concluding that senescence patterns in fields of the Palouse express differential development of drought conditions, sometimes over remarkably short distances. Simulations with the SMR model demonstrated the effect that a spatially-heterogeneous soil depth has on PAW, and even lacking a crop growth component, was able to explain up to 20% ($R = 0.45$) of the variability in a late season NDVI image. On the other hand, some of the more prominent features visible with RapidEye™ were entirely missed at fields with more uniform soil depth. The brownest areas generally also had the least organic matter, earliest soil water depletion, and were located in landscape positions (ridges and hilltops) conducive to water erosion. It is expected that incorporating soil organic matter into approximations of available water capacity will greatly improve model estimates where root penetration is not impeded by a restricting layer and PAW is controlled by water retention properties of the soil.

The SMR model is well-suited to the unique climate, soils, and topography of the Palouse region—something which very few if any other models can claim. By incorporating a dynamic root zone soil layer into the SMR water balance simulations, the evolution of water stress, both from saturated and drought conditions, is more realistically represented. A functional hydrologic model is foundational to a cropping systems model that will support dryland cropping systems of the Palouse region. We suggest that the strengths of the original SMR model and its early modifications, together with contribution from this work, qualify SMR as a functional hydrologic model for Palouse agriculture.

3. REFERENCES

Allen DE, Kingston G, Rennenberg H, Dalal RC, Schmidt S. 2010. Effect of nitrogen fertilizer management and waterlogging on nitrous oxide emission from subtropical sugarcane soils. *Agriculture, Ecosystems & Environment* **136**(3-4): 209-217. DOI: 10.1016/j.agee.2009.11.002

Brooks ES, Boll J, Snyder AJ, Ostrowski KM, Kane SL, Wulfhorst JD, Van Tassel LW, Mahler R. 2010. Long term sediment loading trends in Paradise creek watershed. *Journal of Soil Water Conservation* **65**(6): 331-341. DOI: 10.2489/jswc.65.6.331

Cannell RQ, Belford RK, Gales K, Dennis CW, Prew RD. 1980. Effects of waterlogging at different stages of development on the growth and yield of winter wheat. *Journal of the Science of Food and Agriculture* **31**(2): 117-132. DOI: 10.1002/jsfa.2740310203

Christen EW, Ayars JE. 2001. Subsurface drainage system design and management in irrigated agriculture: best management practices for reducing drainage volume and salt load, Technical Report 38-01, 130pp. CSIRO Land and Water: Griffith, NSW, Australia. Accessed December 15, 2015 at http://www.clw.csiro.au/publications/technical2001/tr38-01.pdf.

Fiez TE, Miller BC, Pan WL. 1994. Winter wheat yield and grain protein across varied landscape positions. *Agronomy Journal* **86**(6): 1026-1032.

Fiez TE, Pan WL, Miller BC. 1995. Nitrogen use efficiency of winter wheat among landscape positions. *Soil Science Society of America Journal* **59**(6): 1666-1671.

Gauer LE, Grant CA, Gehl DT, Bailey LD. 1992. Effects of nitrogen fertilization on grain protein content, nitrogen uptake, and nitrogen use efficiency of six spring wheat (*Triticum aestivum L.*) cultivars, in relation to estimated moisture supply. *Canadian Journal of Plant Science* **72**(1): 235-341.

Gessler PE, Chadwick OA, Chamran F, Althouse L, Holmes K. 2000. Modeling soil-landscape and ecosystem properties using terrain attributes. *Soil Science Society of America Journal* **64**: 2046-2056.

Gregory PJ. 2006. *Plant Roots: Growth, Activity and Interactions with the Soil*, 328pp. Blackwell Publishing Ltd.

Huggins D, Pan W, Smith J. 2010. (Chapter 17) Yield, protein and nitrogen use efficiency of spring wheat: evaluating field-scale performance. In *Climate Friendly Farming—Final Report*, CSANR Research Report 2010-001. Washington State University Center for Sustaining Agriculture and Natural Resources. Accessed December 14, 2015 at http://csanr.wsu.edu/wp-content/uploads/2013/02/CSANR2010-001.Ch17.pdf.

Huggins D, Uberuaga D. 2010. (Chapter 14) Field heterogeneity of soil organic carbon and relationships to soil properties and terrain attributes. In *Climate Friendly Farming—Final Report*, CSANR Research Report 2010-001. Washington State University Center for Sustaining Agriculture and Natural Resources. Accessed December 14, 2015 at http://csanr.wsu.edu/wp-content/uploads/2013/02/CSANR2010-001.Ch14.pdf.

Ibrahim HM, Huggins DR. 2011. Spatio-temporal patterns of soil water storage under dryland agriculture at the watershed scale. *Journal of Hydrology* **404**(3-4): 186-197. DOI: 10.1016/j.jhydrol.2011.04.029

Kok H, Papendick RI, Saxton KE. 2009. STEEP: Impact of long-term conservation farming research and education in Pacific Northwest wheatlands. *Journal of Soil and Water Conservation* **64**(4): 253-264. DOI: 10.2489/jswc.64.4.253

Kramer PJ, Boyer JS. 1995. (Chapter 5) Roots and root systems. In *Water Relations of Plants and Soils*. Academic Press, Inc.: San Diego, CA; 115-166.

Moore ID, Gessler PE, Nielsen GA, Peterson GA. 1993. Soil attribute prediction using terrain analysis. *Soil Science Society of America Journal* **57**: 443-452.

Mosier A, Wassmann R, Verchot L, King J, Palm C. 2004. Methane and nitrogen oxide fluxes in tropical agricultural soils: sources, sinks and mechanisms. *Environment, Development and Sustainability* **6**(1-2): 11-49. DOI: 10.1023/B:ENVI.0000003627.43162.ae.

Mulla DJ, Bhatti AU, Hammond MW, Benson JA. 1992. A comparison of winter wheat yield and quality under uniform versus spatially variable fertilizer management. *Agriculture Ecosystems & Environment* **38**(4): 301-311. DOI: 10.1016/0167-8809(92)90152-2.

Pan W, Schillinger W, Huggins D, Koenig R, Burns J. 2007. (Chapter 10) Fifty years of predicting wheat nitrogen requirements in the Pacific Northwest USA, 6pp. In *Managing Crop Nitrogen for Weather*, Bruulsema T (ed). International Plant Nutrition Institute: Norcross, GA.

Randall GW, Huggins DR, Russelle MP, Fuchs DJ, Nelson WW, Anderson JL. 1997. Nitrate losses through subsurface tile drainage in Conservation Reserve Program, alfalfa, and row crop systems. *Journal of Environmental Quality* **26**(5): 1240-1247.

Rasmussen PE, Rohde CR. 1991. Tillage, soil depth, and precipitation effects on wheat response to nitrogen. *Soil Science Society of America Journal* **55**(1): 121-124.

Steffens D, Hutsch BW, Eschholz T, Losak T, Schubert S. 2005. Water logging may inhibit plant growth primarily by nutrient deficiency rather than nutrient toxicity. *Plant Soil and Environment* **51**(12): 545-552.

APPENDIX A: CHAPTER TWO APPENDED TABLES AND FIGURES

Table A-I. Complete table of top correlations between field measurements and vegetation indices

Grower	Variable	Depth (cm)	Index	Image Date	r^2	N	p-value	r
Colfax	*Yield*	NA	OSAVI	8 July	0.88	12	<.001	0.94
	$GWC_{SPR.}$	0-90	OSAVI	27 July	0.88	11	<.001	0.94
	TC_{2011}	0-60	NDRE	8 July	0.85	12	<.001	0.92
	TN_{2011}	0-60	NDVI	8 July	0.83	12	<.001	0.91
	Δ*IN*	0-90	NDVI	15 June	0.77	12	<.001	0.88
	BD	0-60	MCARI	8 July	0.79	12	<.001	-0.89
	AWC	0-60	OSAVI	8 July	0.76	12	<.001	0.87
	Δ*GWC*	0-90	NDVI	8 July	0.64	12	0.002	0.80
	TWI	NA	OSAVI	27 July	0.62	11	0.003	0.79
	VWC_{FALL}	0-90	MCARI	8-June	0.58	12	0.004	-0.76
	$ECa_{SPR.}$	NA	OSAVI	27 July	0.49	11	0.016	-0.70
	Δ*VWC*	0-30	NDVI	8 July	0.52	10	0.018	0.72
	sand	0-90	OSAVI	15 June	0.44	12	0.019	-0.66
	GWC_{FALL}	0-30	NDVI	29 June	0.44	12	0.020	-0.66
	$IN_{SPR.}$	0-90	NDVI	15 June	0.42	12	0.022	0.65
Genesee	*sand*	0-60	OSAVI	15 July	0.86	12	<.001	0.93
	$ECa_{FALL.}$	NA	MCARI	15 July	0.85	12	<.001	-0.92
	clay	0-30	NDVI	15 July	0.79	12	<.001	-0.89
	TN_{2012}	0-90	NDRE	15 July	0.75	12	<.001	0.86
	silt	0-150	NDRE	15 July	0.73	12	<.001	0.85
	TC_{2012}	0-120	NDRE	15 July	0.69	12	<.001	0.83
	AWC	0-90	NDRE	15 July	0.58	12	0.004	0.76
	Δ*IN*	0-120	MCARI	15 June	0.58	11	0.007	0.76
	Δ*GWC*	0-30	NDRE/NDVI	27 June	0.67	8	0.012	-0.82
	$IN_{SPR.}$	0-30	NDVI	15 June	0.57	8	0.017	0.80
	Yield	NA	NDRE	15 July	0.44	12	0.018	0.66
Leland	$IN_{SPR.}$	0-120	NDRE	9 July	0.94[a]	11	<.001	0.97
	$TAW_{OBS.}$	NA	OSAVI	27 June	0.88	12	<.001	0.94
	$D_{OBS.}$	NA	OSAVI	27 June	0.81	12	<.001	0.90
	Δ*IN*	0-90	NDRE	9 July	0.79[b]	11	<.001	0.89
	Δ*GWC*	0-60	OSAVI	15 June	0.72	12	<.001	0.85

Table A-I. Continued

	AWC	0-90	NDVI	15 June	0.71	12	<.001	0.84
	silt	0-90	NDVI	15 June	0.69	12	<.001	0.83
	$TAW_{AVG.}$	NA	NDVI	15 June	0.69	12	<.001	0.83
	Δ*VWC*	0-60	OSAVI	15 June	0.67	12	<.001	0.82
	clay	0-90	NDVI	15 June	0.67	12	0.001	-0.82
	$ECa_{SPR.}$	NA	MCARI/OSAVI	27 June	0.61	12	0.003	0.78
	BD	0-60	NDVI	15 June	0.58	12	0.004	-0.76
	TN_{2011}	0-120	OSAVI	15 June	0.56	12	0.005	0.75
	Δ*EC*a	NA	MCARI/OSAVI	27 June	0.38	12	0.032	0.62
Troy	*Yield*	NA	OSAVI	29 June	0.72	12	<.001	0.85
	Δ*EC*a	NA	MCARI/OSAVI	29 June	0.53	12	0.007	0.73
	$IN_{SPR.}$	0-60	NDRE/NDVI	15 June	0.50	12	0.009	-0.71
	Δ*IN*	0-60	NDRE/NDVI	15 June	0.50	12	0.010	-0.71
	IN_{FALL}	0-150	NDRE/NDVI	6 June	0.46	12	0.015	-0.68
	$TAW_{AVG.}$	NA	OSAVI	16 July	0.42	12	0.022	0.65
	AWC	0-120	NDVI	29 June	0.37	12	0.035	0.61
	$GWC_{SPR.}$	0-30	NDVI	16 July	0.36	12	0.041	0.60

[a]Obtained with outlier removed. If outlier is included r^2=0.64

[b]If outlier is included, r^2=0.56

Table A-II. Sample Pearson correlation coefficient between total carbon (TC) and NDRE computed from reflectance data collected by the RapidEye™ sensor over the 2013 growing season

		Pearson Correlation Coefficient				
		Depth Increment				
	2013 NDRE					
Grower	Image Date	0-30 cm	30-60 cm	60-90 cm	90-120 cm	120-150 cm
Genesee	15 June	0.66	0.63	0.56	0.49	0.53
	27 June	0.72	0.69	0.61	0.54	0.57
	15 July	0.74	0.83	0.86	0.86	0.81
	24 July	0.61	0.81	0.88	0.91	0.86
Colfax	8 June	0.79	0.65	0.51	0.47	0.46
	15 June	0.81	0.66	0.54	0.51	0.50
	29 June	0.90	0.81	0.66	0.60	0.57
	8 July	0.90	0.92	0.81	0.76	0.72
	27 July	0.40	0.69	0.76	0.75	0.73

Table A-III. Distribution of leaf area index (LAI) at peak LAI for the 2013 growing season for the crop types shown in parenthesis, SW=spring wheat, WW=winter wheat, SB=spring barley. Stdev=standard deviation, CV=coefficient of variation

Microsite	LAI			
	Colfax (SW)	Troy (WW)	Genesee (SB)	Leland (WW)
1	2.3	4.0	5.0	3.7
2	3.2	3.8	3.1	3.5
3	2.0	3.4	4.7	3.5
4	1.7	3.6	3.2	4.1
5	2.9	3.0	2.3	4.7
6	3.2	2.5	3.7	3.8
7	2.1	4.2	5.8	3.4
8	1.7	4.4	2.4	3.8
9	2.1	3.9	3.2	3.6
10	2.6	4.5	3.6	3.3
11	3.2	3.1	5.4	3.7
12	3.8	3.1	2.1	3.9
Average	2.6	3.6	3.7	3.7
Stdev	0.7	0.6	1.2	0.4
CV	0.3	0.2	0.3	0.1

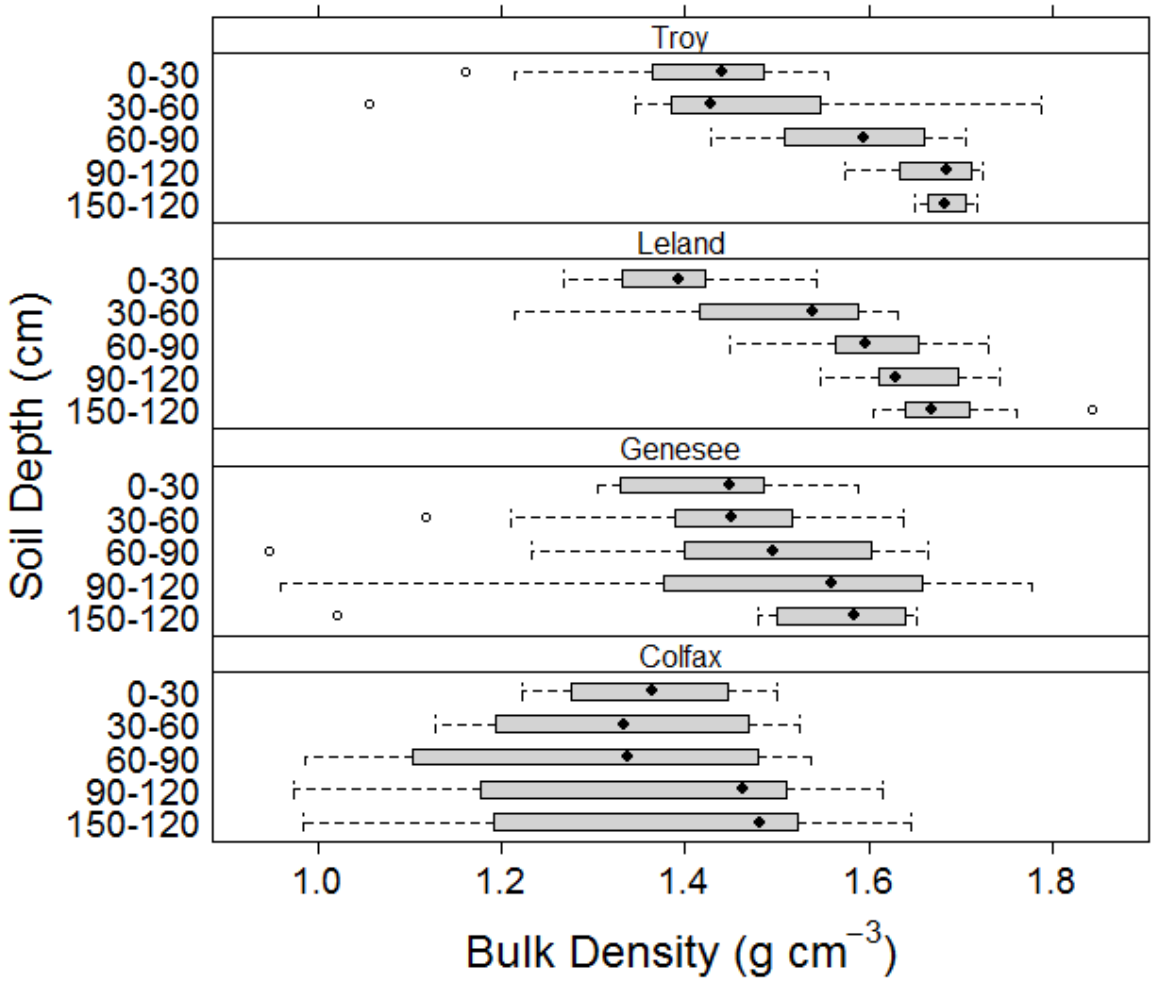

Figure A-1. Variation in bulk density with depth at the four study sites. The sharp increase in bulk density with depth at the Troy and Leland fields occurs with an associated increase in clay content in the argillic horizon.

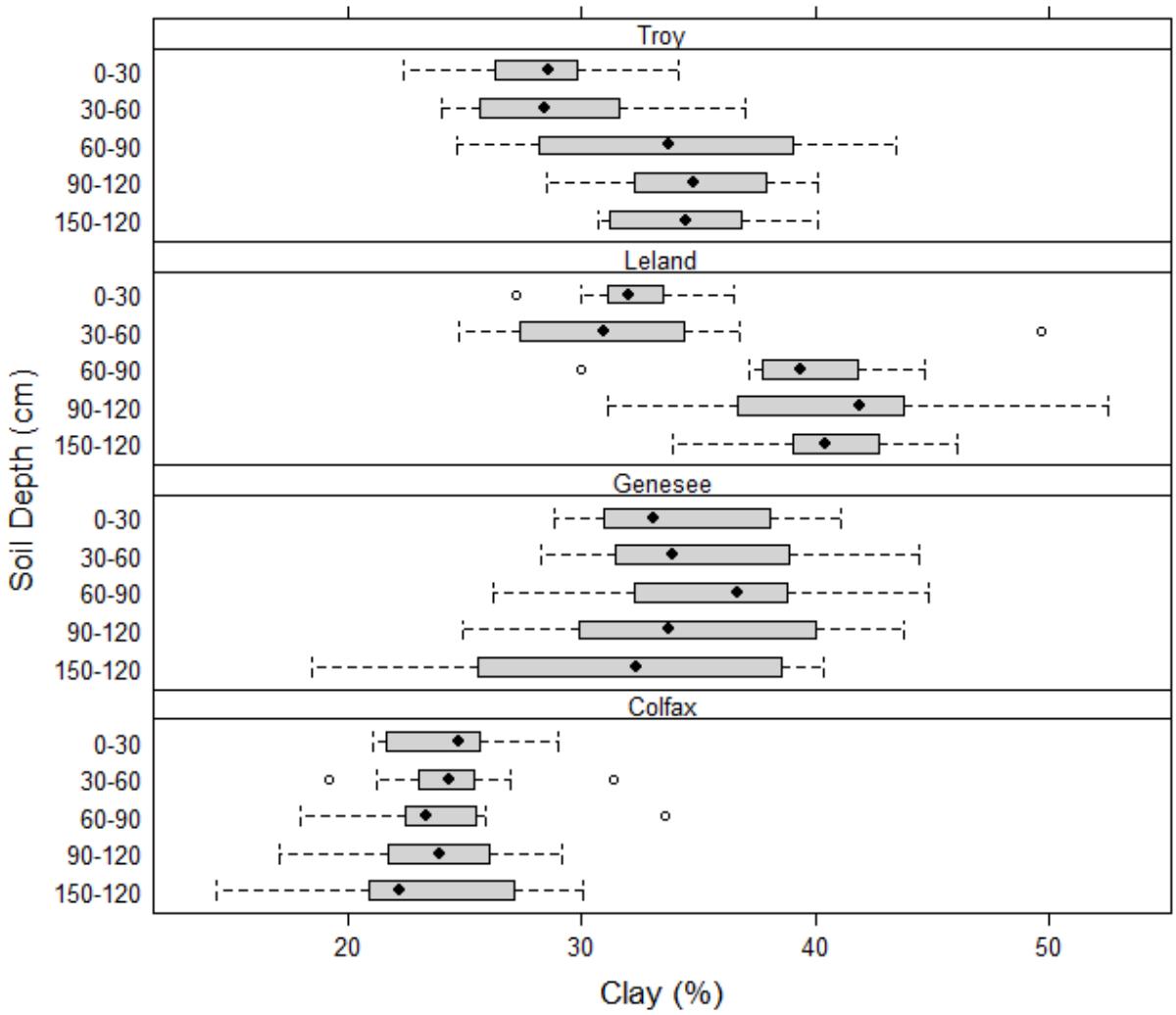

Figure A-2. Clay content variation with depth at the four field sites. Strong argillic horizons are present at the Troy and Leland fields as indicated by the sharp increase in clay content at 60-90 cm.

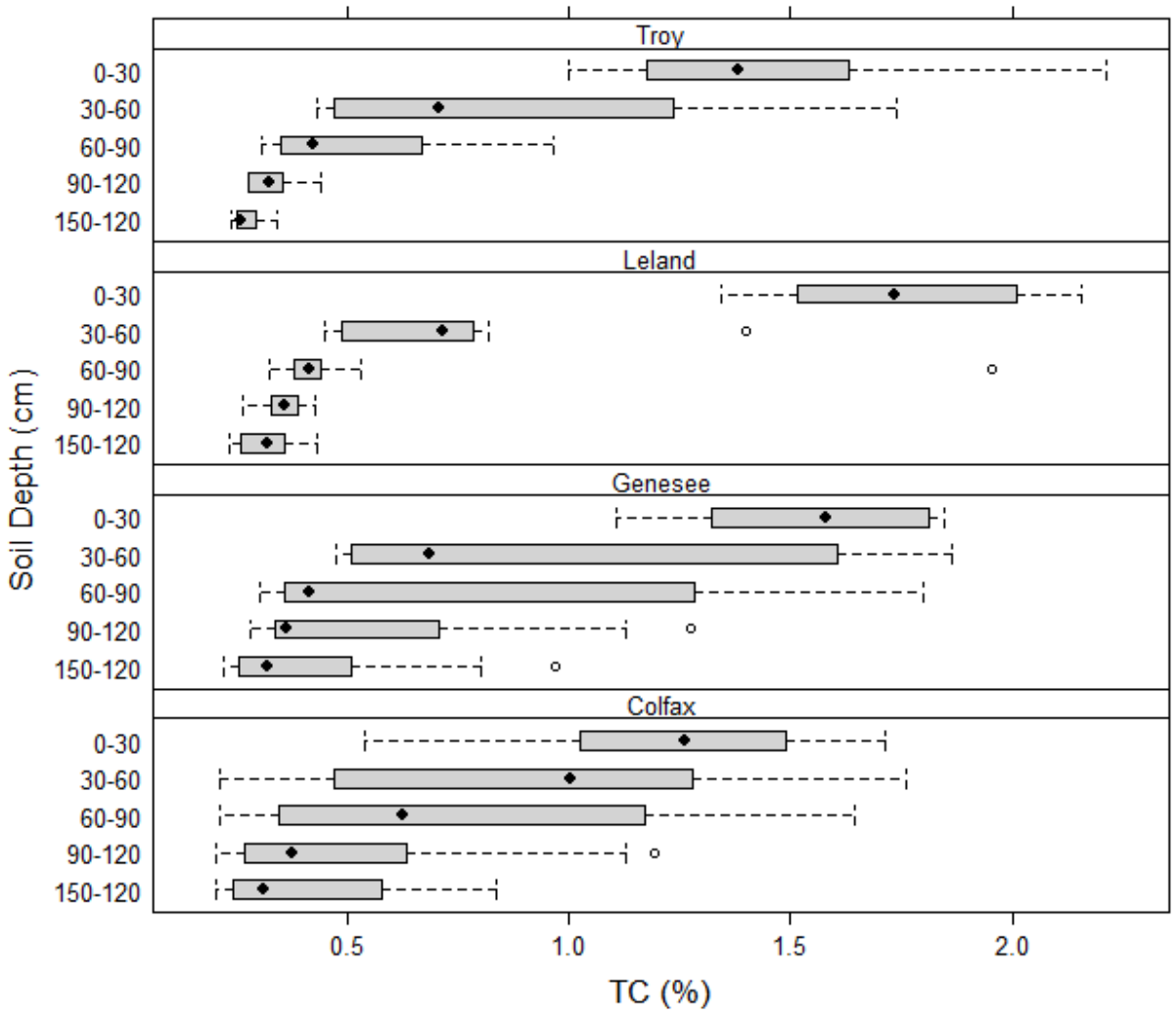

Figure A-3. Variation in total carbon (TC) content with depth shown for the four fields. The variability in subsoil TC at the Genesee and Colfax fields was detected with RapidEye™ satellite imagery through the effect TC has on crop productivity.

APPENDIX B: CHAPTER TWO CORRELATION MATRICES AND TABLE OF VEGETATION INDICES

Table B-I. Average value and coefficient of variation (CV) for the six vegetation indices computed for each 2013 RapidEye™ image

Field	Image Date	Approx. Dev. Stage	MCARI		NDRE		NDVI		OSAVI		NDRE/NDVI		MCARI/OSAVI	
			Avg.	CV	Avg.	CV	Avg.	CV	Avg.	CV	Avg.	CV	Avg.	CV
Colfax	8 June	stem extension	0.05	0.59	0.30	0.28	0.38	0.35	0.38	0.35	0.79	0.09	0.13	0.34
	15 June	stem extension	0.05	0.55	0.31	0.29	0.40	0.33	0.39	0.33	0.80	0.09	0.13	0.38
	29 June	heading	0.03	0.72	0.39	0.32	0.42	0.38	0.41	0.38	0.98	0.14	0.05	0.59
	8 July	heading	0.06	0.33	0.40	0.24	0.50	0.27	0.49	0.27	0.80	0.05	0.12	0.15
	27 July	ripening	0.01	2.55	0.09	0.63	0.07	1.05	0.07	1.05	1.66	2.31	0.02	4.24
Genesee	15 June	stem extension	0.11	0.23	0.37	0.19	0.53	0.20	0.53	0.20	0.71	0.03	0.21	0.06
	27 June	heading	0.09	0.17	0.47	0.13	0.63	0.14	0.62	0.15	0.74	0.02	0.15	0.05
	15 July	heading	0.12	0.18	0.33	0.22	0.49	0.20	0.50	0.21	0.66	0.04	0.25	0.11
	24 July	ripening	0.03	1.13	0.13	0.57	0.18	0.64	0.18	0.64	0.79	0.17	0.13	1.13
Leland	6 June	heading	0.08	0.12	0.53	0.04	0.66	0.04	0.64	0.05	0.81	0.02	0.12	0.09
	15 June	heading	0.09	0.14	0.45	0.09	0.60	0.09	0.59	0.10	0.76	0.03	0.15	0.08
	27 June	heading	0.06	0.16	0.40	0.09	0.51	0.08	0.47	0.09	0.77	0.04	0.12	0.12
	9 July	ripening	0.01	1.32	0.10	0.23	0.12	0.30	0.11	0.30	0.87	0.16	0.06	1.60
Troy	6 June	stem extension	0.05	0.31	0.12	0.41	0.57	0.17	0.56	0.18	0.20	0.29	0.09	0.19
	15 June	heading	0.07	0.18	0.47	0.14	0.59	0.14	0.59	0.15	0.79	0.03	0.13	0.10
	29 June	heading	0.08	0.18	0.47	0.11	0.61	0.10	0.58	0.11	0.77	0.05	0.13	0.13
	16 July	ripening	0.02	0.99	0.19	0.40	0.22	0.46	0.21	0.45	0.92	0.17	0.07	1.08

Table B-II. Correlation matrix for variables significantly correlated with vegetation indices at the Colfax field

Depth (cm)	Variable	TC_{2011}	$GWC_{SPR.}$	*Yield*	TN_{2011}	Δ*IN*	*BD*	*AWC*	Δ*GWC*	*TWI*	VWC_{FALL}	$ECa_{SPR.}$	Δ*VWC*	*sand*	GWC_{FALL}	$IN_{SPR.}$
NA	TC_{2011}	1														
0-90	$GWC_{SPR.}$	0.89*	1													
0-60	*Yield*	0.86*	0.66	1												
0-60	TN_{2011}	0.99*	0.89*	0.85*	1											
0-90	Δ*IN*	0.63	0.29	0.83*	0.58	1										
0-60	*BD*	-0.82*	-0.74*	-0.69	-0.82*	-0.46	1									
0-60	*AWC*	0.82*	0.62	0.73*	0.82*	0.62	-0.92*	1								
0-90	Δ*GWC*	0.64	0.57	0.85*	0.63	0.61	-0.45	0.38	1							
NA	*TWI*	0.54	0.64	0.35	0.54	0.18	-0.62	0.53	0.10	1						
0-90	VWC_{FALL}	-0.65	-0.46	-0.89*	-0.63	-0.69	0.51	-0.47	-0.93*	-0.10	1					
NA	$ECa_{SPR.}$	-0.63	-0.56	-0.50	-0.56	-0.57	0.49	-0.56	-0.21	-0.52	0.16	1				
0-30	Δ*VWC*	0.60	0.44	0.84*	0.53	0.70	-0.37	0.35	0.85*	0.06	-0.85*	-0.33	1			
0-90	*sand*	-0.30	0.08	-0.39	-0.33	-0.51	0.39	-0.61	-0.04	0.05	0.27	0.14	0.00	1		
0-30	GWC_{FALL}	-0.40	-0.15	-0.72*	-0.36	-0.70	0.17	-0.16	-0.78*	0.15	0.87*	0.08	-0.86*	0.17	1	
0-90	$IN_{SPR.}$	0.55	0.38	0.46	0.50	0.72*	-0.44	0.59	0.16	0.36	-0.11	-0.79*	0.26	-0.25	-0.14	1

* $p<0.01$

Table B-III. Correlation matrix for variables significantly correlated with vegetation indices at the Genesee field

Depth (cm)	Variable	*sand*	*ECa*$_{FALL.}$	*clay*	*TN*$_{2012}$	*silt*	*TC*$_{2012}$	*IN*$_{SPR.}$	Δ*IN*	Δ*GWC*	*Yield*	*AWC*
0-60	*sand*	1										
NA	*ECa*$_{FALL.}$	-0.78*	1									
0-30	*clay*	-0.79*	0.73*	1								
0-90	*TN*$_{2012}$	0.81*	-0.54	-0.68	1							
0-150	*silt*	0.67	-0.54	-0.84*	0.72*	1						
0-120	*TC*$_{2012}$	0.76*	-0.43	-0.62	0.98*	0.68	1					
0-90	*IN*$_{SPR.}$	0.45	-0.56	-0.64	0.25	0.29	0.22	1				
0-120	Δ*IN*	0.48	-0.40	-0.35	0.33	0.10	0.30	0.9*	1			
0-30	Δ*GWC*	0.57	-0.39	-0.09	-0.04	-0.12	-0.03	0.21	0.19	1		
NA	*Yield*	0.45	-0.49	-0.57	0.69	0.68	0.64	0.46	0.29	-0.45	1	
0-30	*AWC*	0.65	-0.73*	-0.92*	0.58	0.8*	0.50	0.30	0.03	-0.10	0.48	1

* $p<0.01$

Table B-IV. Correlation matrix for variables significantly correlated with vegetation indices at the Leland field

Depth (cm)	Variable	$IN_{SPR.}$	$TAW_{OBS.}$	$D_{OBS.}$	Δ*IN*	Δ*GWC*	*AWC*	*silt*	$TAW_{AVG.}$	Δ*VWC*	*clay*	$ECa_{SPR.}$	*BD*	TN_{2011}	Δ*EC*a
0-120	$IN_{SPR.}$	1													
NA	$TAW_{OBS.}$	0.53	1												
NA	$D_{OBS.}$	-0.12	0.53	1											
0-90	Δ*IN*	0.35	0.55	0.40	1										
0-60	Δ*GWC*	0.37	0.91*	0.57	0.68	1									
0-90	*AWC*	0.99*	0.51	-0.09	0.44	0.38	1								
0-90	*silt*	0.19	0.65	0.58	0.79*	0.87*	0.24	1							
NA	$TAW_{AVG.}$	0.49	0.92*	0.50	0.73*	0.95*	0.48	0.79*	1						
0-60	Δ*VWC*	0.33	0.48	0.41	0.97*	0.59	0.42	0.76*	0.64	1					
0-90	*clay*	-0.35	-0.65	-0.45	-0.77*	-0.81*	-0.40	-0.91*	-0.75*	-0.73*	1				
NA	$ECa_{SPR.}$	-0.15	0.01	0.32	-0.12	-0.11	-0.20	-0.25	-0.08	-0.12	0.18	1			
0-60	*BD*	-0.35	-0.75*	-0.41	-0.74*	-0.87*	-0.39	-0.71*	-0.86*	-0.58	0.72*	0.06	1		
0-120	TN_{2011}	0.31	0.60	0.66	0.55	0.59	0.33	0.60	0.70	0.56	-0.44	-0.03	-0.46	1	
NA	Δ*EC*a	-0.58	-0.10	0.55	-0.07	-0.07	-0.58	0.03	-0.11	0.01	0.20	0.62	0.18	0.28	1

* $p<0.01$

Table B-V. Correlation matrix for variables significantly correlated with vegetation indices at the Troy field

Depth (cm)	Variable	*yield*	Δ*EC*a	$IN_{SPR.}$	Δ*IN*	IN_{FALL}	$TAW_{AVG.}$	*AWC*	$GWC_{SPR.}$
NA	*yield*	1							
NA	Δ*EC*a	-0.27	1						
0-60	$IN_{SPR.}$	-0.26	0.32	1					
0-60	Δ*IN*	-0.27	0.26	0.99*	1				
0-150	IN_{FALL}	-0.43	0.18	0.24	0.17	1			
NA	$TAW_{AVG.}$	0.63	-0.43	-0.01	-0.02	-0.05	1		
0-120	*AWC*	0.75*	-0.46	0	0.01	-0.25	0.93*	1	
0-30	$GWC_{SPR.}$	0.17	-0.28	0.17	0.14	0.2	0.44	0.45	1

* $p<0.01$

Table B-VI. Correlation matrix for vegetation indices on two selected dates determined for the Leland field

Index (Date)	MCARI (6-Jun)	MCARI (9-Jul)	NDRE (6-Jun)	NDRE (9-Jul)	NDVI (6-Jun)	NDVI (9-Jul)	OSAVI (6-Jun)	OSAVI (9-Jul)	NDRE/ NDVI (6-Jun)	NDRE/ NDVI (9-Jul)	MCARI /OSAVI (6-Jun)	MCARI /OSAVI (9-Jul)
MCARI (6-Jun)	1											
MCARI (9-Jul)	-0.04	1										
NDRE (6-Jun)	0.16	-0.34	1									
NDRE (9-Jul)	0.05	0.61	-0.02	1								
NDVI (6-Jun)	0.66	-0.28	0.84*	-0.03	1							
NDVI (9-Jul)	0.09	0.88*	-0.10	0.89*	-0.04	1						
OSAVI (6-Jun)	0.67	-0.30	0.83*	-0.03	1	-0.06	1					
OSAVI (9-Jul)	0.09	0.87*	-0.09	0.89*	-0.04	1	-0.05	1				
NDRE/NDVI (6-Jun)	-0.93*	-0.04	0.10	0.03	-0.46	-0.06	-0.46	-0.06	1			
NDRE/NDVI (9-Jul)	-0.05	-0.84*	0.15	-0.29	0.05	-0.69	0.09	-0.68	0.14	1		
MCARI/OSAVI (6-Jun)	0.93*	0.08	-0.21	0.05	0.33	0.11	0.35	0.11	-0.95*	-0.10	1	
MCARI/OSAVI (9-Jul)	-0.13	0.95*	-0.39	0.48	-0.34	0.75*	-0.38	0.75*	-0.01	-0.84*	0.02	1

* $p<0.01$

APPENDIX C: ADDITIONAL NOTES ON METHODOLOGY

C.1. 5TM/5TE Moisture Sensor Calibration Procedure

With regard to moisture sensor water content readings, a few key observations pointed to the need for some type of field calibration. These were: 1) unrealistically low wilting point (e.g. 0.04 cm cm^{-1} in silt loam), 2) unrealistically high saturated water content (e.g. 0.50 cm cm^{-1} in argillic soils) and 3) a large difference in volumetric water content (VWC) ranges between the sensor-reported values and VWC determined from soil samples. In general, the likelihood of a particular sensor exhibiting any one of the three mentioned characteristics was observed to increase with depth, especially in higher clay, higher bulk density (BD) horizons. Inadequate soil-to-sensor contact is suggested as a probable cause of loss of accuracy under field conditions.

A soil sampling campaign was undertaken to improve sensor accuracy. The time of sampling was chosen to capture the wet and dry ends of the seasonal soil moisture cycle. At minimum, soil samples were collected fall and spring of each year (2012-2014). The spring sample preceded sowing of spring cereals while the fall sample was taken post-harvest for spring cereals and pre-plant for winter wheat. Additional soil samples were acquired in-season. Typically this would include two in-season measurements during the 2013 growing season and one during the 2014 growing season. Water contents were determined for these samples by the gravimetric method (samples dried at 105°C for 24 h) and converted to VWC using known BD.

The sample VWC was regressed against sensor-reported VWC in order to obtain a slope and intercept for sensor correction using ordinary least squares regression. Sensors were individually calibrated for all measurement years using the slope for scaling and intercept for bias correction. Regression outliers were removed so long as the following criteria could be satisfied: r^2>0.6, RMSE <0.05, N>=4, and at least one wet/dry point defined as a 20% difference in water content on a cm per cm basis. A probable cause of regression outliers was the disparity between the volume of soil measured by the sensor (point-based measurement) and the volume of soil samples, which were aggregated over the entire 30-cm depth increment. The distribution of moisture in a 0-30 cm sample is treated uniformly in gravimetric analysis while the sensor is most heavily influenced by the immediately surrounding soil.

C.2. Inputs to the GRASS Module: *i.atcorr*

The *i.atcorr* module (GRASS Development Team, 2012) performs atmospheric correction on satellite data using the Second Simulation of Satellite Signal in the Solar Spectrum (6S) radiative transfer model (Vermote *et al.*, 1997). The user has the option to supply atmospheric conditions, aerosol model, and spectral conditions or to choose from pre-defined conditions and models. We supplied the model with atmospheric conditions specified by the optical depth parameter at 550 nm and spectral conditions according to the published RapidEye™ spectral response curves (BlackBridge, 2012). We chose "midlattitude summer" atmospheric profile, and "homogenous surface" for ground reflectance with no directional effect from the list of pre-set options. Aerosol optical depth was retrieved from the AERONET database (Aerosol Robotic Network) from the station in Rimrock, ID (46°N 116°W). The filter function used for each RapidEye™ band was obtained from the *Iwave.cpp* file available at *https://code.google.com/p/xatmorr/source*.

C.3. Calibration of GRASS Module: *R.sun*

The effect of haze and cloud cover on irradiance received by the land surface is simulated in the *R.sun* module (Hofierka and Suri, 2002) using three input parameters: Linke turbidity factor LT, beam radiation coefficient K_{B}, and diffuse radiation coefficient K_{D}. The LT is founded on the work of Linke (1922) and accounts for absorption and scattering of the solar beam by atmospheric gases and aerosols under cloudless sky conditions (Kasten, 1980, 1996; Louche *et al.*, 1986; Grenier and Cabot, 1994; Ineichen and Perez, 2002). It may be conceptualized as the equivalent number of clear, dry atmospheres needed to produce the same extinction of extraterrestrial radiation through a turbid, wet atmosphere. Approximations of LT were made using observed aerosol optical depth, water vapor, and Angstrom parameters (Aerosol Robotic Network) based on the method of Remund and Domeisen (2010). Atmospheric properties were obtained from the AERONET database at daily intervals from January 2012 through October 2014 using data from the AERONET station in RimRock, ID (46°N 116°W).

The K_{B} and K_{D} coefficients are used for simulating effects of cloud cover on irradiance received by land. They are simply the ratio of real-sky (cloudy) to clear-sky (cloudless) irradiance for each component radiation component. The equations used for computing K_{B} and K_{D} are:

$$(a)\ K_{\mathrm{B}} = \frac{B_{\mathrm{R}}}{B_{\mathrm{C}}} \quad \text{and} \ (b)\ K_{\mathrm{D}} = \frac{D_{\mathrm{R}}}{D_{\mathrm{C}}} \tag{C-1}$$

where B and D are the beam and diffuse irradiance values, respectively, and subscripts R and C stand for real and clear-sky conditions, respectively. The *R.sun* module arrives at clear-sky global irradiance

values by summing the calculated beam, diffuse, and reflected components. Thus, to determine K_{B} and K_{D} from observed data, it was first necessary to partition measured global irradiance into beam and diffuse components. This was accomplished using the equations of Vignola and McDaniels (1986), which express the beam component as a function of global irradiance normalized by extraterrestrial radiation. The modeled irradiance values B_{C} and D_{C} of Equation (A-1) were computed according to Hofierka and Suri (2002) for a horizontal surface using the estimated LT. The coefficient K_{B} was then calculated as the partitioned observed beam irradiance B'_{R} divided by B_{C}. The remaining observed global irradiance was assumed to be diffuse, and the reflected component zero, since measurements were made on a horizontal surface. Accordingly, Equation (C-1) is rewritten in terms of B'_{R}, D_{C}, and measured global irradiance G'_{R}, as follows:

$$(a)\ K_{\mathrm{B}} = \frac{B'_{\mathrm{R}}}{B_{\mathrm{C}}} \ \text{ and } \ (b)\ K_{\mathrm{D}} = \left(\frac{G'_{\mathrm{R}} - B'_{\mathrm{R}}}{D_{\mathrm{C}}}\right) \qquad \text{(C-2)}$$

Consistently the K_{D} computed from Equation (C-2b) was greater than one. The error stems from the fact that beam components used for calculating Equation (C-2a) were derived by two very different methods, with B_{C} based on equations of astrophysics and B'_{R} based on empirical observation; hence, K_{B} and K_{D} were treated as calibration parameters and used only to correct modeled clear-sky irradiance to satisfy the condition: $K_{\mathrm{B}} \cdot B_{\mathrm{C}} + K_{\mathrm{D}} \cdot D_{\mathrm{C}} = G'_{\mathrm{R}}$. Upon calibration of K_{B} and K_{D} on a horizontal surface, the *R.sun* module was used for simulating irradiance on variable topographies according to Hofierka and Suri (2002).

C.4. Calculating Frequency of Saturation from 5TM/5TE Soil Moisture Sensors

Sustained periods of surface saturation result when water perches near the soil surface, such that there is a lack of available pore space into which water can drain. In this research we used 5TM and 5TE soil moisture probes (Decagon Devices, Pullman, WA) installed 30 cm beneath the ground surface in order to quantify the drainage activity above hydraulically-restricting layers in terms of the average number of days per year that the water table rises to within 30 cm of the soil surface. The moisture sensors provided continuous, hourly measurements of VWC, while measurements of perched water depth (PWD), defined as the vertical distance measured from the top of the ground surface to the top of the water table, were made from shallow wells in the field in order to relate VWC to PWD. Manual PWD measurements were taken periodically from 2012 to 2014, while automated data were collected at selected field locations using pressure sensors (model WT-HR, Intech Instruments Ltd, Christchurch, New Zealand).

It was observed that the 5TM/5TE moisture sensors reported a range of water contents under saturated conditions, so it was not possible to assign a static threshold water content on which to base saturation. Instead, saturation was determined visually from time-series plots of VWC from the 30-cm sensor. Sustained, high VWC readings indicate the presence of a nearby water table. By "sustained" is meant that the surface soil is unable to drain to field capacity within at least a couple days. The total number of days of sustained high water content were tabulated and reported as days per year of saturation. Figure (C-I) shows a comparison of VWC, manual PWD measurements, and pressure sensor measurements at site 9 of the Troy catchment. In Figure C-1a there is occasional disparity between VWC and measured water table depth, such that when the moisture sensor is beneath the water table according to PWD measurements, the water content is rapidly rising or falling, which does not fit the notion of "sustained". The cause of this disparity, whether error in PWD measurement, error in VWC measurement, or otherwise, is unknown. However, in terms of actual water content, the error may be very small because, as Brooks *et al.* (2007) have pointed out, large fluctuations in PWD result in very small differences in water content in soils with a shallow, hydraulically-restrictive layer. In Figure C-1a, the saturation line has been shifted from PWD=300 mm (dashed line) up to the PWD=180 mm (bottom border of blue-shaded region) in order to improve the visual agreement. Days with water content falling within the blue-shaded region are counted as days of saturation.

C.5. References

Aerosol Robotic Network. National Aeronautics and Space Administration—Goddard Space Flight Center, Holben B (Principle Investigator), Rimrock, ID. URL http://aeronet.gsfc.nasa.gov.

GRASS Development Team, 2012. Geographic Resources Analysis Support System (GRASS) Software. Open Source Geospatial Foundation Project. http://grass.osgeo.org.

Grenier JC, Delacasiniere A, Cabot T. 1994. A spectral model of Linke turbidity factor and its experimental implications. *Solar Energy* **52**(4): 303-313. DOI: 10.1016/0038-092X(94)90137-6

Hofierka J, Suri M. 2002. The solar radiation model for open source GIS: implementation and applications. In *Proceedings of the Open Source GIS-GRASS Users Conference, 2002—Trento, Italy, 11-13 September 2002* [online], Ciolli M, Zatelli P (eds). Accessed December 13, 2015 at http://www.ing.unitn.it/~grass/conferences/GRASS2002/proceedings/proceedings/pdfs/Hofierka_Jaroslav.pdf.

Ineichen P, Perez R. 2002. A new airmass independent formulation for the Linke turbidity coefficient. *Solar Energy* **73**(3): 151-157. DOI: 10.1016/S0038-092X(02)00045-2

Kasten F. 1980. A simple parameterization of the pyrheliometric formula for determining the Linke turbidity factor. *Meteorologische Rundschau* **33**(4): 124-127.

Kasten F. 1996. The Linke turbidity factor based on improved values of the integral Rayleigh optical thickness. *Solar Energy* **56**(3): 239-244. DOI: 10.1016/0038-092X(95)00114-7

Linke F. 1922. Transmissions-Koeffizient und Trubungsfaktor. *Beitr. Phys. Atmos.* **10**: 91-103.

Louche A, Peri G, Iqbal M. 1986. An analysis of Linke turbidity factor. *Solar Energy* **37**(6): 393-396. DOI: 10.1016/0038-092X(86)90028-9

Remund J, Dameisen D (eds). 2010. Aerosol optical depth and Linke turbidity climatology, IEA SHC Task 36 Final Report, 30pp. Solar Heating & Cooling Programme of the International Energy Agency. Accessed December 23, 2015 at http://meteonorm.com/images/uploads/downloads/ieashc36_ report_TL_AOD _climatologies.pdf.

Vermote EF, Tanre D, Deuze JL, Herman M, Morcrette JJ. 1997. Second simulation of the satellite signal in the solar spectrum, 6S: an overview. *IEEE Transactions on Geoscience and Remote Sensing* **35**(3): 675-686. DOI: 10.1109/36.581987.

Vignola F, McDaniels DK. 1986. Beam-global correlations in the Pacific Northwest. *Solar Energy* **36**(5): 409-418. DOI: 10.1016/0038-092X(86)90088-5

C.6. Figures

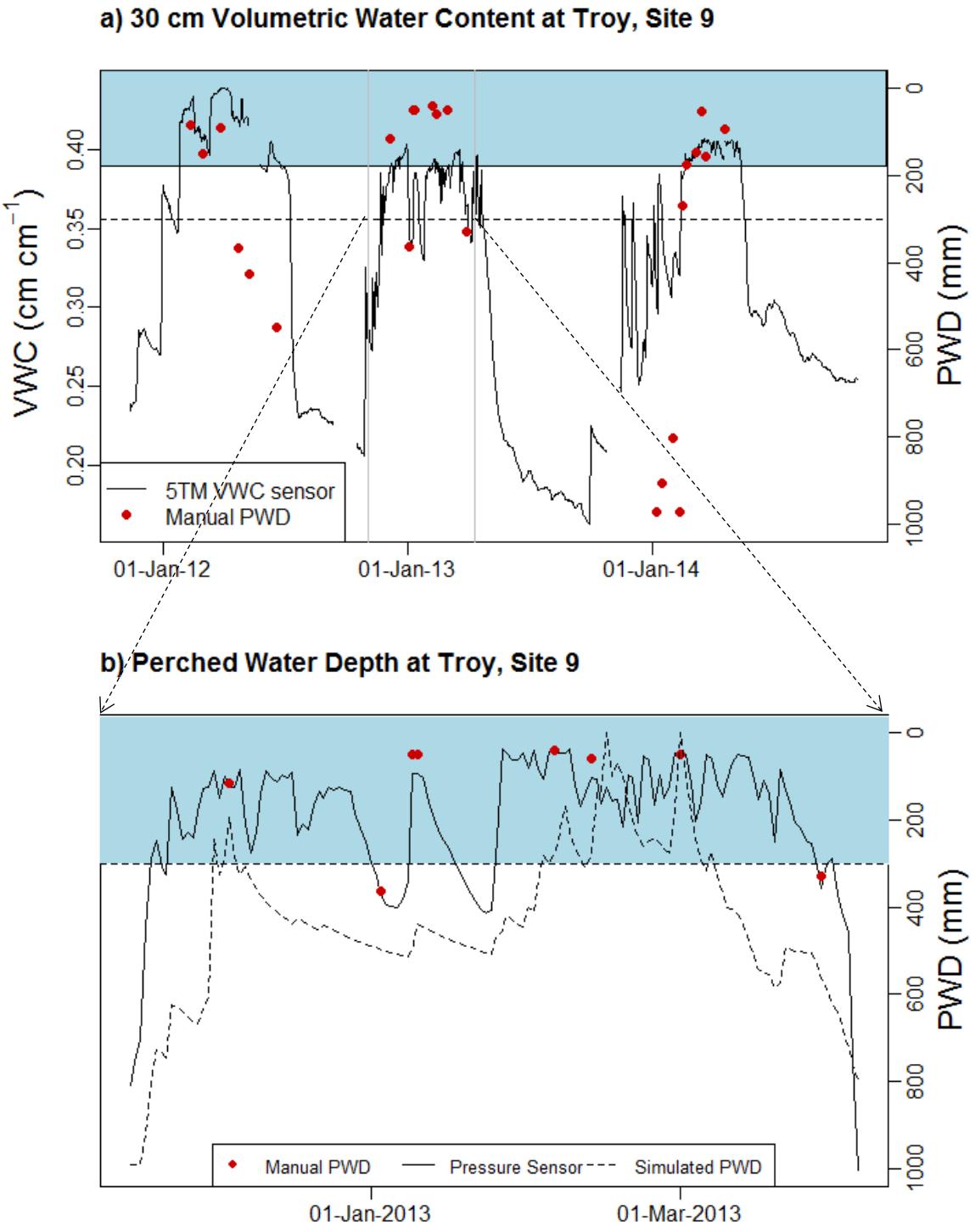

Figure C-1. Frequency of saturation determined using 5TM/5TE soil moisture sensors. VWC is shown in C-1a and pressure sensor readings of PWD for the 2013 season are shown in C-1b. The red dots show all manual PWD measurements. The surface soil is considered saturated whenever water content falls within the blue-shaded region of C-1a.